

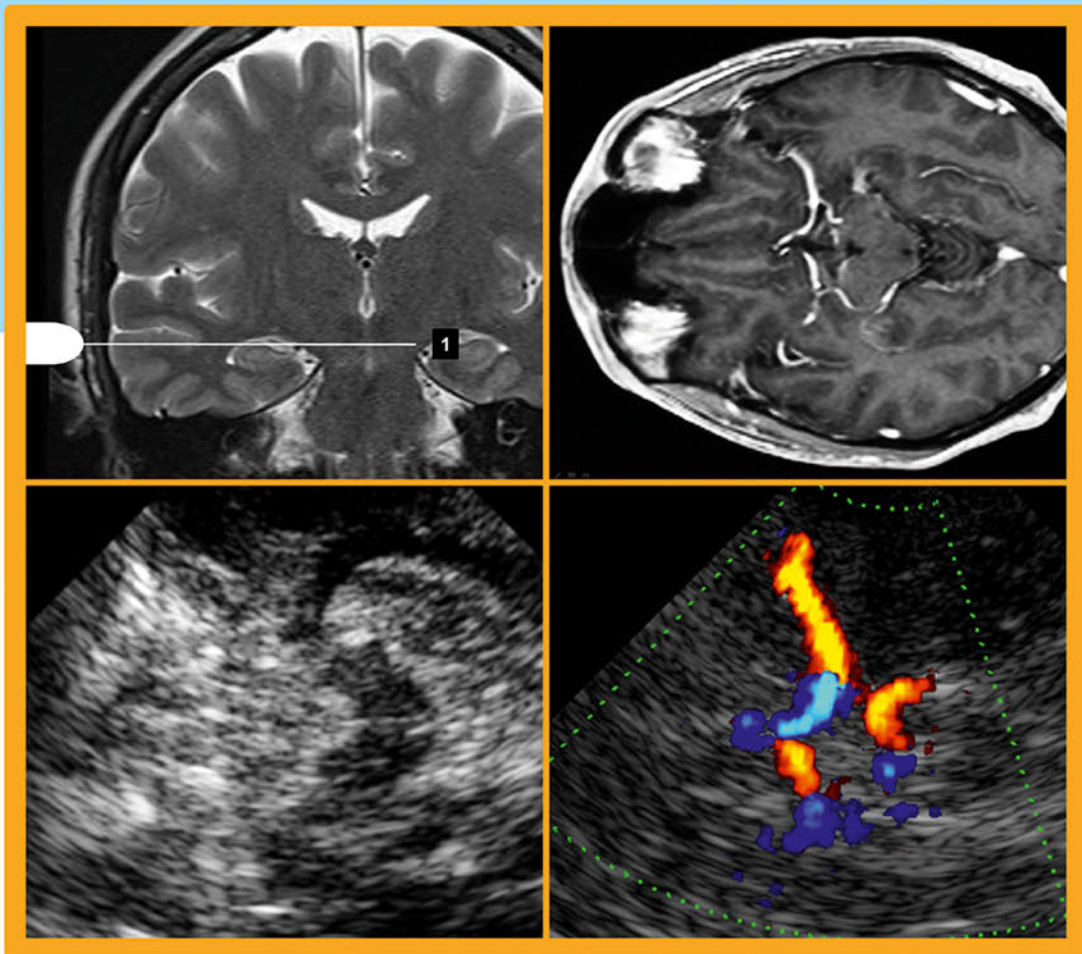
Neurosonology and Neuroimaging of Stroke

A Comprehensive Reference

José M. Valdueza
Stephan J. Schreiber
Jens-Eric Roehl
Florian Connolly
Randolf Klingebiel

Second Edition

plus videos



MediaCenter.thieme.com
plus e-content online



Thieme

Find videos and ultrasound reference charts online at MediaCenter.thieme.com!

Simply visit MediaCenter.thieme.com and, when prompted during the registration process, enter the code below to get started today.

Q6WY-NQKP-8KW8-BE46

Neurosonology and Neuroimaging of Stroke

A Comprehensive Reference

2nd Edition

José M. Valdueza, MD

Professor of Neurology
Charité – Universitätsmedizin Berlin
Berlin, Germany
Director, Center of Neurology
Segeberger Kliniken Gruppe
Bad Segeberg, Germany

Stephan J. Schreiber, MD

Professor of Neurology
Charité – Universitätsmedizin Berlin
Berlin, Germany
Head, Department of Neurology
Asklepios Hospital Brandenburg
Brandenburg an der Havel, Germany

Jens-Eric Roehl, MD

Senior Neurologist
Department of Neurology
Klinikum Ernst von Bergmann
Potsdam, Germany

Florian Connolly, MD

Senior Neurologist
Department of Neurology
Charité – Universitätsmedizin Berlin
Berlin, Germany

Randolf Klingebiel, MD

Professor of Neuroradiology
Charité – Universitätsmedizin Berlin
Berlin, Germany
Head, Department of Diagnostic and Interventional
Neuroradiology
Evangelisches Krankenhaus Bielefeld
Bielefeld, Germany

1305 illustrations

Thieme
Stuttgart • New York • Delhi • Rio de Janeiro

Library of Congress Cataloging-in-Publication Data

Names: Valdueza, José M., author. | Schreiber, Stephan J., author. | Roehl, Jens-Eric, author. | Connolly, Florian, author. | Klingebiel, Randolph, author.

Title: Neurosonology and neuroimaging of stroke : a comprehensive reference / José M.Valdueza, Stephan J. Schreiber, Jens-Eric Roehl, Florian Connolly, Randolph Klingebiel.

Description: 2nd edition. | Stuttgart ; New York : Thieme, [2017] | Preceded by Neurosonology and neuroimaging of stroke / José M. Valdueza ... [et al.]. c2008 | Includes bibliographical references and index.

Identifiers: LCCN 2016035027 (print) | LCCN 2016036354 (ebook) | ISBN 9783131418722 (hardback : alk. paper) | ISBN 9783131760227 (e-book) | ISBN 9783131760227

Subjects: | MESH: Ultrasonography, Doppler, Transcranial—methods | Cerebrovascular Disorders—ultrasonography | Cerebrovascular Circulation | Case Reports

Classification: LCC RC78.7.U4 (print) | LCC RC78.7.U4 (ebook) | NLM WL 154 | DDC 616.07/543—dc23

LC record available at <https://lccn.loc.gov/2016035027>

1st Russian edition 2012

© 2017 by Georg Thieme Verlag KG

Thieme Publishers Stuttgart
Rüdigerstrasse 14, 70469 Stuttgart, Germany
+49 [0]711 8931 421, customerservice@thieme.de

Thieme Publishers New York
333 Seventh Avenue, New York, NY 10001 USA
+1 800 782 3488, customerservice@thieme.com

Thieme Publishers Delhi
A-12, Second Floor, Sector-2, Noida-201301
Uttar Pradesh, India
+91 120 45 566 00, customerservice@thieme.in

Thieme Publishers Rio, Thieme Publicações Ltda.
Edifício Rodolpho de Paoli, 25º andar
Av. Nilo Peçanha, 50 – Sala 2508
Rio de Janeiro 20020-906 Brasil
+55 21 3172 2297 / +55 21 3172 1896

Cover design: Thieme Publishing Group
Typesetting by DiTech Process Solutions

Printed in Germany by Aprinta Druck GmbH,
Wemding

5 4 3 2 1

ISBN 978-3-13-141872-2

Also available as an e-book:
eISBN 978-3-13-176022-7

Important note: Medicine is an ever-changing science undergoing continual development. Research and clinical experience are continually expanding our knowledge, in particular our knowledge of proper treatment and drug therapy. Insofar as this book mentions any dosage or application, readers may rest assured that the authors, editors, and publishers have made every effort to ensure that such references are in accordance with **the state of knowledge at the time of production of the book.**

Nevertheless, this does not involve, imply, or express any guarantee or responsibility on the part of the publishers in respect to any dosage instructions and forms of applications stated in the book. **Every user is requested to examine carefully** the manufacturers' leaflets accompanying each drug and to check, if necessary in consultation with a physician or specialist, whether the dosage schedules mentioned therein or the contraindications stated by the manufacturers differ from the statements made in the present book. Such examination is particularly important with drugs that are either rarely used or have been newly released on the market. Every dosage schedule or every form of application used is entirely at the user's own risk and responsibility. The authors and publishers request every user to report to the publishers any discrepancies or inaccuracies noticed. If errors in this work are found after publication, errata will be posted at www.thieme.com on the product description page.

Some of the product names, patents, and registered designs referred to in this book are in fact registered trademarks or proprietary names even though specific reference to this fact is not always made in the text. Therefore, the appearance of a name without designation as proprietary is not to be construed as a representation by the publisher that it is in the public domain.

This book, including all parts thereof, is legally protected by copyright. Any use, exploitation, or commercialization outside the narrow limits set by copyright legislation without the publisher's consent is illegal and liable to prosecution. This applies in particular to photostatic reproduction, copying, mimeographing or duplication of any kind, translating, preparation of microfilms, and electronic data processing and storage.

Preface

Stroke is one of the most commonly occurring brain diseases and, in spite of its often homogeneous clinical appearance, its causes vary considerably. The implementation of a tailored and targeted therapy in each individual case requires rapid etiological classification and a qualified evaluation of the vascular status. Knowledge of normal vascular anatomy, variants, and anomalies are essential for proper clinical assessment.

In the 1970s, conventional angiography was practically the only method capable of visualizing brain-supplying arteries. In the 1980s, magnetic resonance imaging (MRI) and computed tomography (CT) were developed and gradually implemented into clinical practice. Since the end of the 1990s, the latter methods have evolved into sophisticated angiologic techniques. However, despite being well established, they do have limitations: MRI requires patient compliance and may not be used in patients with a pacemaker. CT involves radiation exposure and CT angiography (CTA) requires the administration of a contrast agent. An excellent alternative diagnostic modality to study the brain-supplying arteries is diagnostic ultrasound. The technique is in fact a powerful, noninvasive, inexpensive, and dynamic tool which not only captures a snapshot of vessels, but shows real hemodynamics over time. Ultrasound can be used quickly and spontaneously. It follows rules and pathways but defies full standardization, thereby allowing space for individualized decision-making on a case-by-case basis. The sonographer has the advantage of being directly at the patient's side and is therefore capable of speaking with the patient, winning their confidence, and diminishing their anxiety. It is the doctor and not the machine guiding the probe and it is the clinical question that motivates the investigation.

In clinical neurology, ultrasound became available in the early 1970s. The neurovascular focus developed in the 1980s with the use of extracranial color-coded duplex sonography (ECCS) and transcranial Doppler (TCD) techniques. The development of transcranial color-coded duplex sonography (TCCS) in the early 1990s was an important advance, as TCCS's diagnostic sensitivity exceeded that of TCD. B-mode and color-mode images generated using TCCS greatly facilitated vessel identification by offering additional spatial information about vessel courses in relation to bone, parenchymal structures, and ventricles. In the mid-1990s, we shifted our routine vascular diagnostic procedures away from TCD to TCCS. The combination of extra- and intracranial duplex ultrasound permits an almost comprehensive assessment of all brain-supplying vessels with a single bedside device. TCD remains the primary method for functional assessments such as right-left shunt diagnosis, assessment of

cerebrovascular reactivity, autoregulation, and bilateral continuous monitoring for spontaneous microemboli.

What is the best diagnostic approach for patients with acute and chronic brain ischemia? Several angiologic methods are now available for the treatment of stroke patients: DSA, MRA, CTA, and ultrasound. Each technique may yield information that is partly competing and partly complementary regarding vessel anatomy, vessel wall properties, and circulation physiology. Stroke physicians should be aware of the strengths and weaknesses of each of the available methods. In this book, we point out both the advantages and limitations of each of these methods, but the reader should also consider availability and investigator skill.

The concept of this book is based on the combined teaching experience gained by the authors (J.M. Valdueza, S.J. Schreiber, J.-E. Roehl, and F. Connolly) in ultrasound courses, seminars, and lectures over the past 15 years. We realized that the presentation and discussion of real cases provoked the greatest interest among our listeners, which we have again considered by adding new and instructive clinical case reports.

The book is divided into two parts. Part A outlines the necessary basic principles, with a particular focus on the precise description of ultrasound anatomy and the related examination techniques. The online materials accompanying this book include video sequences of a complete extra- and intracranial arterial and venous duplex examination and of fusion imaging with MRI. Part A also includes a discussion of the basic principles of cerebral hemodynamics and a comprehensive presentation of pathologic findings in extracranial and intracranial stenoses and occlusions. The relevant stroke aspects from a clinical and radiologic point of view are presented in a separate chapter. Part A ends with an overview of the currently available neuroradiologic techniques—DSA, MRA, and CTA (R. Klingebiel).

In Part B, we present 45 case histories of selected patients managed either in the Department of Neurology, Charité – Universitätsmedizin Berlin (Germany), or in the Neurological Center in Bad Segeberg (Germany). Each case is divided into two sections: the case report and a discussion. In the case reports, the diagnostic algorithm and the therapeutic strategy are presented in chronological order. Each case report begins with a short history of the presenting complaint and a description of the initial radiologic findings. On these grounds, we have formulated a hypothesis and angiologic questions to be answered using ultrasound. The findings of extra- and intracranial color-coded duplex sonography are controlled for plausibility and the postulated hypothesis is confirmed or

rejected. A final diagnosis is then made on the basis of the findings of all the diagnostic procedures, including the parenchymal and vascular imaging. In more than half of the cases, additional video sequences of the ultrasound studies are provided on Thieme's MediaCenter to give a better impression of the real examination situation and also to emphasize the advantages of the ultrasound technique as a single noninvasive real-time imaging method. Complex cases are accompanied by schematics which illustrate the occlusive process and collateral situation to help the reader understand the specifics of the individual vascular constellation.

The case discussion is divided into clinical and angiologic–anatomic sections. The clinical discussion provides a short overview of the presented disease and outlines specific diagnostic and therapeutic aspects of the case to help readers manage vascular patients on a high level. The angiologic–anatomic discussion focuses on ultrasound-related and general angiologic questions arising from the individual case. Special emphasis is placed on explaining the strengths and weaknesses of each imaging method. Our particular interest is to promote the duplex ultrasound technique while giving the user a better understanding of the technique's potential within the clinical context.

This is the book's second edition. The first edition, published in 2008, was soon sold out. After a reprint and a Russian edition, we were asked by the publishers to prepare a second, extended, edition. The concept of the first edition—the presentation of the principles of neurosonology through real-life clinical scenarios—has not changed. Based on the technical developments and many valuable suggestions from colleagues worldwide, both parts of the book have been expanded.

In Part A, we have extended the anatomic and pathologic contents to give a better survey of the clinically relevant aspects. In particular, orbital and vascular-related parenchymal sonography as well as fusion imaging with ultrasound and MRI has been added in the anatomy

section. In Part B, we have added rarer but important clinical entities like subarachnoid hemorrhage, sickle cell disease, arteriovenous dural fistula, intracranial aneurysm, central retinal occlusion, cerebral reversible vasoconstriction syndrome, agenesis of the internal carotid artery (ICA), and transient global amnesia, as well as complex vascular conditions in severe atherosclerosis not presented before. Also, some cases from the first edition were substituted to provide better ultrasound images, e.g. proximal ICA stenosis, proximal middle cerebral artery stenosis, moyamoya disease, traumatic four-vessel dissection, and ICA near-occlusion.

The present book is aimed at all doctors—in particular neurologists, neurosurgeons, internists, angiologists, and (neuro-) radiologists—who treat neurologic or neurosurgical patients with vascular diseases.

Finally, we would like to thank all those who directly or indirectly contributed to this book. We thank Dr. Georg Bohner and Dr. Christian Gaebel for contributing the neuroradiologic images and evaluations of the newly included cases from the Charité hospital and the clinic in Bad Segeberg. We thank Dr. Niksha Ranpura, Dr. Si Hung Liu, and Christopher Leonards, who contributed to the linguistic improvement of this project, and Michael Blanz, who edited all the videos. We especially want to thank Angelika-Marie Findgott, Dr. Martina Habeck, and Stephan Konnry from Thieme Publishers for their quick and reliable support in all developmental phases of this second edition. Last but not least, we would like to express our profound gratitude to our families for their constant support and understanding.

José M. Valdueza, MD
Stephan J. Schreiber, MD
Jens-Eric Roehl, MD
Florian Connolly, MD
Randolf Klingebiel, MD

Contents

Preface	v
Videos	xiv
Abbreviations	xix

Part A Principles and Rules

1 Flow and Ultrasound Basics	2	Other Tests to Assess Differences Between the Right and Left Sides as Markers of Impaired Collateral Function.....	84
Flow Dynamics	2	Parameters of Cerebral Hemodynamics	86
Physics of Flow	2	Cerebral Blood Flow Velocity.....	86
Flow Pattern and Flow Velocity	2	Resistance Indices.....	86
Ultrasound Principles	3	Cerebral Blood Flow Volume	86
Doppler Effect	3	Cerebral Circulation Time.....	87
Doppler Shift and Flow Velocity.....	4	Cerebral Blood Volume	88
Ultrasound Systems	6	4 Pathogenesis of Stroke	90
Ultrasound Transducer	7	Arterial Ischemia.....	90
Imaging Modalities, Parameters, and Settings ..	8	Pathophysiology	90
Imaging Modalities.....	8	Classification of Arterial Stroke.....	91
Parameters and Settings.....	12	Microembolic Signals.....	100
Artifacts.....	15	Spontaneous Microemboli.....	100
Artifacts in Gray-scale Imaging.....	15	Detection of Microemboli in Patent Foramen Ovale	102
Refraction and Mirror Artifacts.....	16	Venous Ischemia	103
Artifacts in Color-mode Imaging	17	5 Vascular Pathology	106
Artifacts in Doppler Spectrum Analysis.....	17	Arterial Pathology.....	106
Safety Considerations	17	Vessel Wall Pathology	106
2 Vascular Anatomy and Structure of Ultrasound		Tortuosity.....	107
Examination	18	Intima-media Thickness.....	108
General Arterial Anatomy.....	18	Atherosclerotic Plaques	108
Extracranial Arterial Anatomy.....	18	Arterial Stiffness.....	113
Intracranial Arterial Anatomy.....	21	Dissection.....	113
General Structure of Arterial Ultrasound Examination.....	24	Fibromuscular Dysplasia (FMD).....	114
Special Arterial Anatomy and Ultrasound Anatomy	25	Vasculitis/Arteritis.....	115
Extracranial Arteries	25	Carotidynia and Carotid Artery Vasospasm .	115
Intracranial Arteries.....	34	Stenoses and Occlusions.....	118
General Venous Anatomy	61	Ultrasound Criteria of Stenoses	118
Intracranial Venous Anatomy	62	Ultrasound Criteria of Occlusions	125
Extracranial Venous Anatomy.....	62	Extracranial Pathology	125
General Structure of Venous Ultrasound Examination.....	64	Extracranial Anterior Circulation.....	125
Special Venous Anatomy and Ultrasound Anatomy	64	Extracranial Posterior Circulation.....	133
Intracranial Veins and Sinuses	64	Intracranial Pathology.....	138
Extracranial Veins.....	71	Stenoses	138
3 Intracranial Hemodynamics and Functional Tests ..	79	Occlusions	144
Analysis of Cerebral Blood Flow	79	Intracranial Anterior Circulation	145
Autoregulation	80	Intracranial Posterior Circulation.....	153
Testing of Autoregulation	81	Collateral Pathways	161
Neurovascular Coupling	82	Intracranial Collateral Pathways.....	162
Testing of Neurovascular Coupling.....	82	Intracranial Collateral Pathways in ICA	
Metabolic Coupling	83	Occlusive Processes	167
Testing of Metabolic Coupling.....	83	Intracranial Collateral Pathways in VA	
		Occlusive Processes	172

Extracranial Collateral Pathways in VA		Midline and Midline Shift	180
Occlusive Processes	173	Intracranial Hemorrhage	180
Clinical Relevance of Collateral Pathways ...	173	Parenchymal Hemorrhage	180
Venous Pathology	175	Subdural and Epidural Hematoma	182
Cerebral Venous Thrombosis	175	6 Angiographic Techniques in Neuroradiology	183
Superior Sagittal Sinus Occlusion	175	Choice of Imaging Techniques	183
Deep Cerebral Venous System Occlusion	176	Digital Subtraction Angiography (DSA)	183
Lateral Sinus (Transverse and Sigmoid Sinus)		Historical Development	183
Occlusion	176	Technical Aspects of Diagnostic Angiography ...	184
Flow Abnormalities in Cerebral		Technical Aspects of Mechanical	
Venous Thrombosis	176	Thrombectomy	185
Ultrasonography of the Internal Jugular		Advantages and Disadvantages	185
Vein in Intensive Care Patients	178	Magnetic Resonance Angiography (MRA)	187
Central Venous Cannulation	178	Historical Development	187
Indirect Assessment of Central Venous		Technical Aspects	187
Pressure (CVP)	178	Advantages and Disadvantages	190
Intracranial Stroke-related B-mode		Computed Tomographic Angiography (CTA)	191
Pathology	178	Historical Development	191
Ventricles	178	Technical Aspects	192
Hydrocephalus	179	Advantages and Disadvantages	192
Papilledema and Optic Nerve Sheath Diameter ...	179		

Part B Case Histories

Case 1 Right Extracranial Internal Carotid Artery Stenosis	197	Case 4 Left Temporal Arteriovenous Malformation	215
Clinical Presentation	197	Clinical Presentation	215
Initial Neuroradiologic Findings	197	Initial Neuroradiologic Findings	215
Suspected Diagnosis	197	Suspected Diagnosis	215
Questions to Answer Using Ultrasound Techniques ...	197	Questions to Answer by Ultrasound Techniques	215
Initial Neurosonologic Findings	197	Initial Neurosonologic Findings	215
MRI	197	Conventional Angiography	215
CT Angiography	197	Clinical Course	216
Clinical Course	198	Final Diagnosis	216
Final Diagnosis	198	Discussion	218
Discussion	199	Case 5 Left M1 Middle Cerebral Artery Stenosis	222
Case 2 Free-floating Thrombus of the Left Internal Carotid Artery	205	Clinical Presentation	222
Clinical Presentation	205	Initial Neuroradiologic Findings	222
Initial Neuroradiologic Findings	205	Suspected Diagnosis	222
Diagnosis	205	Conventional Angiography (Day 2)	222
Question to Answer by Ultrasound Techniques	205	Clinical Course	222
Initial Neurosonologic Findings (Day 1)	205	Questions to Answer by Ultrasound Techniques	222
Clinical Course	205	Initial Neurosonologic Findings	222
Neurosonologic Findings (Day 20)	206	Final Diagnosis	224
Final Diagnosis	206	Discussion	224
Discussion	206	Case 6 Left P2 Posterior Cerebral Artery Stenosis	230
Case 3 Left Common Carotid Artery Occlusion	210	Clinical Presentation	230
Clinical Presentation	210	Initial Neuroradiologic Findings	230
Initial Neuroradiologic Findings	210	Suspected Diagnosis	230
Suspected Diagnosis	210	Questions to Answer by Ultrasound Techniques	230
Questions to Answer by Ultrasound Techniques	210	Initial Neurosonologic Findings (Day 2)	230
Initial Neurosonologic Findings	210	Clinical Course	230
Clinical Course	210	Final Diagnosis	232
Final Diagnosis	211	Discussion	232
Discussion	211		

Case 7 Cerebral Circulatory Arrest	235	Clinical Course (2)	270
Clinical Presentation	235	Follow-up Neurosonologic Findings (Day 7)	270
Initial Neuroradiologic Findings	235	Clinical Course (3)	270
Suspected Diagnosis	235	Follow-up Neurosonologic Findings (6 Months)	270
Clinical Course (1)	235	Final Diagnosis	271
Cerebral CT	235	Discussion	276
Question to Answer by Ultrasound Techniques	235		
Initial Neurosonologic Findings	235	Case 12 Extracranial Bilateral Internal Carotid Artery and Right Vertebral Artery Occlusion, and Left Vertebral Artery Stenosis	281
Clinical Course (2)	235	Clinical Presentation	281
Final Diagnosis	236	Initial Neuroradiologic Findings	281
Discussion	236	Suspected Diagnosis	281
		Questions to Answer by Ultrasound Techniques	281
Case 8 Basilar Artery Occlusion in Bilateral Intracranial V4 Vertebral Artery Stenosis	244	Initial Neurosonologic Findings	281
Clinical Presentation	244	Clinical Course	282
Initial Neuroradiologic Findings	244	Final Diagnosis	285
Suspected Diagnosis	244	Discussion	285
Conventional Angiography (Day 1)	244		
Clinical Course (1)	244	Case 13 Right Internal Carotid Artery Stenosis in Fibromuscular Dysplasia and Granulomatosis with Polyangiitis (formerly Wegener's Granulomatosis)	288
Questions to Answer by Ultrasound Techniques	244	Clinical Presentation	288
Initial Neurosonologic Findings (Day 42)	244	Initial Neuroradiologic Findings	288
Neuroradiologic Findings	247	Suspected Diagnosis	288
Clinical Course (2)	247	Question to Answer by Ultrasound Techniques	288
Final Diagnosis	247	Initial Neurosonologic Findings (Day 1)	288
Discussion	247	Clinical Course (1)	288
		Conventional Angiography (Day 5)	289
Case 9 Moyamoya Disease	251	Clinical Course (2)	289
Clinical Presentation	251	Follow-up Neurosonologic Findings (5 Years)	289
Initial Neuroradiologic Findings	251	Final Diagnosis	290
Suspected Diagnosis	251	Discussion	291
Conventional Angiography (Day 3)	251		
Clinical Course (1)	251	Case 14 Isolated Left Carotid Siphon Stenosis	295
Questions to Answer by Ultrasound Techniques	251	Clinical Presentation	295
Initial Neurosonologic Findings (Week 6)	251	Initial Neuroradiologic Findings	295
Clinical Course (2)	255	Suspected Diagnosis	295
Follow-up Neurosonologic Findings (3 Months)	256	Questions to Answer by Ultrasound Techniques	295
Final Diagnosis	256	Initial Neurosonologic Findings	295
Discussion	256	Clinical Course	295
		Final Diagnosis	297
Case 10 Thrombolysis of M1 Middle Cerebral Artery Occlusion	260	Discussion	297
Clinical Presentation	260		
Initial Neuroradiologic Findings	260	Case 15 Near-occlusion of the Right and High-grade Stenosis of the Left Extracranial Internal Carotid Artery	300
Suspected Diagnosis	260	Clinical Presentation	300
Clinical Course (1)	260	Initial Neuroradiologic Findings	300
Questions to Answer by Ultrasound Techniques	260	Suspected Diagnosis	300
Initial Neurosonologic Findings	260	Questions to Answer by Ultrasound Techniques	300
Clinical Course (2)	260	Initial Neurosonologic Findings	300
Follow-up Neurosonologic Findings (1 Hour)	260	Conventional Angiography (Day 3)	301
Clinical Course (3)	261	Clinical Course (1)	301
Final Diagnosis	261	Follow-up Neurosonologic Findings (6 Weeks)	301
Discussion	262	Clinical Course (2)	301
		Follow-up Neuroradiologic Findings (2 Months)	301
Case 11 Secondary Occlusion in Left-sided Extracranial Internal Carotid Artery Dissection	269	Follow-up Neurosonologic Findings (3 Months)	301
Clinical Presentation	269	Final Diagnosis	310
Initial Neuroradiologic Findings	269	Discussion	310
Suspected Diagnosis	269		
Questions to Answer by Ultrasound Techniques	269		
Initial Neurosonologic Findings (Day 1)	269		
Clinical Course (1)	269		
Questions to Answer by Ultrasound Techniques	270		
Follow-up Neurosonologic Findings (Day 2)	270		

Case 16 Giant Cell Arteritis with Bilateral Intracranial V4 Vertebral Artery Stenosis	313	Case 20 Right Internal Carotid Artery Dissection with Fast Recanalization.	345
Clinical Presentation	313	Clinical Presentation	345
Initial Neuroradiologic Findings	313	Initial Neuroradiologic Findings	345
Suspected Diagnosis	313	Suspected Diagnosis	345
Questions to Answer by Ultrasound Techniques	313	Questions to Answer by Ultrasound Techniques	345
Initial Neurosonologic Findings (Day 1)	313	Initial Neurosonologic Findings (Day 1)	345
Clinical Course (1)	313	Evaluation of Collateral Function	345
Follow-up Neurosonologic Findings (6 Weeks)	314	Conventional Angiography	346
Clinical Course (2)	315	Clinical Course (1)	346
Final Diagnosis	315	Follow-up Neurosonologic Findings (Day 20)	347
Discussion	315	Clinical Course (2)	347
		Final Diagnosis	348
		Discussion	348
Case 17 Ascending Left Middle Cerebral Artery Occlusion in an HIV-positive Patient	320	Case 21 Mid-basilar Artery Occlusion Due to Intracranial Dissection	354
Clinical Presentation	320	Clinical Presentation	354
Initial Neuroradiologic Findings	320	Initial Neuroradiologic Findings	354
Suspected Diagnosis	320	Suspected Diagnosis	354
Questions to Answer by Ultrasound Techniques	320	Clinical Course (1)	354
Initial Neurosonologic Findings (Day 1)	320	Follow-up Neurosonologic Findings (Day 3)	354
Conventional Angiography (Day 3)	320	Questions to Answer by Ultrasound Techniques	354
Clinical Course	321	Initial Neurosonologic Findings (Day 3)	354
Final Diagnosis	322	Conventional Angiography (Day 4)	355
Discussion	322	Clinical Course (2)	355
		Final Diagnosis	356
		Discussion	356
Case 18 Traumatic Bilateral Internal Carotid and Vertebral Artery Dissection with Right-sided Embolic Middle Cerebral Artery Occlusion.	327	Case 22 Right Mid-part M1 Middle Cerebral Artery Occlusion with Prominent Early Temporal Branch and Patent Foramen Ovale	362
Clinical Presentation	327	Clinical Presentation	362
Neuroradiologic Findings (Day 2)	327	Initial Neuroradiologic Findings	362
Suspected Diagnosis	327	Suspected Diagnosis	362
Conventional Angiography with Endovascular Thrombectomy (Day 2)	327	Questions to Answer by Ultrasound Techniques	362
Clinical Course (1)	327	Initial Neurosonologic Findings (Day 1)	362
Questions to Answer by Ultrasound Techniques	327	Clinical Course (1)	362
Initial Neurosonologic Findings (Day 3)	328	Questions to Answer by Ultrasound Techniques	363
Clinical Course (2)	330	Neurosonologic Findings (Day 10)	363
Second Conventional Angiography (Day 4)	330	Neuroradiologic Findings (Day 11)	364
Clinical Course (3)	331	Clinical Course (2)	364
Follow-up Neurosonologic Findings (Day 21)	331	Final Diagnosis	365
Follow-up MRI and MR Angiography (8 Months)	332	Discussion	366
Follow-up Neurosonologic Findings (After 1 Year)	332		
Clinical Course (4)	334	Case 23 Takayasu's Arteritis with Right-sided Subclavian Steal	372
Final Diagnosis	334	Clinical Presentation	372
Discussion	334	Initial Neuroradiologic Findings	372
		Suspected Diagnosis	372
		Questions to Answer by Ultrasound Techniques	372
Case 19 Bilateral Extracranial Vertebral Artery Dissection with Distal Occlusion of the Right Vertebral Artery	339	Initial Neurosonologic Findings	372
Clinical Presentation	339	Conventional Angiography	372
Initial Neuroradiologic Findings	339	Clinical Course (1)	373
Suspected Diagnosis	339	Question to Answer by Ultrasound Techniques (6 Months)	373
Questions to Answer by Ultrasound Techniques	339	Neurosonologic Findings (6 Months)	373
Initial Neurosonologic Findings	339	Clinical Course (2)	374
Conventional Angiography	339	Questions to Answer by Ultrasound Techniques (8 Months)	376
Clinical Course	340		
Final Diagnosis	340		
Discussion	340		

Neurosonologic Findings (8 Months)	376	Conventional Angiography	403
Final Diagnosis	376	Clinical Course	403
Discussion	376	Final Diagnosis	403
		Discussion	406
Case 24 Dissection of the Right Extracranial Internal Carotid Artery and Left M1 Middle Cerebral Artery	380	Case 28 Subclavian Steal in Left Subclavian Artery and Right Internal Carotid Artery Occlusion Leading to Extracranial- Intracranial Bypass Surgery	409
Clinical Presentation	380	Clinical Presentation	409
Initial Neuroradiologic Findings	380	Initial Neuroradiologic Findings	409
Suspected Diagnosis	380	Suspected Diagnosis	409
Clinical Course (1)	380	Questions to Answer by Ultrasound Techniques	409
MRI and MR Angiography (10:00 Hours)	380	Initial Neurosonologic Findings (Day 1)	409
Questions to Answer by Ultrasound Techniques	380	Conventional Angiography (Day 2)	410
Neurosonologic Findings (12:00 Hours)	380	Clinical Course (1)	410
Conventional Angiography (16:00 Hours)	381	Follow-up Neurosonologic Findings (4 Weeks)	410
Clinical Course (2)	382	Clinical Course (2)	410
Questions to Answer by Ultrasound Techniques	383	Final Diagnosis	410
Follow-up Neurosonologic Findings (6 Months)	383	Discussion	415
Conventional Angiography	384	Case 29 Cerebral Venous Thrombosis	420
Clinical Course (3)	384	Clinical Presentation	420
Final Diagnosis	384	Initial Neuroradiologic Findings	420
Discussion	384	Suspected Diagnosis	420
		Questions to Answer by Ultrasound Techniques	420
Case 25 Progressive Right M1 Middle Cerebral Artery Occlusion Treated with Extracranial-Intracranial Bypass Surgery	388	Initial Neurosonologic Findings (Day 1)	420
Clinical Presentation	388	CT Angiography (CTA) (Day 1)	420
Initial Neuroradiologic Findings	388	Clinical Course (1)	420
Suspected Diagnosis	388	Question to Answer by Ultrasound Techniques	420
Questions to Answer by Ultrasound Techniques	388	Follow-up Neurosonologic Findings (Day 90)	420
Initial Neurosonologic Findings (Day 2)	388	Question to Answer by Ultrasound Techniques	421
Conventional Angiography (Day 4)	388	Follow-up Neurosonologic Findings (Day 180)	421
Clinical Course (1)	389	Clinical Course (2)	421
Clinical Course (2) and Follow-up Neuroradiologic Findings	391	Final Diagnosis	421
Follow-up Neurosonologic Findings (10 Months)	391	Discussion	424
Clinical Course (3)	392	Case 30 Multilocular Extra- and Intracranial Stenoses and Occlusions	427
Final Diagnosis	392	Clinical Presentation	427
Discussion	392	Initial Neuroradiologic Findings (Day 1)	427
		Suspected Diagnosis	427
Case 26 Extracranial Left Vertebral Artery Dissecting Aneurysm Following Basilar Artery Stenting	396	Questions to Answer by Ultrasound Techniques	427
Clinical Presentation	396	Initial Neurosonologic Findings (Day 20)	427
Initial Neuroradiologic Findings	396	Conventional Angiography (Day 22)	428
Suspected Diagnosis	396	Clinical Course (1)	428
Conventional Angiography	396	Questions to Answer by Ultrasound Techniques	428
Clinical Course (1)	396	Follow-up Neurosonologic Findings (Day 29)	428
Questions to Answer by Ultrasound Techniques	396	Clinical Course (2)	429
Initial Neurosonologic Findings (Day 1)	396	Follow-up Neurosonologic Findings (3 Months)	429
Cranial CT and CT Angiography (Day 1)	397	Final Diagnosis	429
Clinical Course (2)	397	Discussion	437
Final Diagnosis	397	Case 31 Dissection of the Left Internal Carotid Artery C6 Segment	440
Discussion	399	Clinical Presentation	440
		Initial Neuroradiologic Findings	440
Case 27 Diffuse Cerebral Angiomatosis	402	Suspected Diagnosis	440
Clinical Presentation	402	Questions to Answer by Ultrasound Techniques	440
Initial Neuroradiologic Findings	402	Initial Neurosonologic Findings (Day 2)	440
Suspected Diagnosis	402	Follow-up Neuroradiologic Findings (Day 2)	440
Questions to Answer by Ultrasound Techniques	402		
Initial Neurosonologic Findings	402		

Clinical Course (1)	440	Final Diagnosis	474
Follow-up Neurosonologic Findings (Day 120)	440	Discussion	474
Follow-up Neuroradiologic Findings (Day 120)	442		
Clinical Course (2)	442	Case 36 Postpartum Angiopathy (Reversible Cerebral Vasoconstriction Syndrome)	476
Final Diagnosis	442	Clinical Presentation	476
Discussion	442	Initial Neuroradiologic Findings	476
		Conventional Angiography (Day 2)	476
Case 32 Right Temporal Hemorrhage in Pial Arteriovenous Malformation	444	Suspected Diagnosis	476
Clinical Presentation	444	Clinical Course (1)	476
Initial Neuroradiologic Findings	444	Questions to Answer by Ultrasound Techniques	476
Suspected Diagnosis	444	Initial Neurosonologic Findings (Day 5)	476
Questions to Answer by Ultrasound Techniques	444	Neuroradiologic Findings (Day 6)	478
Initial Neurosonologic Findings	444	Follow-up Neurosonologic Findings (Day 6)	478
MRI, MR Angiography, and Dynamic MR Angiography	444	Follow-up Neurosonologic Findings (Days 7–17)	478
Conventional Angiography	444	Clinical Course (2)	478
Clinical Course	446	Follow-up Neurosonologic Findings (6 Months)	479
Final Diagnosis	446	Final Diagnosis	479
Discussion	446	Discussion	479
Case 33 Subarachnoid Hemorrhage after Rupture of Left Supraorbital Internal Carotid Artery Aneurysm	448	Case 37 Left Anterior Choroidal Artery Infarction in Left Supraorbital Internal Carotid Artery Occlusion	483
Clinical Presentation	448	Clinical Presentation	483
Initial Neuroradiologic Findings	448	Initial Neuroradiologic Findings	483
Conventional Angiography	448	Suspected Diagnosis	483
Diagnosis	448	Questions to Answer by Ultrasound Techniques	483
Clinical Course (1)	448	Neurosonologic Findings (Day 3)	483
Questions to Answer by Ultrasound Techniques	448	Digital Subtraction Angiography (Day 5)	483
Initial Neurosonologic Findings (Day 2)	448	Clinical Course	487
Neurosonologic Findings (Day 3 to Day 5)	448	Final Diagnosis	487
Neurosonologic Findings (Day 6)	449	Discussion	487
CT (Day 6)	450		
Conventional Angiography (Day 9)	451	Case 38 Left-sided Amaurosis in Left Central Retinal Artery Occlusion	489
Neurosonologic Findings (Day 9)	451	Clinical Presentation	489
Neurosonologic Findings (Day 10 to Day 17)	452	Initial Neuroradiologic Findings	489
CT and CTA (Day 16)	452	Suspected Diagnosis	489
Neurosonologic Findings (Day 18 to Day 40)	454	Questions to Answer by Ultrasound Techniques	489
Clinical Course (2)	454	Initial Neurosonologic Findings	489
Discussion	454	Clinical Course (1)	489
		Follow-up Neuroradiologic Findings (Day 3)	489
		Clinical Course (2)	490
		Follow-up Neurosonologic Findings (3 Months)	490
		Final Diagnosis	490
		Discussion	490
Case 34 Right-sided Occipital Dural Arteriovenous Fistula	460	Case 39 Combined Chronic Right-sided Extracranial Internal Carotid Artery and Middle Cerebral Artery Occlusion	494
Clinical Presentation	460	Clinical Presentation	494
Initial Neuroradiologic Findings	460	Initial Neuroradiologic Findings	494
Suspected Diagnosis	460	Suspected Diagnosis	494
Questions to Answer by Ultrasound Techniques	460	Questions to Answer by Ultrasound Techniques	494
Initial Neurosonologic Findings	460	Neurosonologic Findings (Day 2)	494
Conventional Angiography	464	Clinical Course	495
Clinical Course (1)	464	Final Diagnosis	496
Clinical Course (2)	465	Discussion	496
Final Diagnosis	465		
Discussion	465	Case 40 Left Internal Carotid Artery Occlusion and Ipsilateral Arteriovenous Malformation in Inflammatory Bowel Disease	500
		Clinical Presentation	500
Case 35 Left Distal Vertebral Artery Occlusion and Right Vertebral Artery Hypoplasia with Retrograde Basilar Artery Flow	470	Initial Neuroradiologic Findings	500
Clinical Presentation	470		
Initial Neuroradiologic Findings	470		
Suspected Diagnosis	470		
Questions to Answer by Ultrasound Techniques	470		
Neurosonologic Findings (Day 3)	470		
Clinical Course	474		

Suspected Diagnosis	500	Follow-up Neurosonologic Findings over 4 Years	524
Questions to Answer by Ultrasound Techniques	500	Clinical Course	524
Initial Neurosonologic Findings	500	Neuroradiologic Findings	524
MRI, MR Angiography, and Dynamic MR		Neurosonologic Findings after Bone Marrow	
Angiography	502	Transplantation	524
Clinical Course	502	Discussion	525
Follow-up Neurosonologic Findings (10 Months)	502		
Final Diagnosis	506	Case 44 Transient Global Amnesia with Left	
Discussion	506	Hippocampal Diffusion-weighted Lesion	
		and Asymptomatic Right Middle Cerebral	
Case 41 Right Internal Carotid Artery as the		Artery Infarction in High-grade Right M1	
Remaining Patent Brain-supplying		Stenosis.	529
Artery	509	Clinical Presentation	529
Clinical Presentation	509	Initial Neuroradiologic Findings	529
Initial Neuroradiologic Findings	509	Suspected Diagnosis	529
Suspected Diagnosis	509	Questions to Answer by Ultrasound Techniques	529
Questions to Answer by Ultrasound Techniques	509	Initial Neurosonologic Findings (Day 1)	529
Neurosonologic Findings (Day 2)	509	Clinical Course	530
Clinical Course	512	Final Diagnosis	530
Final Diagnosis	515	Discussion	530
Discussion	515		
		Case 45 Bilateral Proximal Vertebral Artery	
Case 42 Left Internal Carotid Artery Aplasia as an		Stenosis and Bilateral Middle Cerebral	
Incidental Diagnosis in Optic Neuritis in		Artery Aneurysm	535
Lupus Erythematosus	517	Clinical Presentation	535
Clinical Presentation	517	Initial Neuroradiologic Findings	535
Suspected Diagnosis	517	Suspected Diagnosis	535
Initial Neuroradiologic Findings	517	Questions to Answer by Ultrasound Techniques	535
Questions to Answer by Ultrasound Techniques	517	Initial Neurosonologic Findings (Day 1)	535
Initial Neurosonologic Findings	517	Clinical Course (1)	535
Clinical Course	521	Follow-up Neurosonologic Findings	539
Final Diagnosis	521	MRI	539
Discussion	521	Clinical Course (2)	539
		Conventional Angiography	539
Case 43 Sickle Cell Disease	524	Follow-up Neurosonologic Findings	539
Clinical Presentation	524	Clinical Course (3)	539
Questions to Answer by Ultrasound	524	Final Diagnosis	539
Initial Neurosonologic Findings	524	Discussion	539
References			545
Index			599

Videos

Part A

Chapter 1

- Video A1.1** Ultrasound perfusion imaging of a healthy person
Video A1.2 Ultrasound perfusion imaging in old middle cerebral artery territorial infarction

Chapter 2

Extracranial arterial ultrasound anatomy

- Video A2.1** Common, internal, and external carotid arteries during tapping of the superficial temporal artery
Video A2.2 Common, internal, and external carotid arteries and superior thyroid artery
Video A2.3 External carotid artery and lingual artery during functional testing
Video A2.4 Superficial temporal artery and occipital artery
Video A2.5 Axillary artery and brachial artery during functional testing
Video A2.6 From the common carotid artery to the V2 segment of the vertebral artery
Video A2.7 Common carotid artery and vertebral artery
Video A2.8 From the V2 segment of the vertebral artery to the subclavian artery
Video A2.9 From the subclavian artery to the V3 segment of the vertebral artery

Intracranial arterial ultrasound anatomy

- Video A2.10** Application of echo-contrast agent to improve the temporal insonation quality
Video A2.11 Overview of arteries in the five axial insonation planes (transtemporal insonation)
Video A2.12 Overview of the five axial insonation planes (transtemporal insonation, fusion imaging with MRI)
Video A2.13 Overview of arteries in the five axial insonation planes (transtemporal insonation, fusion imaging with MRI)
Video A2.14 Overview of arteries in the anterior and posterior coronal planes (transtemporal insonation)
Video A2.15 Transtemporal axial insonation of the internal carotid artery (proximal and distal segments)
Video A2.16 Transtemporal coronal insonation focusing on the internal carotid artery, middle cerebral artery, and basilar artery (fusion imaging with MRI)
Video A2.17 Middle meningeal artery and C6 segment of the internal carotid artery
Video A2.18 Internal carotid artery siphon and ophthalmic artery at rest and during digital tapping of the bulb
Video A2.19 Ophthalmic artery
Video A2.20 Optic nerve sheath, central retinal artery and vein
Video A2.21 Midbrain plane (fusion imaging with MRI)
Video A2.22 Middle cerebral artery (from M1 to M3)
Video A2.23 Middle cerebral artery and posterior cerebral artery (fusion imaging with MRI)
Video A2.24 Internal carotid artery, middle cerebral artery, and anterior cerebral artery
Video A2.25 Early temporal M1 branch of the middle cerebral artery
Video A2.26 Anterior cerebral artery (from A1 to the pericallosal artery)
Video A2.27 V3 and V4 segments of the vertebral artery, cerebellar arteries (fusion imaging with MRI)
Video A2.28 V3 and V4 segments of the vertebral artery, posterior inferior cerebellar artery, basilar artery, anterior inferior cerebellar artery
Video A2.29 Vertebral artery, cerebellar arteries (posterior inferior, anterior inferior, superior), and basilar artery
Video A2.30 Vertebral artery V4 segment hypoplasia with mono- or biphasic flow signals
Video A2.31 Posterior cerebral artery, superior cerebellar artery, basilar artery
Video A2.32 Posterior cerebral artery and superior cerebellar artery during visual stimulation
Video A2.33 Posterior cerebral artery from P1 to P3, including the calcarine artery

- Video A2.34** Posterior cerebral artery and calcarine artery during visual stimulation
Video A2.35 Posterior communicating artery, posterior cerebral artery, and superior cerebellar artery with a normal posterior cerebral artery P1 segment, a hypoplastic P1 segment, or a bilateral fetal-type posterior cerebral artery
Video A2.36 M1 segment of the middle cerebral artery and P2 segment of the posterior cerebral artery during tapping of the extracranial internal carotid artery, vertebral artery, and eye bulb

Intracranial venous ultrasound anatomy

- Video A2.37** Overview of venous vessels in the transtemporal axial planes (fusion imaging with MRI)
Video A2.38 Deep middle cerebral vein
Video A2.39 Basal vein of Rosenthal and P2 segment of the posterior cerebral artery
Video A2.40 Basal vein of Rosenthal and its inflow to the vein of Galen and straight sinus
Video A2.41 Straight sinus with nonpathologic high flow velocity
Video A2.42 Transverse sinus, straight sinus, and intracranial arteries
Video A2.43 Transverse sinus at rest and during ipsi- and contralateral compression of the internal jugular vein
Video A2.44 Superior sagittal sinus
Video A2.45 Sphenoparietal sinus
Video A2.46 Superior petrosal sinus
Video A2.47 Inferior petrosal sinus

Extracranial venous ultrasound anatomy

- Video A2.48** Internal jugular vein and valve
Video A2.49 Thyrolinguofacial trunk
Video A2.50 Internal jugular vein at rest and during Valsalva maneuver with and without valve insufficiency
Video A2.51 Vertebral vein at rest and during compression of the internal jugular vein

Chapter 3

- Video A3.1** Normal cerebral circulation time on digital subtraction angiography and extracranial duplex ultrasound

Chapter 4

- Video A4.1** Microembolic signals in the middle cerebral artery in internal carotid artery disease and during patent foramen ovale testing

Chapter 5

- Video A5.1** Calcified plaque in the V0/V1 segment of the vertebral artery
Video A5.2 Internal carotid artery plaque with contrast enhancement
Video A5.3 Dissection of the proximal V2 segment of the vertebral artery with true and false lumen
Video A5.4 Dissection of the distal V1 segment of the vertebral artery with wall hematoma
Video A5.5 Common carotid artery dissection with wall hematoma, membrane, and false lumen
Video A5.6 Common carotid artery dissection with false lumen
Video A5.7 Musical murmurs in intracranial stenosis and in functional stenosis of the posterior communicating artery
Video A5.8 Acute thrombotic occlusion of the internal carotid artery
Video A5.9 Occlusion of the common carotid artery with secondary filling of the internal carotid artery via the external carotid artery
Video A5.10 Stenosis of the V2 segment of the vertebral artery
Video A5.11 Stenosis of the C6 segment of the internal carotid artery
Video A5.12 Stenosis of the proximal M2 segment of the middle cerebral artery
Video A5.13 Occlusion of the proximal M1 segment of the middle cerebral artery
Video A5.14 Occlusion of the distal M1 segment of the middle cerebral artery with stepwise flow velocity reduction
Video A5.15 Stenosis of a cortical branch of the posterior cerebral artery (occipitotemporal artery)
Video A5.16 Collaterals via the basilar artery, posterior cerebral artery, and ophthalmic artery in internal carotid artery occlusion
Video A5.17 Collaterals via the sphenoparietal sinus and via the straight sinus and transverse sinus in cerebral venous thrombosis

Part B

Case 1

- Video B1.1** High-grade stenosis of the internal carotid artery
- Video B1.2** Internal carotid artery plaque enhancement

Case 2

- Video B2.1** Free-floating thrombus of the internal carotid artery on day 1, B-mode
- Video B2.2** Free-floating thrombus of the internal carotid artery on day 1, color-mode
- Video B2.3** Internal carotid artery normalization after surgery on day 20

Case 3

- Video B3.1** Retrograde flow in the A1 segment of the anterior cerebral artery in common carotid artery occlusion
- Video B3.2** Mild poststenotic flow pattern in the M1 segment of the middle cerebral artery, retrograde flow in the A1 segment of the anterior cerebral artery, and functional stenosis of the anterior communicating artery

Case 4

- Video B4.1** Arteriovenous malformation and surrounding vessels
- Video B4.2** Posterior cerebral artery feeder and musical murmurs
- Video B4.3** Normal left and arterialized right basal vein of Rosenthal
- Video B4.4** Shortening of the cerebral circulation time

Case 6

- Video B6.1** Stenosis of the distal P2 segment of the posterior cerebral artery

Case 8

- Video B8.1** Stenosis of the V4 segment of the vertebral artery

Case 9

- Video B9.1** Steno-occlusive and collateral vessels in moyamoya disease

Case 10

- Video B10.1** Distal occlusion of the M1 segment of the middle cerebral artery with collateral flow via the A1 segment of the anterior cerebral artery before rt-PA therapy
- Video B10.2** Recanalization of the middle cerebral artery and normalization of the A1 segment of the anterior cerebral artery after rt-PA therapy

Case 11

- Video B11.1** Internal carotid artery dissection with prestenotic flow pattern on day 2
- Video B11.2** Poststenotic flow pattern in the middle cerebral artery and increased flow velocity in the posterior cerebral artery on day 2
- Video B11.3** Retrograde flow in the left ophthalmic artery and normal flow in the right ophthalmic artery on day 2
- Video B11.4** Improved internal carotid artery flow on day 7
- Video B11.5** Improved middle cerebral artery flow and decreased posterior cerebral artery collateral flow on day 7
- Video B11.6** Decreased retrograde flow in the left ophthalmic artery on day 7
- Video B11.7** Normalized internal carotid artery flow 6 months later
- Video B11.8** Normalized middle cerebral artery flow 6 months later

Case 14

- Video B14.1** Carotid siphon stenosis

Case 15

- Video B15.1** Stenosis of the left internal carotid artery and near-occlusion of the right internal carotid artery
- Video B15.2** Intracranial poststenotic flow pattern and collateral flow pathways

Case 17

Video B17.1 Normal right middle cerebral artery and occluded left middle cerebral artery with collateral flow via the anterior cerebral artery

Case 19

Video B19.1 Dissection of the distal right vertebral artery with a normal left vertebral artery and a high-resistance flow signal in the right V2 segment

Case 20

Video B20.1 Internal carotid artery dissection with high-resistance flow signal

Video B20.2 Marked poststenotic flow pattern in the M1 segment of the middle cerebral artery, retrograde flow in the A1 segment of the anterior cerebral artery, and functional stenosis of the anterior communicating artery

Case 22

Video B22.1 Mid-part occlusion of the M1 segment of the middle cerebral artery with a patent early temporal branch

Case 23

Video B23.1 Takayasu's arteritis with antegrade poststenotic flow in the left V2 segment of the vertebral artery and retrograde flow in the right V2 segment

Video B23.2 Bilateral poststenotic flow in the posterior cerebral artery, antegrade flow in the left V4 segment of the vertebral artery, and retrograde flow in the right V4 segment

Video B23.3 Normalized posterior cerebral artery flow after bypass surgery

Case 24

Video B24.1 Stenosis of the M1 segment of the middle cerebral artery

Video B24.2 Collateral flow via the anterior and posterior communicating arteries

Case 25

Video B25.1 Near-occlusion of the M1 segment of the middle cerebral artery with leptomeningeal collateral flow via the anterior cerebral artery

Video B25.2 Leptomeningeal collateral flow via the posterior cerebral artery

Case 26

Video B26.1 Dissecting aneurysm in the V2 segment of the vertebral artery

Case 28

Video B28.1 V2 segment of the vertebral artery with subclavian steal phenomenon Grade 2 at rest and Grade 3 after arm compression

Video B28.2 Internal carotid artery occlusion with collateral flow via the posterior communicating artery and poststenotic flow patterns in the middle cerebral artery and anterior cerebral artery

Case 29

Video B29.1 Increased venous flow in the collateral vessels in cerebral venous thrombosis

Case 30

Video B30.1 Stenosis of the left M1 segment of the middle cerebral artery and the left carotid siphon on day 20

Video B30.2 Stenosis of the right M1 segment of the middle cerebral artery with leptomeningeal collateral flow via the posterior cerebral artery on day 20

Video B30.3 Collateral flow via the left posterior communicating artery with poststenotic flow in the left middle and anterior cerebral arteries on day 29

Case 32

Video B32.1 Middle cerebral artery feeder and draining cortical veins in pial arteriovenous malformation

Case 35

Video B35.1 Retrograde filling of the basilar artery and the left V4 segment of the vertebral artery via a retrograde left P1 segment of the posterior cerebral artery in vertebral artery occlusion

Case 39

Video B39.1 Insonation of the deep middle cerebral vein with missing M1 segment in middle cerebral artery occlusion

Case 40

Video B40.1 Thrombotic occlusion of the internal carotid artery

Video B40.2 Shortening of the cerebral circulation time

Video B40.3 Arteriovenous malformation nidus

Video B40.4 Arteriovenous malformation nidus and draining veins on time-resolved dynamic magnetic resonance angiography

Case 41

Video B41.1 Collateral flow pathways and poststenotic flow patterns in one internal carotid artery as the remaining patent artery

Case 45

Video B45.1 Stenosis of the left proximal vertebral artery with secondary distal filling via external carotid artery collaterals

Video B45.2 Aneurysm of the M1 segment of the middle cerebral artery

Video B45.3 Poststenotic flow in the left V4 segment of the vertebral artery and PICA-ending-like flow in the right V4 segment

Abbreviations

ACA	anterior cerebral artery	CW	circle of Willis
AChA	anterior choroidal artery	DMCV	deep middle cerebral vein
ACoA	anterior communicating artery	DSA	digital subtraction angiography
ACV	anterior cerebral vein	DWI	diffusion weighted imaging
ADB	angiomatosis Divry–Van Bogaert	ECA	external carotid artery
ADC	apparent diffusion coefficient	ECAS	extracranial atherosclerosis
AICA	anterior inferior cerebellar artery	ECCG	electrocardiogram
ASA	atrial septal aneurysm	EC–IC	extracranial–intracranial
AT	acceleration time	EDV	end-diastolic velocity
ATA	anterior temporal artery	ESR	erythrocyte sedimentation rate
AVM	arteriovenous malformation	FFT	fast Fourier transform
AxA	axillary artery	FLAIR	fluid attenuated inversion recovery
BA	basilar artery	FMD	fibromuscular dysplasia
BCT	brachiocephalic trunk	FS	fat saturation
BFV	blood flow velocity	FT	fetal type
BHI	breath-holding index	FT-PCA	fetal-type posterior cerebral artery
BIF	bifurcation	GE	gradient echo
BP	blood pressure	GCA	giant cell arteritis
BrA	brachial artery	COGIF	Consensus on Grading Intracranial Flow Obstruction
BVF	blood volume flow	HITS	high-intensity transient signals
BVR	basal vein of Rosenthal	HSV	herpes simplex virus
BZI	border zone infarction	ICA	internal carotid artery
CA	calcarine artery	ICAS	intracranial atherosclerosis
CANCA	cytoplasmic antineutrophilic cytoplasmic antibody	ICH	intracranial hemorrhage
CAS	carotid artery stenting	ICP	intracranial pressure
CBF	cerebral blood flow	ICU	intensive care unit
CBV	cerebral blood volume	ICV	internal cerebral vein
cc	cervico-cranial	IJV	internal jugular vein
CCA	common carotid artery	IMT	intima-media thickness
CCT	cerebral circulation time; cranial computed tomography	IPH	intraparenchymal hemorrhage
ce	contrast-enhanced	IPS	inferior petrosal sinus
CEA	carotid endarterectomy	ISS	inferior sagittal sinus
CoS	confluence of sinuses	LDL	low-density lipoprotein
CPP	cerebral perfusion pressure	LI	Lindegaard Index
CRA	central retinal artery	LMC	leptomeningeal collateral
CRAO	central retinal artery occlusion	LSA	lenticulostriate artery
CS	cavernous sinus	MAP	mean arterial pressure
CSF	cerebrospinal fluid	MCA	middle cerebral artery
CT	computed tomography	MES	microembolic signal
CTA	computed tomographic angiography	MI	mechanical index
CVR	cerebrovascular reactivity	MIP	maximal intensity projection
CVT	cerebral venous thrombosis	MMA	middle meningeal artery
		MMD	moyamoya disease

MRA	magnetic resonance angiography	SOV	superior ophthalmic vein
MRI	magnetic resonance imaging	SPECT	single photon emission computed tomography
MRV	magnetic resonance venography	SpPS	sphenoparietal sinus
MSCT	multislice CT	SPS	superior petrosal sinus
MSCTA	multislice CTA	SSP	subclavian steal phenomenon
MTT	mean transit time	SSS	superior sagittal sinus
NIHSS	National Institutes of Health Stroke Scale	STeA	superficial temporal artery
OA	ophthalmic artery	StS	straight sinus
OccA	occipital artery	SWS	Sturge–Weber syndrome
OTA	occipitotemporal artery	TAV	time-averaged velocity
PC	phase-contrast	TCCS	transcranial color-coded duplex sonography
PCA	posterior cerebral artery	TCD	transcranial Doppler
PCoA	posterior communicating artery	TEE	transesophageal echocardiography
PET	positron emission tomography	TGA	transient global amnesia
PFO	patent foramen oval	TIA	transient ischemic attack
PI	pulsatility index	TIBI	Thrombolysis In Brain Ischemia grading system
PICA	posterior inferior cerebellar artery	TICA	terminal intracranial carotid artery
POA	parietooccipital artery	TOF	time-of-flight
PRF	pulse repetition frequency	TS	transverse sinus
PSV	peak systolic velocity	TTE	transthoracic echocardiography
PTA	percutaneous transfemoral angioplasty	UFI	ultrasound fusion imaging
PTT	partial thromboplastin time	VA	vertebral artery
RI	resistance index	VG	vein of Galen
RLS	right-to-left shunt	VMR	vasomotor reactivity
rt-PA	recombinant tissue plasminogen activator	VV	vertebral vein
SA	subclavian artery	WG	Wegener granulomatosis
SAH	subarachnoid hemorrhage	WMS	Wyburn–Mason syndrome
SCA	superior cerebellar artery	WUS	wake-up stroke
SCD	sickle cell disease		
SCOI	small centrum ovale infarction		
SiS	sigmoid sinus		
SLE	systemic lupus erythematosus		

Part A Principles and Rules

1	Flow and Ultrasound Basics	2
2	Vascular Anatomy and Structure of Ultrasound Examination	18
3	Intracranial Hemodynamics and Functional Tests	79
4	Pathogenesis of Stroke	90
5	Vascular Pathology.	106
6	Angiographic Techniques in Neuroradiology.	183

1

Flow and Ultrasound Basics

Flow Dynamics	2	Imaging Modalities, Parameters, and Settings	8
Physics of Flow	2	Imaging Modalities	8
Flow Pattern and Flow Velocity	2	Parameters and Settings	12
Ultrasound Principles	3	Artifacts	15
Doppler Effect	3	Artifacts in Gray-scale Imaging	15
Doppler Shift and Flow Velocity	4	Refraction and Mirror Artifacts	16
Ultrasound Systems	6	Artifacts in Color-mode Imaging	17
Ultrasound Transducer	7	Artifacts in Doppler Spectrum Analysis	17
		Safety Considerations	17

Flow Dynamics

Physics of Flow

The flow of a liquid substance in a tubular system can be described by the following physical rules. According to the Hagen–Poiseuille law, flow velocity in a straight tube depends on the pressure gradient (ΔP), the vessel radius (r) and the vessel length (l) (Fig. A1.1). This function, in general, also applies to the human vascular system, in which pressure is generated by the pump function of the heart. However, the

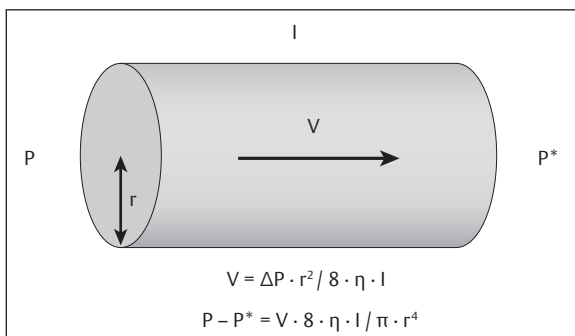


Fig. A1.1 The Hagen–Poiseuille law. V = mean velocity; $P - P^* = \Delta P$ = pressure gradient; l = vessel length; r = vessel radius, η = dynamic fluid viscosity.

pressure gradient is difficult to assess accurately because the diameter of the blood vessels in the system varies and vessels rarely follow a straight path. This restricts the direct application of the Hagen–Poiseuille law in clinical practice.

Flow Pattern and Flow Velocity

Flow in a vessel system can be linear or turbulent depending on the vessel size and flow velocity (Fig. A1.2, Fig. A1.3, Fig. A1.4). The example in Fig. A1.2 shows the



Fig. A1.2 The pattern of flow of water in the Colorado river as it flows through the Grand Canyon (Colorado, USA). Note the normal, calm flow in the wider segments of the river and the increase in flow and turbulence in the narrow segment. (Reproduced from Google Earth, Mount View, USA.)

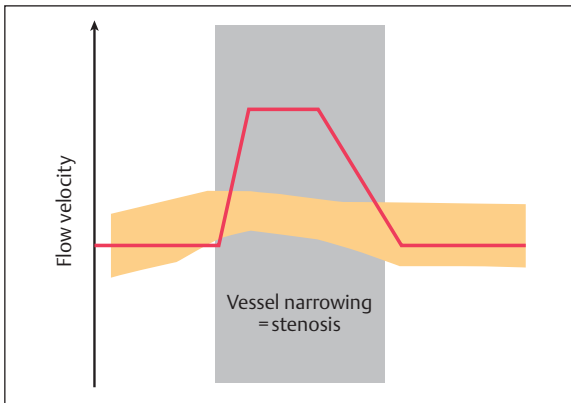


Fig. A1.3 Schematic of the changes in flow velocity around and within a vessel narrowing: Normal initial flow velocity, increased velocity within the stenosis and normalized flow afterward.

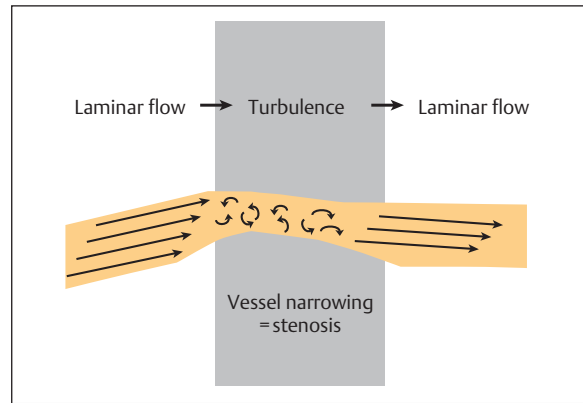


Fig. A1.4 Schematic of the flow pattern around and within a vessel narrowing: Initial laminar flow changing to turbulent flow within the stenosis and within a short segment distal to the narrowing, followed again by a normal laminar flow.

water flow in a segment of the Colorado river as it flows through the Grand Canyon (Colorado, USA). The width of the river changes, from a relatively wide stretch with calm flow to a narrow section where cataracts can be seen. The river then widens again and the flow becomes calmer. Within the calm areas the water flow is steady but flow velocity increases noticeably within the narrowing, i.e., within the stenosis (**Fig. A1.3**). Flow in the wider segments of the river is laminar, but it becomes turbulent within the narrowed areas (**Fig. A1.4**). Similarly, in the human vasculature flow velocity increases in any case of vessel narrowing. In addition, this phenomenon can be observed in vessel segments with a raised pressure gradient, i.e., hyperperfusion within a normal-sized vessel. If flow velocity reaches a certain magnitude, it changes from laminar to turbulent. This is why turbulent flow is an ultrasound criterion always searched for in suspected vessel stenosis. However, turbulence can also be seen over varying lengths distally adjacent to a stenosis, in regions with vessel elongation, kinking, or hyperperfusion, which may limit its diagnostic value.

Ultrasound Principles

Doppler Effect

Diagnostic ultrasound enables the visualization and measurement of the phenomenon of flow dynamics. Ultrasound is generated by oscillating piezoelectric elements, emitting frequencies in the nonaudible range between 20 kHz and 1 GHz (Hz = Hertz = number of oscillations per second). This frequency travels through body tissues in the form of a wave. While traveling through tissue at a speed of ~1,500 m/s, the wave is reflected by various structures which may be resting (tissue) or moving (blood cells, mainly erythrocytes). The reflected wave is then analyzed. When there is a frequency shift between the emitted and received frequency, a “Doppler effect” has occurred, named after the Austrian physicist Christian A. Doppler (**Fig. A1.5**).



Fig. A1.5 Christian A. Doppler (1803–1853).

The Doppler effect can easily be explained using audible sound. Consider a tuning fork emitting sound with a frequency of $A = 440$ Hz (**Fig. A1.6**). This frequency travels through air with the speed of sound (330 m/s) toward an observer, who can hear exactly the same frequency of 440 Hz. However, if the observer rides a bicycle at a speed of 18 km/h (5 m/s) toward the tuning fork his speed would lead to the subjective experience of a higher frequency, i.e., 447 Hz in our example.

The human auditory system (**Fig. A1.7**) is able to recognize a Doppler shift of audible frequencies. A familiar example is that when an emergency ambulance passes us in the street we hear characteristic changes in the received sound pitch of its sirens. All ultrasound systems are constructed to a pattern which resembles the human hearing system (**Fig. A1.8**). The difference between emitted and received frequencies (Doppler shift) is caused by the reflection of ultrasound by various moving reflectors—the corpuscular blood components.

The received frequency is amplified (corresponding to the function of the tympanic membrane and

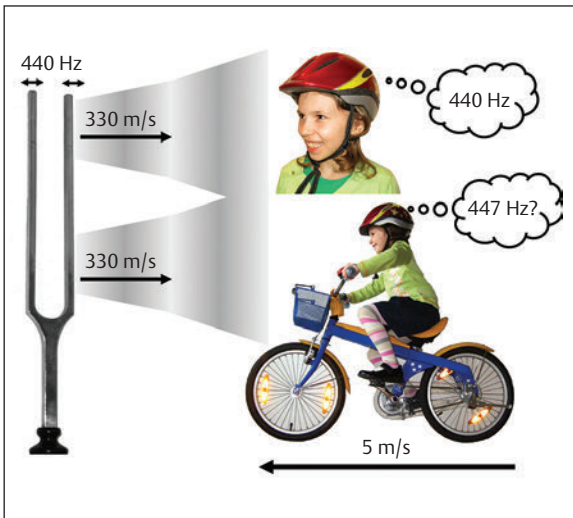


Fig. A1.6 Example of the Doppler effect occurring within the range of the audible sound. An observer evaluates the sound emitted by a tuning fork. **Top:** The observer stands still. The emitted frequency is identical to the received frequency. **Bottom:** The observer is moving toward the acoustic source, therefore passing more quickly through the sound waves, resulting in a subjectively higher received frequency.

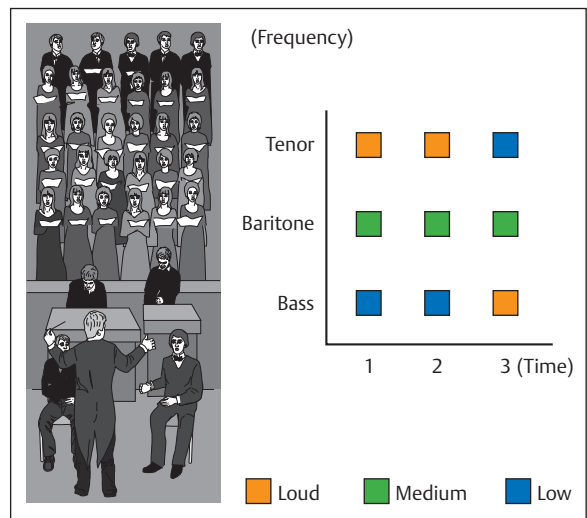


Fig. A1.9 Explanation of Fourier analysis, using a choir as an example. A frequency analysis is performed over time. At defined time points the song is analyzed and documented in colored boxes according to the active singers (= frequencies) and to the strength at which they sing, i.e., point 1 depicts the moment when the tenor is loudest, the baritone sings at moderate volume, and the bass has the weakest sound.

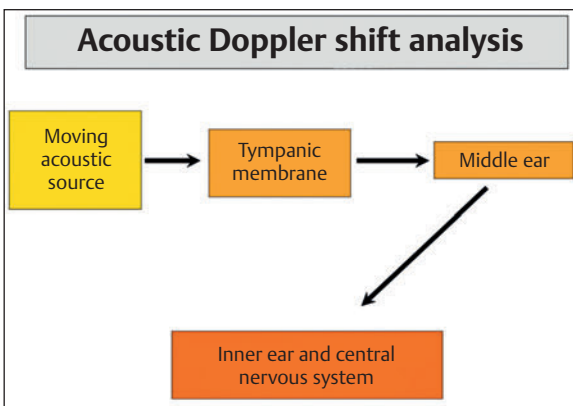


Fig. A1.7 Schematic of the human auditory apparatus and its ability to detect a frequency shift of a moving acoustic source.

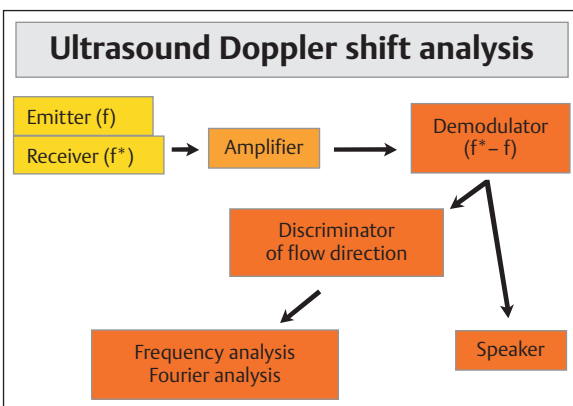


Fig. A1.8 Schematic demonstrating the analogy of a diagnostic ultrasound machine to the human auditory system.

ossicles). A demodulator subtracts the received from the emitted frequency ($f^* - f$) which is then directly sent to a speaker, as the Doppler shift is within the audible kHz range of the human ear. In addition, flow direction is determined, depending on whether $f^* - f$ is positive or negative. Finally, the received frequency spectrum is processed by Fourier analysis. This calculation can be explained by the following example: An observer is asked to analyze the male voices of a choir. At time points 1, 2, and 3 seconds, he is asked to mark on a diagram how loud he can hear the tenor, baritone, and bass. At time points 1 and 2, the tenor is the loudest, the baritone is moderately loud, and the bass is the quietest. At time point 3, the tenor is silent while the bass is loudest (**Fig. A1.9**). Applying this to Doppler frequencies, a large Doppler shift translates into high flow velocity and a small Doppler shift translates into a low flow velocity, while the volume depends on the number of reflectors moving with a given flow velocity. In our example (**Fig. A1.10**), most erythrocytes are flowing fast, a moderate number are slower, and a small number are very slow, which is usually the case in regions with a laminar flow pattern.

Extension of frequency step numbers of time points per second leads to a typical Doppler spectrum (**Fig. A1.11**). The exact number of frequency steps varies from 64 to 256 depending on the Doppler or duplex ultrasound system being used.

Doppler Shift and Flow Velocity

To convert the Doppler shift (measured as a frequency in kHz) into flow velocities (cm/s or m/s), the Doppler formula needs to be applied (**Equation A1.1**). As the formula includes the cosine of the insonation angle, exact flow

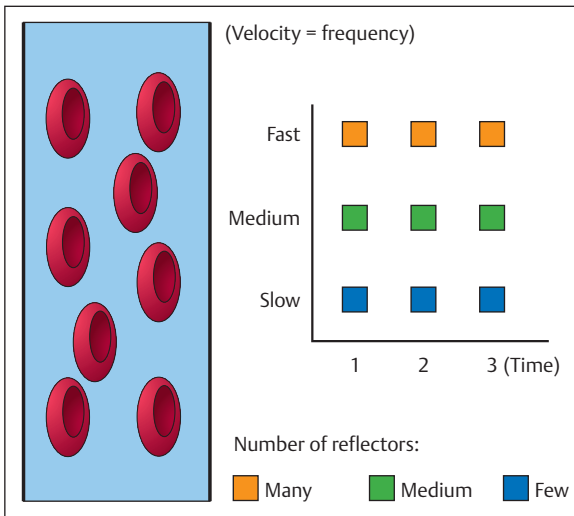


Fig. A1.10 Fourier analysis of ultrasound-generated Doppler signals: Transferring the example of the choir to blood flow analysis. The detected frequencies now resemble the detected Doppler shift, the amplification from the number of reflectors generating an equal Doppler shift.

$$v = \frac{c(f^* - f)}{2f \cos \alpha}$$

$\alpha < 20^\circ$

$$v = \frac{c(f^* - f)}{2f}$$

v	=	Flow velocity
c	=	Velocity of sound within the tissue
f	=	Emitted frequency
f^*	=	Received frequency
$f - f^*$	=	Doppler shift
α	=	Insonation angle
\cos	=	Cosine

Equation A1.1

velocity can only be calculated if the ultrasound beam is directly in line with the direction of blood flow in the vessel segment being analyzed (cosine of 0° insonation angle = 1). Therefore, whenever the insonation angle is greater than 0° the calculated velocity will be “false low.” As blood vessels hardly ever point directly toward the ultrasound transducer, an acceptable flow velocity can only be calculated if the insonation angle is less than 30° (error from real Doppler shift is $\leq 13\%$) or if the insonation angle is known and corrected for (Fig. A1.12). Every duplex ultrasound system offers the feature of angle correction, which is easily achieved by adjusting a flow-line-symbol visualized within the sample volume. For correct measurements, the sample volume needs to be in the center of flow and not too close to the edges of the visible vessel. The flow-line then needs to be adjusted in line with the blood flow or flow-jet seen in the color mode (see also Fig. A5.54). Most ultrasound systems offer the option to correct for angles from 0° to more than 70° , but a correction of more than 60° will result in additional system-dependent errors (falsely high velocities)

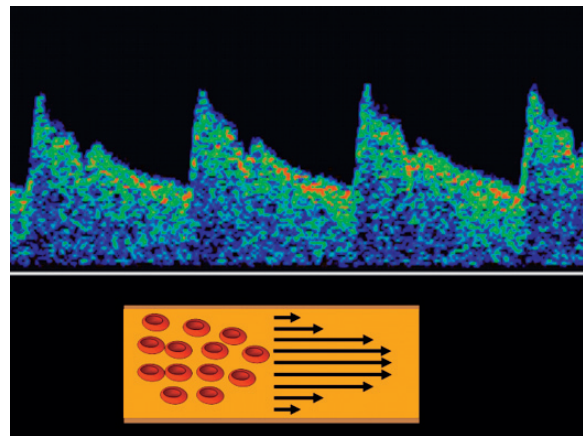


Fig. A1.11 Top: Doppler spectrum of a transcranial (TCD) ultrasound system. Note the “systolic window,” i.e., in laminar flow most erythrocytes are fast flowing, therefore the highest intensities (orange colored) are close to the highest flow velocities. Intensity near the zero line is low as only few erythrocytes are slow. **Bottom:** Blood vessel with schematic laminar flow lines, fastest erythrocytes (and high number) in the vessel middle, slowest erythrocytes (and low number) near the vessel wall.

that can be as high as 40% (Daigle et al 1990, Steinman et al 2005). Therefore, it is usually recommended not to correct for more than 60° to avoid inaccurate flow velocity measurements (Fig. A1.13). In general, it is desirable to apply angle correction for all vessels to minimize angle-dependent errors of velocity measurement. However, to avoid introducing additional errors or increasing inter- and intraobserver variability, angle correction is usually recommended in straight vessel segments that are visible over at least 1.5 cm of length (Giller 1994). Extracranially, this criterion is mostly fulfilled and therefore angle correction is an accepted and required part of every velocity measurement. This does not apply to intracranial insonation, however, as most vessel segments are tortuous, thus impeding exact angle correction (Fig. A1.14). Consequently, recommendations in the literature for transcranial color-coded duplex sonography (TCCS) vary from “correction” via “fixed correction” to “no correction.” For the above reasons, we do not recommend routine angle correction in TCCS examinations but registering the highest measurable velocity instead. In case of a specific question, for instance in unclear side-to-side velocity differences, it may be helpful to apply angle correction if the sample volume can be positioned in a satisfactory long vessel segment of at least 1 cm aligned with the direction of the vessel in the color-mode image (Nedelmann et al 2009b).

The reflected ultrasound waves contain a spectrum of frequencies. From these, several diagnostically relevant hemodynamic and blood flow parameters are generally calculated automatically by modern ultrasound machines, provided that a correct envelope curve has been fitted (Fig. A1.15) (for further details about hemodynamic parameters, see also Chapter 3, “Parameters of Cerebral Hemodynamics”).

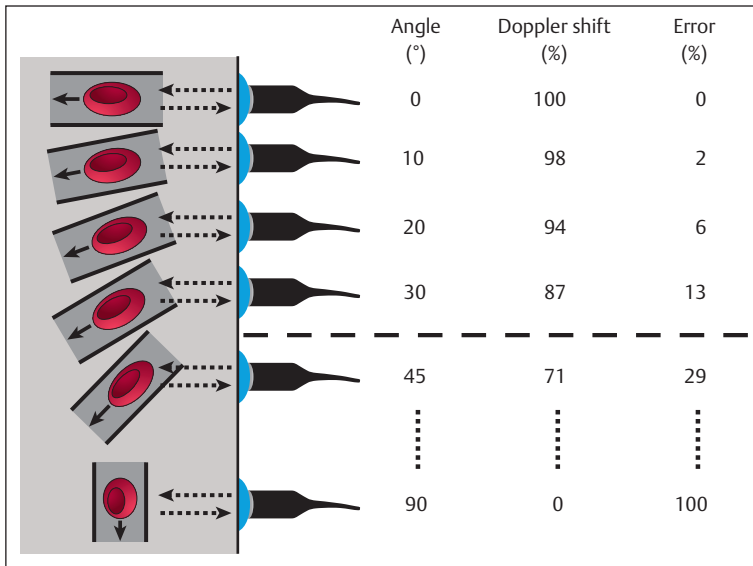


Fig. A1.12 Relation of insonation angle and error in Doppler shift determination.

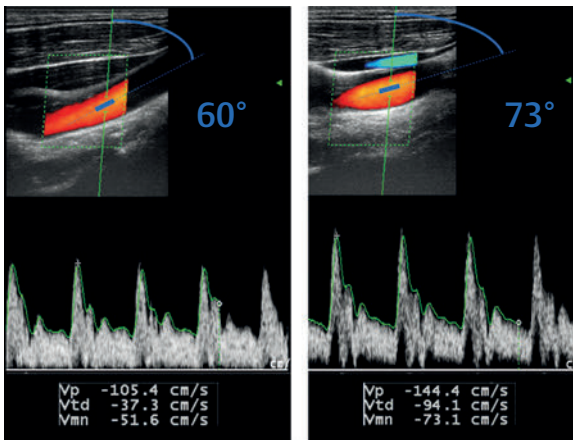


Fig. A1.13 Duplex ultrasound of the CCA, longitudinal plane. Identical vessel segments but different angulation of the ultrasound probe at the neck, subsequently requiring two different angle corrections (blue bar): 60° and 73°. The former leads to a correct flow velocity of 105 cm/s, the latter to a system-related false high velocity of 144 cm/s.

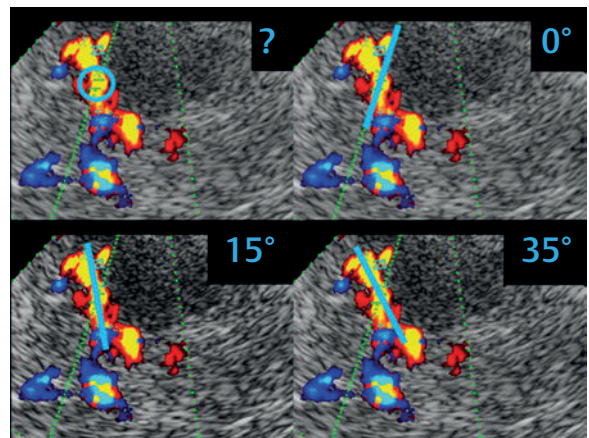


Fig. A1.14 Dilemma of exact angle correction in curved vessel segments. The blue circle (top left) indicates the segment of interest. Which angle correction would you choose: 0° (top right), 15° (bottom left), or 35° (bottom right)? Exact angle correction is not possible in short, curved vessel segments.

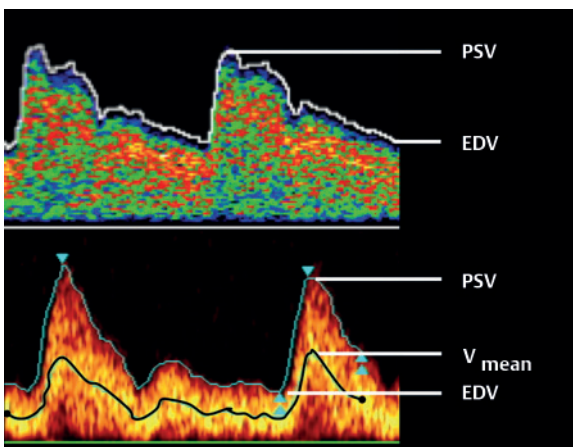


Fig. A1.15 Hemodynamic parameters derived from Doppler spectrum analysis. **Top:** TCD system. **Bottom:** Duplex ultrasound system. PSV = peak systolic velocity; EDV = end diastolic velocity; $V_{mean} = TAV_{mean}$ = intensity-weighted mean velocity.

Ultrasound Systems

This section focuses on the characteristics and function of duplex ultrasound systems. The use of these systems for routine vascular diagnostics, particularly for determination of stenoses and occlusion, is the current standard for extracranial examinations and is the foreseeable standard for intracranial assessment. With systems becoming smaller and lighter, this applies not only to assessments in the ultrasound laboratory but also to assessments of patients in intensive care units. Pure Doppler ultrasound is being modified to perform functional tests. The majority of ultrasound diagnostics in the cases presented in this book are derived from duplex ultrasound. If data are derived from Doppler systems, the particular specifications are discussed. In general, the same basic principles are applied in Doppler and duplex systems, and system settings can be adjusted in a similar manner.

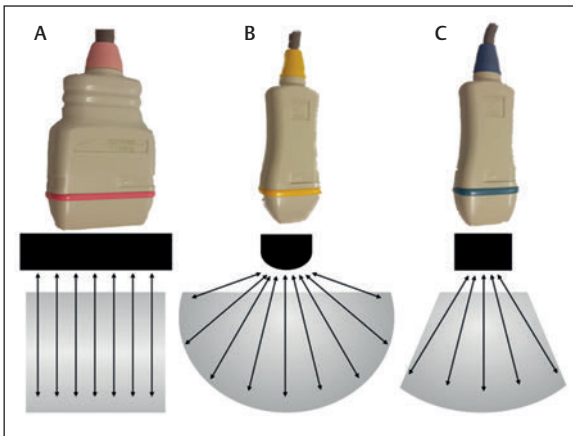


Fig. A1.16 Examples of the three transducer types and frequencies often used for insonation of the vessels supplying the brain. (A) Linear transducer, frequency range 5–18 MHz, for extracranial insonation; (B) Sector transducer, frequency range 4–8 MHz, for extracranial insonation; (C) Trapezoid transducer, 1–3 MHz, for transcranial insonation.

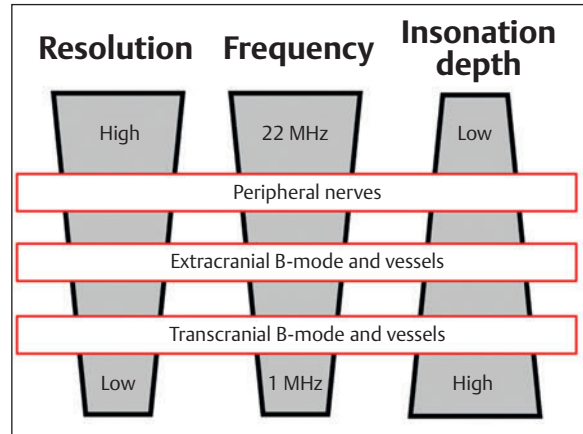


Fig. A1.17 Schematic visualization of the relationship between insonation frequency, achievable spatial resolution, and possible insonation depth. Usually, for each region of interest a compromise between the three variables has to be used.

Ultrasound Transducer

The transducer combines the emission of ultrasound waves into the tissue and the simultaneous registration of reflected ultrasound in quick succession to the emitted impulse. Duplex ultrasound transducers contain a series of piezoelectric elements working simultaneously. When exposed to an alternating voltage, these crystals start to vibrate and therefore emit mechanical waves into the surrounding tissues. This also works in reverse, enabling the detection of mechanical—i.e., ultrasound—waves, and their conversion into electrical current. More than 500 piezoelectric elements may be integrated into current modern transducers. Their configuration on the probe varies and determines the appearance of the image. Three main types of transducer configuration are usually used for insonation of the extra- and intracranial arteries and veins (**Fig. A1.16**). For extracranial insonation, high-frequency transducers with a frequency range between 5 MHz and 18 MHz and a linear or sector ultrasound beam configuration are used. The higher the frequency the higher the achievable spatial resolution, but the lower the potential insonation depth (**Fig. A1.17** and **Fig. A1.18**).

The linear transducer has the advantage of providing undistorted images with high spatial resolution, but it requires a large contact surface. For extracranial insonation, this is generally not a problem, so that linear probes are most frequently used. The high-frequency sector transducer has the advantage of providing images from a wider fan-shaped range but causes image distortion. For transcranial insonation, lower frequencies in the range of 1–3 MHz are required to permit transmission and reception of sound through the bones of the skull. However, this is limited to regions of the skull where the bone is naturally thin, i.e., a “bone window” is present (for further details, see also Chapter 2, “Intracranial Arteries” under “Special Arterial Anatomy and Ultrasound Anatomy,” and **Fig. A2.45**). Using a linear transducer for transcranial insonation would result in small, narrow images, whereas the trapezoidal ultrasound field produced by a sector transducer allows insonation with

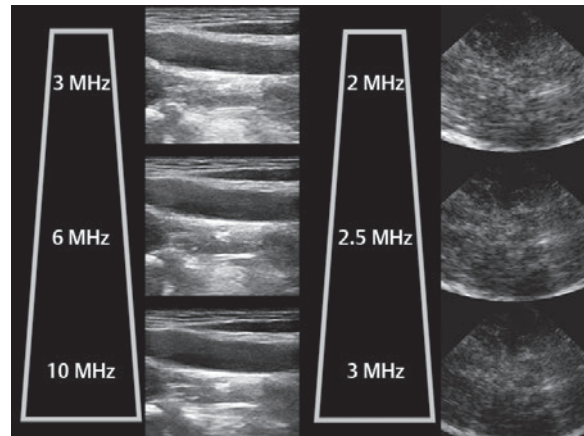


Fig. A1.18 **Left:** extracranial duplex sonography, longitudinal plane. **Right:** Transcranial duplex, axial insonation, midbrain plane. Example images acquired with one extracranial and transcranial probe adjusted to different insonation frequencies. **Note:** the lower the insonation frequency the brighter the image, but this is accompanied by a loss in spatial resolution.

maximum image information even through a small bone window (**Fig. A1.16**).

The ultrasound fields of all transducer types are focused by the spatial arrangement of the piezoelectric elements on the surface of the transducer, by electronic control, or both. The ultrasound field can be divided into a near field and a far field. The transitional area between the two is the focal zone with the best lateral spatial image resolution, i.e., the ability to distinguish two objects that are adjacent to one another within the same insonation depth. A typical 2-MHz probe achieves a lateral resolution of up to 3 mm, a 15-MHz probe of up to 0.4 mm (David et al 2000). Modern ultrasound systems allow calculation of two or more focus zones simultaneously (**Fig. A1.19**). The localization of the focus zone can be adjusted in all duplex ultrasound systems and should always be optimized according to the insonated region of interest.

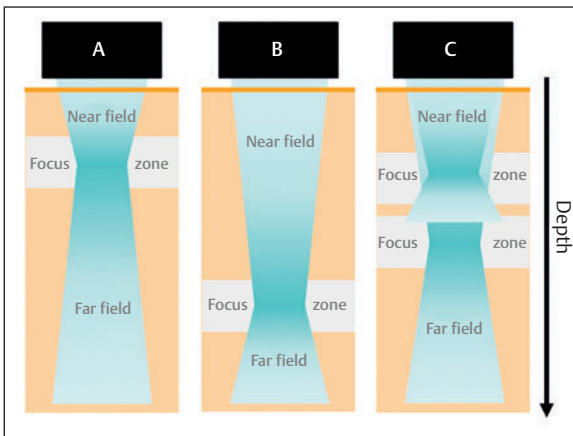


Fig. A1.19 Schematic of focused ultrasound fields with near field, far field, and the focus zone. For image optimization, the focus can be adjusted in most duplex ultrasound systems. (A) Focus adjustment for small insonation depth; (B) Focus adjustment for high insonation depth; (C) Parallel use of multiple focus zones.

The axial resolution along the ultrasound beam—i.e., the ability to distinguish two objects along the ultrasound beam—depends on the insonation frequency and the length and form of the ultrasound pulse wave (see below). The higher the frequency and the shorter the pulses, the higher the axial resolution. A typical 2-MHz probe achieves an axial resolution of up to 0.8 mm, a 15-MHz probe of up to 0.15 mm (David et al 2000).

The mode in which the piezoelectric element operates in all duplex transducers is a pulsed emission of waves (pulsed-wave [PW] mode), which enables the system to determine the insonation depth from which the signal is being reflected. Pure Doppler ultrasound systems may alternatively be switched to the continuous-wave mode, where a minimum of two piezoelectric elements work simultaneously. One of these constantly emits ultrasound while the other constantly receives the reflected waves. The disadvantage of the continuous-wave mode is the lack of information regarding the depth from which a signal is derived. In duplex ultrasound systems, this simple mode is not used.

Imaging Modalities, Parameters, and Settings

Imaging Modalities

Brightness-mode Imaging

The brightness mode (B-mode) permits two-dimensional visualization of tissue and is based on ultrasound signals being reflected from the insonated structures. The resulting image is a compound of information from the parallel connected piezoelectric elements of the ultrasound transducer. The reflected amplitudes along each single ultrasound beam (A-mode data) are gray-scale coded, and within the image, arranged according to their reflection depth (**Fig. A1.20**). The sum of all adjacent ultrasound beams adds up to the final B-mode image.

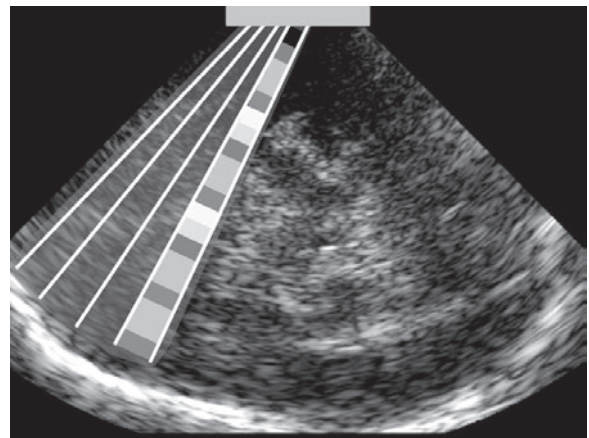


Fig. A1.20 B-mode imaging: Transcranial insonation. The image is derived from the analysis of the echo reflection pattern along several ultrasound beams, allocated to the corresponding insonation depth. The brightness within the image corresponds to the strength of the received echo, hence the term *brightness mode*.

Color-mode Imaging

While B-mode images are focusing on tissue properties, the color mode analyses blood flow. Based on the Doppler shift principle, regions with a detectable blood flow are color-coded within all or part of the B-mode image depending on the size of the color box chosen (**Fig. A1.21**). In the velocity mode, the direction toward or away from the probe is coded with a color. The brightness of the color increases, or the color changes, with increasing flow velocity. Further information that may be gained from the color-mode signal is the recognition of turbulence (aliasing)—routinely looked for during extracranial insonation. All ultrasound images of extra- and intracranial blood vessels in this book have been obtained using this insonation mode.

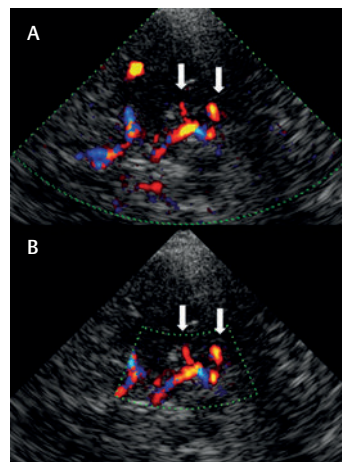


Fig. A1.21 Relation of color box size and color image quality. (A) Example of a large color box in intracranial transtemporal duplex ultrasound. (B) Adapted small color box, resulting in improved imaging of at least one proximal PCA branch (arrows).

In most ultrasound systems flow toward the probe is coded red and flow away from the probe coded blue, as can be seen on all transcranial insonation images. Extracranially, in most ultrasound laboratories, the color of brain-supplying arteries is set to red, despite their flow away from the probe, and the color of the veins to blue, despite their flow toward the probe. Another potential point of confusion is the definition of cranial and caudal or anterior and posterior positions on the monitor. In our laboratory the orientation is adjusted according to the flow direction as follows: In the extracranial longitudinal examination the proximal vessel segments are on the right and the distal segments on the left side of the monitor screen. In the transverse examination the lateral parts are positioned on the right side of the screen during the right-sided examination and on the left side during the left-sided examination. In the transcranial axial examination the anterior parts are on the left and the posterior parts on the right side. In the coronal examination the distal vessel segments are allocated to the left side of the screen, the proximal segments to the right side.

The sensitivity of detection of a flow signal within the color box depends on several factors: the chosen pulse repetition frequency (PRF) and gain (see following paragraphs) but also on the size of the color box, which can be adjusted manually. The smaller the box, the better the resolution and sensitivity; the larger the box, the lower the image quality and the lower the system's image frame rates. To optimize imaging while avoid misinterpretation of findings an adjusted color box should be used, sufficient to give a good overview to the area of interest. If there are difficulties with depiction of color signals, a reduction in the size of the color box can help (Fig. A1.21).

Power-mode Imaging

Power-mode imaging is another option to visualize blood flow. Here, the signal is not derived from the Doppler frequency (Fig. A1.22A) but from changes in Doppler amplitude, i.e., intensity of the reflected signal. This result in angle-independent registration of flow while the flow direction is not coded (Fig. A1.22B). The mode is more flow sensitive than the color velocity mode, as persistence and higher amplification can be used. In particular, it may facilitate the detection of low-flow signals—from venous vessels or small arteries, for example. However, the mode is susceptible to artifacts caused by movement of the patient or the insonated tissue, and in our experience it is only relevant for intracranial and not extracranial insonation. Some ultrasound systems permit a technical combination of the above modes resulting in a color-coded power mode (Fig. A1.22C). Most of the transcranial ultrasound images in this book have been obtained using this combined insonation mode.

B-flow Imaging

The B-flow technique is a method of analyzing flow without using Doppler shift information (Umemura and Yamada 2001). Two or more impulses are sent into the tissue under study and the returning echo amplitudes are subtracted. For tissues without movements between the pulses, the subtraction leads to erasure of signals

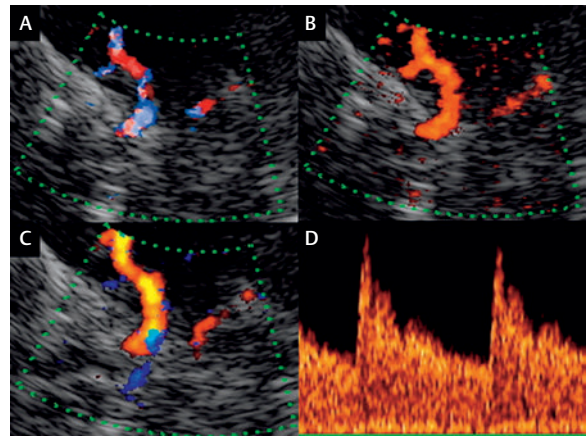


Fig. A1.22 TCCS, transtemporal bone window, axial midbrain plane. (A) Color-mode image, mainly of the MCA. (B) Power-mode image of the same region. (C) Combined color- and power-mode. (D) Doppler spectrum analysis of blood flow in the M1-MCA segment.

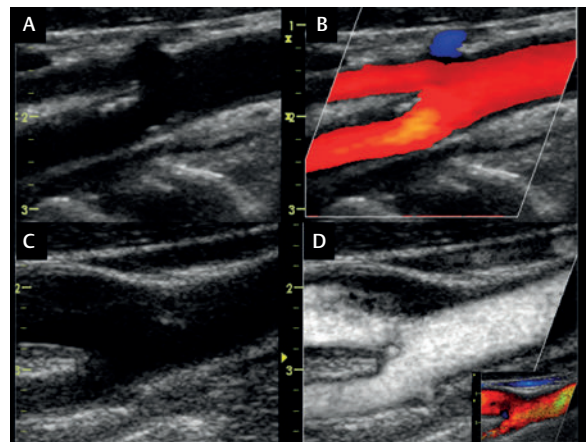


Fig. A1.23 Extracranial duplex ultrasound, longitudinal plane. (A,B) B-mode image and corresponding color-mode signal of a carotid bifurcation. (C,D) B-mode image and corresponding B-flow signal of a carotid bulb—which can improve visualization and can also be color-coded by the ultrasound system. (Images with kind permission by Dr. W. Sanad, Dept. of Cardiology, Charité—Universitätsmedizin Berlin, Germany.)

while moving reflectors lead to a measurable signal difference, which is then displayed as a gray-scale image. Advantages of the method are rapid image generation, higher spatial resolution, and no blooming artifact (frequently seen in color-mode imaging). This facilitates the delineation of the plaque surface in extracranial ultrasound imaging. In transcranial insonation, where aliasing and blooming artifacts may be rather helpful and are purposely used for vessel identification, the signal yield of the B-flow technique is often lower compared with the other color modes (Fig. A1.23).

Doppler Spectrum Analysis

For a detailed description of Doppler spectrum analysis see Chapter 3, “Parameters of Cerebral Hemodynamics.” In addition to the information gathered by the color mode, a sample volume (see below under “Parameters

and Settings”) can be placed along a single ultrasound beam and velocities, velocity distribution, and pulsatility indices (PI) can be analyzed. Most modern duplex ultrasound systems permit simultaneous online registration of the B-mode image, color-mode image, and the Doppler spectrum analysis—called the triplex mode. This is particularly helpful and timesaving when analyzing tortuous or oblique vessel courses, particularly of the intracranial arterial system. Depending on the ultrasound system, the triplex mode might result in reduced color-mode quality, so when choosing the individual optimal system setting, a reduced Doppler PRF (see “Pulse Repetition Frequency, Insonation Depth, and the Aliasing Phenomenon” below) may have to be considered.

Ultrasound Fusion Imaging

Ultrasound fusion imaging (UFI) is a technical approach that has only recently become available for use in clinical settings. UFI allows online transcranial or extracranial ultrasound analysis in freely selectable insonation planes with simultaneous visualization of corresponding pre-registered CT or MR datasets. During an ultrasound examination, the system provides an exact matched image slice of the second image modality which adapts instantly and online to any movement of the ultrasound probe. For study initiation, the radiologic DICOM datasets are recalculated by the ultrasound system into a three-dimensional dataset, in which external marker points (e.g., eye, ear, nose for TCCS) can manually be defined. During the matching process and actual ultrasound analysis, the patient needs to be positioned within an electromagnetic field continuously emitted by an antenna aimed toward the study region. In addition, a small electromagnetic field sensor is fixed to the patient and remains in place until the end of the study: this acts as a motion control sensor that allows the system to make online corrections for any movement of the patient. A second electromagnetic field sensor is first used to match the predefined CT/MRI marker points with the corresponding surface points of the studied patient. When matching is confirmed, the sensor is then attached to the standard TCCS insonation probe of the ultrasound system and the study can be started (Fig. A1.24, Fig. A1.25).

The technique is promising for teaching purposes (identification of insonation planes in comparison with CT or MRI) but also in clinical conditions with initial radiologic imaging that require frequent or bedside follow-up studies, such as subdural hematoma or intracranial mass hemorrhage, or even for intraoperative surgical guidance (Prada et al 2015, Schreiber et al 2014c). For further reading, see “Intracranial Arteries” under “Special Arterial Anatomy and Ultrasound Anatomy” in Chapter 2.

Tissue Harmonic Imaging

Tissue harmonic imaging is a technique used to improve B-mode ultrasound. This requires ultrasound probes that can emit one frequency, f_0 , and detect reflected signals as harmonics of the emitted frequency, for example $2f_0$. Harmonic frequencies were discovered using contrast-enhanced ultrasound (see below), but normal

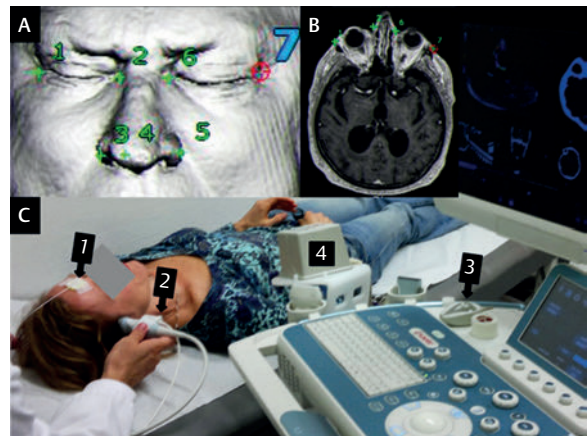


Fig. A1.24 Synopsis of the UFI technique: (A) Surface rendering from routine CT or MRI DICOM datasets with manually chosen external marker points. (B) Visualization of marker point localization on axial images. (C) Ultrasound examination settings: 1—motion control sensor fixed to the patient’s forehead, 2—detachable motion control sensor at the ultrasound probe during insonation, 3—pointer for registration of marker points (for the registration process, sensor 2 is detached from the probe and fixed to the pointer), 4—antenna, constantly emitting an electromagnetic field for identification of both motion control sensor positions.

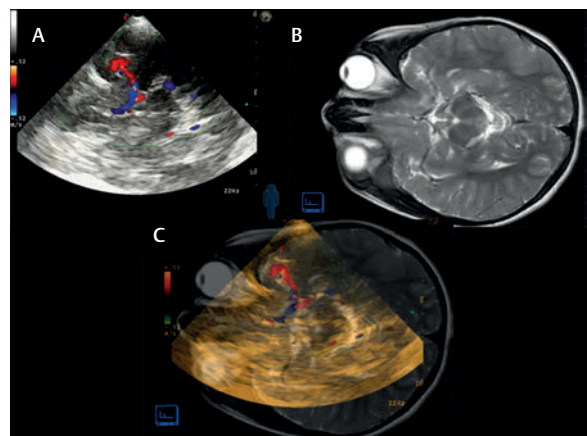


Fig. A1.25 Example images of the applied fusion imaging technique: (A) Transtemporal color-coded sonography, axial imaging plane with visualization of the midbrain, the M1-segment of the MCA, the A1-segment of the anterior cerebral artery, and partially the P2-segment of the PCA. (B) Corresponding T2-weighted MRI plane showing the midbrain as well as the flow void signals of the circle of Willis. (C) Overlay image between both imaging modalities.

tissue without the use of contrast also generates harmonic echoes which are used for image generation. The technique reduces artifacts and improves the spatial resolution because of the higher frequencies used (see also “Ultrasound Transducer” under “Ultrasound Systems” above).

Harmonic Imaging and Ultrasound Contrast Agents

A particular problem of the above-mentioned conventional ultrasound modes is the lack of sensitivity for small blood vessels and the vascular periphery. Within this

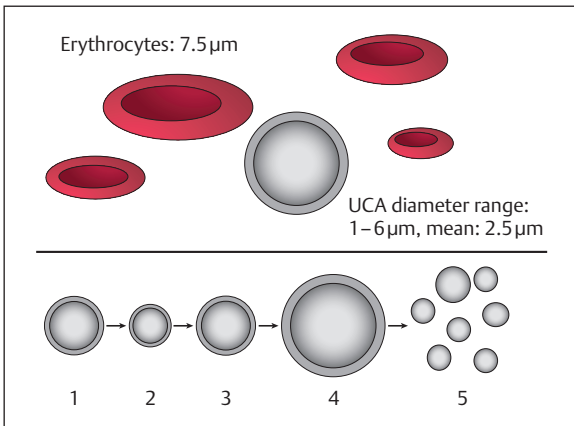


Fig. A1.26 Top: Ultrasound contrast agents consist of microbubbles that are smaller than an erythrocyte. The core of the bubble is gaseous and may contain air, perfluorocarbon, fluoropropane, or sulfur hexafluoride. The stabilizing shell may consist of palmitic acid, galactose, albumin, surfactant, or lipid. The bubbles persist for several minutes in the circulation and then, depending on the content, are resorbed or exhaled by normal breathing. **Bottom:** Mechanical energy applied to the bubble results in triggered oscillations (1–4). If the insonation energy is high, the bubble may fragment (5).

region the flow velocities are low. The resulting Doppler shift comes into the range of spontaneous movements of the insonated tissue, which impedes the differentiation between the two signals. Furthermore, the number of available reflectors is much lower within the microcirculation. The use of harmonic imaging in combination with ultrasound contrast agents overcomes this problem and permits the visualization of blood flow within the microcirculation. The underlying principle is that contrast agents do not just reflect the emitted frequency but also show resonance phenomena. Ultrasound contrast agents consist of microbubbles that vibrate or oscillate. Each bubble consists of a stabilizing shell and a gaseous core. If exposed to mechanical energy they start to oscillate; the insonation energy becomes very high they may burst (**Fig. A1.26**). Oscillation phenomena occur marginally in resting tissue, and this facilitates the differentiation between tissue and the stimulated microbubbles, i.e., the perfused microcirculation. The oscillation phenomenon occurs at different frequencies (multiples of the original emission frequency), so harmonic imaging requires transducers that can simultaneously emit one frequency and receive another. Different technical solutions have been suggested to optimize the necessary differentiation between the emitted fundamental and reflected harmonic frequencies. Two commonly used examples, the second harmonic imaging mode and the phase-inversion harmonic imaging mode, are briefly explained in **Fig. A1.27** and **Fig. A1.28**. Other modes that can be employed are signal analysis via power modulation (use of two impulses differing in their intensity) or contrast pulse sequencing (a combination of phase inversion and power modulation). **Fig. A1.29** and **Fig. A1.30** show examples of applied transcranial harmonic imaging in a healthy subject and in a patient with a large middle cerebral artery infarction (see also **Videos** ▶ **A1.1** and **A1.2**).

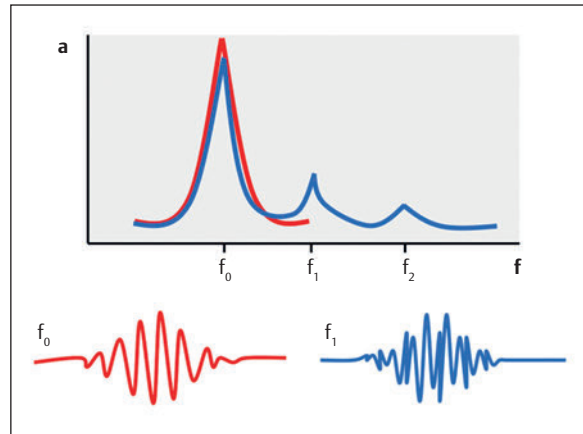


Fig. A1.27 Second harmonic imaging: The diagram shows the emitted frequency band f_0 (red) and the resulting reflected harmonic frequencies (blue). f_1 is the second harmonic frequency ($2 \times f_0$). Note the reduced amplitude of the harmonic signals which impairs the use of higher harmonics for data analysis. (a = amplitude, f = frequency, f_0 = fundamental emitted frequency, f_1 and f_2 = second and third harmonic frequency.)

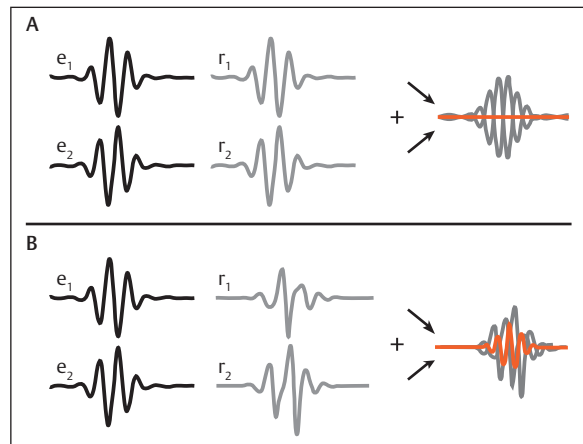


Fig. A1.28 Phase-inversion harmonic imaging: Two impulses with a phase inversion of, e.g., 180° (e_1 and e_2) are sent into the tissue, one shortly after another. **(A)** A linear reflector, for example resting tissue, identically reflects the emitted frequency. During postprocessing, the reflected frequencies (r_1 and r_2) are added which leads to effacement of the signal. **(B)** A nonlinear reflector reflects different frequency spectra, which if added result in a detectable signal.

Ultrafast Imaging

Ultrafast ultrasound imaging is a recently emerging technique which, by using graphical processing unit (GPU)-based platforms, can achieve image frame rates of more than 1,000 frames per second over the whole imaged field of view. Instead of using conventional focused ultrasound beam line acquisition, this technique uses plane wave transmission and computed analysis of the backscattered echoes to calculate ultrasound images (Tanter and Fink 2014). With frame rates in the

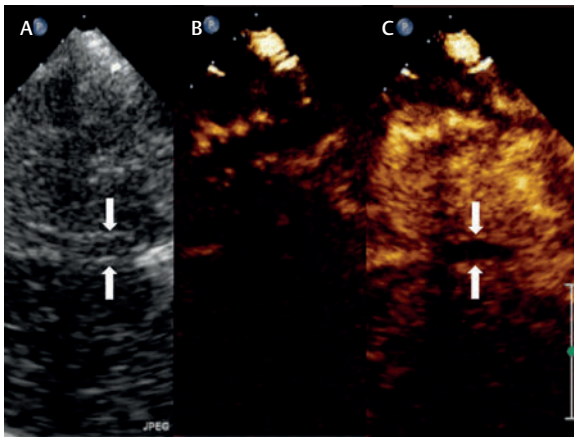


Fig. A1.29 Phase-inversion harmonic imaging applied in transcranial brain perfusion imaging of a healthy subject using a Philips IU22 ultrasound system: (A) B-mode image at the level of the third ventricle (arrows). (B) Corresponding image plane in harmonic imaging mode before contrast arrival. (C) Ultrasound perfusion image after contrast bolus arrival resulting in a homogenous ipsilateral parenchymal signal. Note the missing contrast filling in the third ventricle.

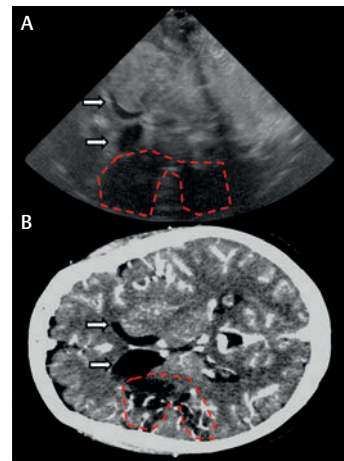


Fig. A1.30 Phase-inversion harmonic imaging applied in transcranial brain perfusion imaging of a patient with a large chronic MCA infarction using a Philips IU22 ultrasound system: (A) Summation image of the contrast arrival, sampled over 30 seconds. (B) CT angiography source image in an image plane, similar to the ultrasound image. Note the anterior horns of both lateral ventricles (arrows) and the corresponding large contralateral perfusion deficit in both imaging modalities (dotted line).

kilohertz range, the technique makes it possible to measure tissue motion, which led to its first clinical application in shear wave elastography. Since then, the technique has been further developed and can now be used for ultrafast Doppler imaging, permitting a real combination of color-flow and PW Doppler imaging as well as an optimized detection of low-flow signals. In practice the technique makes it possible to retrieve offline Doppler spectrum information from each pixel within a registered image over a time frame of 2–3 cardiac cycles. Experience using the specific advantages of this technique in diagnosis of stroke is not yet available (Fig. A1.31).

Parameters and Settings

Insonation Depth and Sample Volume

The PW mode allows determination of the depth of insonation, which is the depth from which a signal is depicted. Based on the speed of sound in the investigated tissue, which is ~1,500 m/s in the brain, 330 m/s in air, and 3,500 m/s in bone, it is easy to calculate the necessary time for an ultrasound impulse to reach a predefined depth and to measure the reflection. In our example the blood vessel to be studied is at a depth of 8–10 cm (Fig. A1.32). A single impulse needs 0.052 ms to reach 8 cm insonation depth and another 0.052 ms to return to the ultrasound probe. The ultrasound system has therefore to wait 0.104 ms after sending an impulse before starting to use the reflected signal for analysis. The time window of analysis then determines the magnitude of the sample volume. A short time of analysis relates to a small sample volume, a longer time to a larger sample volume. In our example, a time window of 0.026 ms translates into 2 cm sample volume,

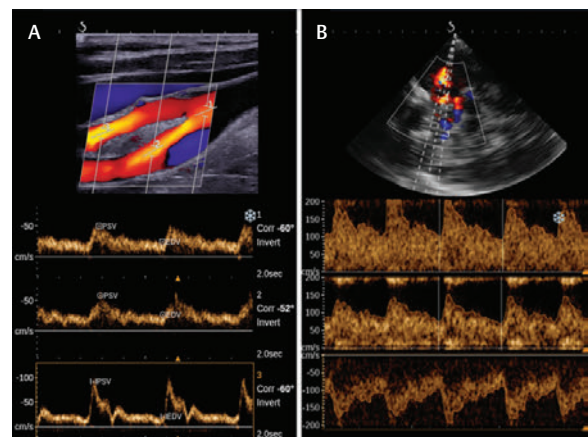


Fig. A1.31 Example images of the ultrafast Doppler imaging technique. Both displayed image sequences contain data from 3–4 cardiac cycles (recordings of 4–5 seconds duration). Within this image, multiple sample volumes can be placed “offline” and the Doppler spectrum analysis for identical time points can be displayed for any location within the image. (A) Extracranial duplex ultrasound: three simultaneous sample volumes are placed in the CCA, the internal carotid artery (ICA), and the ECA. (B) TCCS of the circle of Willis: three simultaneous sample volumes are placed in the ipsilateral proximal and distal MCA as well as in the contralateral MCA. (Images with kind permission of SuperSonic Imagine GmbH, Munich, Germany.)

leading to signals from one vessel only. A time window of 0.052 ms results in a sample volume of 4 cm, permitting signal analysis of both blood vessels. In practice, insonation depth is displayed on the monitor of the system and can easily be adjusted by the available controls. We recommend adjusting the sample volume of Doppler spectrum analysis according to the size of the blood vessel. If the selected volume is too small, it

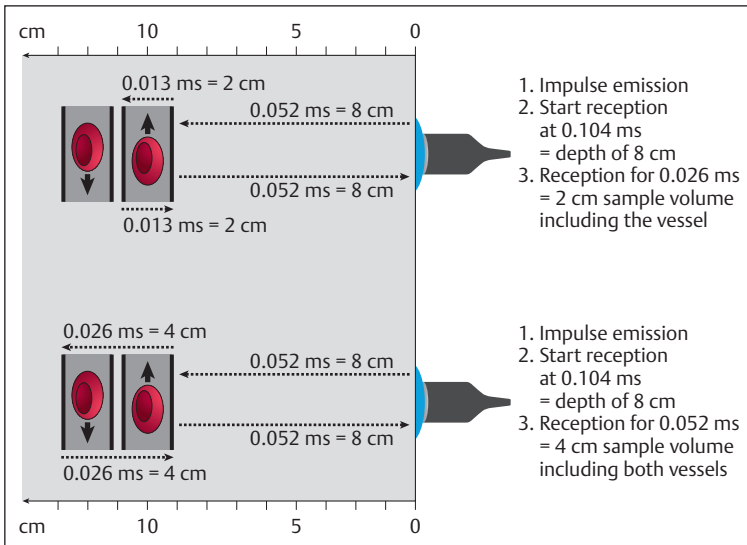


Fig. A1.32 Schematic explanation of insonation depth and sample volume.

may lead to impaired signal quality with visualization of only a part of the total Doppler spectrum. If the selected volume is too large, it may result in the reception of signals from more than one vessel and therefore more than one Doppler spectrum. In our example a small sample volume, placed in the common carotid artery (CCA), will result in the display of a Doppler spectrum without the normal low-flow fraction near the zero line (Fig. A1.33). A sample volume that is too large leads to a simultaneous display of the CCA and jugular vein signal. However, in practical routine application, a medium-sized sample volume placed in the middle of the vessel is sufficient for flow evaluation and fine adjustments are rarely necessary.

Pulse Repetition Frequency, Insonation Depth, and the Aliasing Phenomenon

Ultrasound systems using the PW mode send many repetitive impulses into the tissue. The number of impulses per time unit is called the pulse repetition frequency (PRF) and is measured in Hz. The PRF is closely related to the insonation depth. The greater the insonation depth, the longer the ultrasound impulse needs to return and the lower the possible maximum PRF, which limits the applicable PRF frequency range (Fig. A1.34). For example, if a signal to be studied is from deep blood vessels, the PRF has to be reduced to receive a signal. However, a low PRF increases the risk of an aliasing phenomenon. Aliasing always occurs if the monitored frequency reaches or exceeds the PRF (Fig. A1.35). An easy example for this error is the phenomenon of a wheel apparently moving backward in a movie. The PRF of a standard video is 25 pictures per second, which is fast enough for movements to look smooth to the human eye. If the camera captures a wheel turning slower than 25 times/s the movement appears normal. However, if the wheel turns exactly 25 times/s the camera will always capture the wheel in the same position, i.e., the wheel seems to stand

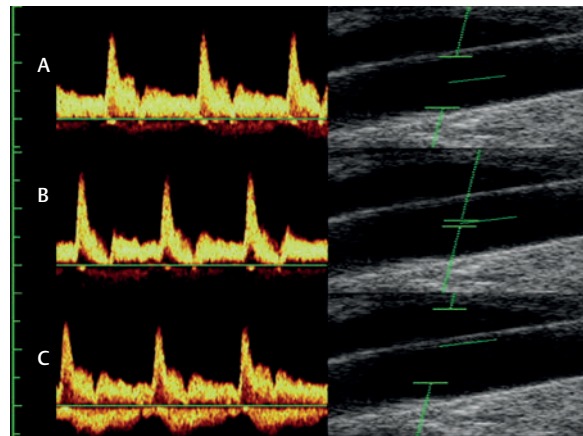


Fig. A1.33 Extracranial duplex: CCA longitudinal plane. Examples of different sample volumes. (A) Optimal sample volume resulting in a complete Doppler spectrum. (B) Sample volume too small. Note in the Doppler spectrum the absent low-flow signals near the zero line. (C) Sample volume too large, resulting in the additional visualization on the Doppler spectrum of the nearby jugular vein.

still. If it turns faster than 25 times/s the wheel appears to move backward. Applying this to the ultrasound analysis of blood flow, aliasing occurs if the Doppler shift frequency exceeds PRF/2. High blood flow velocities result in high Doppler shifts: for example, a stenosis in the distal part of a blood vessel such as the basilar artery at 8 cm might lead to an aliasing phenomenon. The insonation depth of 8 cm requires a low PRF (maximum ~8 kHz) to receive a signal. However, a high-grade stenosis might easily lead to Doppler shifts in excess of 8 kHz, which subsequently results in an aliasing phenomenon. To avoid or to reduce aliasing, the PRF should be adapted as needed. In cases with Doppler spectrum aliasing, the zero line might be moved up or down in addition to the PRF adjustment (Fig. A1.36 and Fig. A1.37).

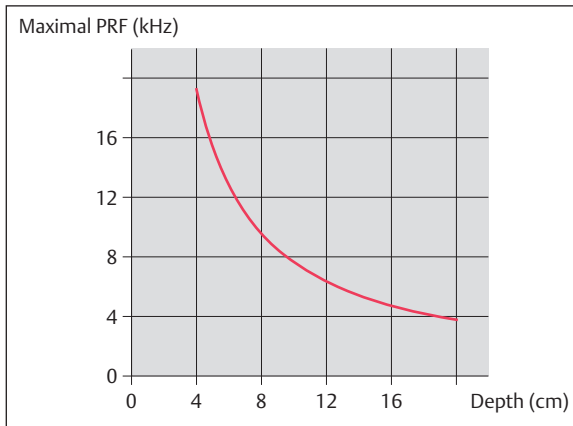


Fig. A1.34 Relation of possible insonation depth and PRF. Example of a pulsed insonation with a 2-MHz insonation probe.

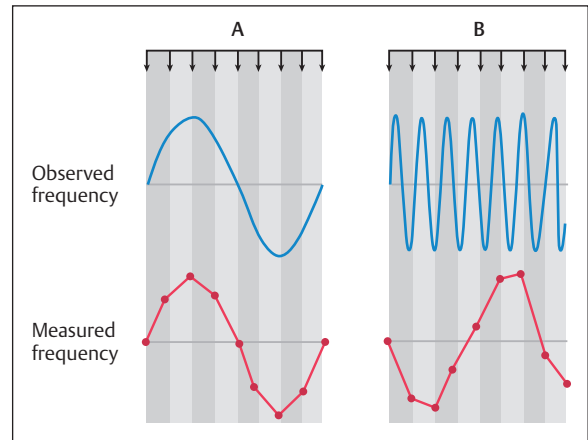


Fig. A1.35 (A) Observation/insonation with PRF greater than twice the observed frequency leads to correct measurement. (B) Observation/insonation with a PRF less than twice the observed frequency leads to an incorrect image of the original frequency.

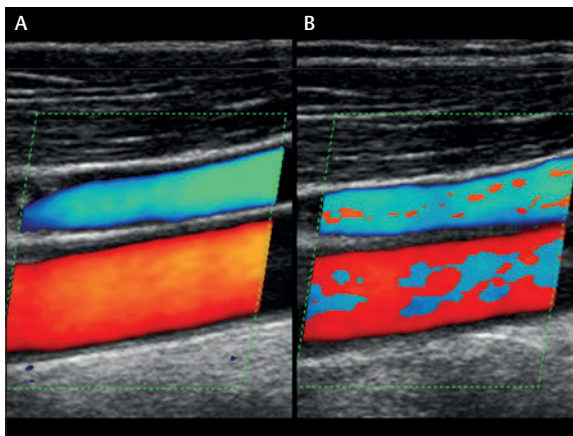


Fig. A1.36 Extracranial duplex: CCA longitudinal plane. (A) Optimal adjusted PRF with homogeneous color signal. (B) Distinct color aliasing in a nonstenosed vessel segment because of low PRF setting.

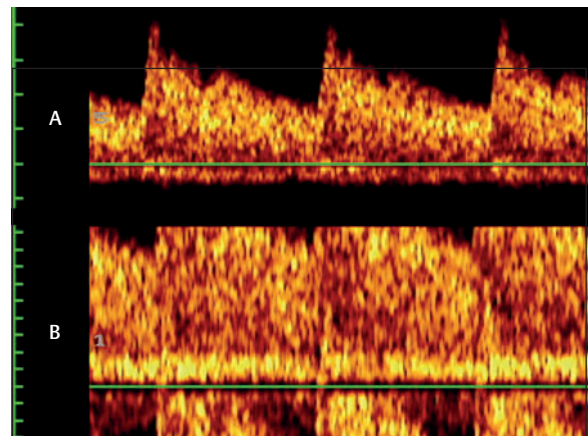


Fig. A1.37 TCCS: Doppler spectrum of the MCA. (A) Optimal adjusted PRF, the MCA spectrum lies above the zero line. (B) Distinct Doppler aliasing. The MCA spectrum breaches the displayed scale.

Power, Gain, and Filter Settings

To improve the signal quality and to reduce unwanted noise, all ultrasound systems allow adjustment of power, gain, and filters. Power is the actual force with which the piezoelectric elements vibrate. For Doppler ultrasound machines it is given in mW/cm^2 and for duplex ultrasound systems the mechanical index (MI) is used: $\text{MI} = P/\sqrt{f}$, where P is the maximal negative axial sound pressure and f is frequency (Meltzer 1996). Increased power will lead to a stronger returning signal. For extracranial ultrasound as well as for insonation through a bone window, the power can be adjusted as needed. However, all ultrasound machines should comply with the US Food and Drug Administration (FDA) and European rules of maximum applicable energy to avoid unwanted bio-mechanical effects such as the elevation of tissue temperature or tissue cavitation (Barnett et al 1997, 2000, Fowlkes and Holland 2000). The second method which enhances the sensitivity of the system is to increase the gain, which is best compared with the action of a hearing aid. If the gain setting is too low, signals are only faint.

A medium setting gives the best results; turning the gain up too high increases the background noise and might then reduce the signal-to-noise ratio. **Fig. A1.38**, **Fig. A1.39**, **Fig. A1.40**, and **Fig. A1.41** demonstrate the effect of gain adjustments on the B-mode image, the color-mode image, and the Doppler spectrum. For the B-mode image it is also important to adjust for depth-dependent loss in signal intensity (time gain compensation) (**Fig. A1.39**). The amplification of the Doppler spectrum should be adjusted so that the system is able to fit an exact envelope curve onto the spectrum.

The number of shades of gray displayed within a B-mode image can be adjusted using the dynamic range (compression). It influences the contrast of the image and is usually set between 55 and 65 dB (**Fig. A1.39**).

Within the Doppler spectrum analysis, all ultrasound systems allow the use of filters which permit erasure of low frequencies, i.e., the signals near the zero line. Early developers wanted to be able to reduce artifacts generated by vessel wall or tissue vibrations, or movements. The effect of a low-frequency filter can be seen in **Fig. A1.42**, in which the filter function is gradually

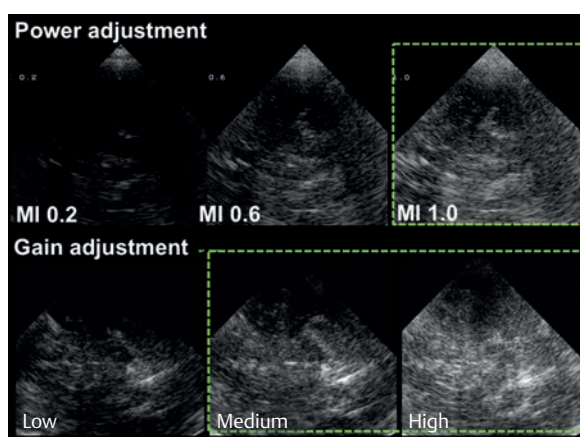


Fig. A1.38 TCCS, B-mode imaging, transtemporal axial midbrain plane. **Top:** Effect of raising the power of image quality. Increasing power from an MI of 0.2 to 1 leads to increased signal yield. **Bottom:** Effect of gain function on image quality. Increasing gain from low to high leads to increased image intensities. Green fields indicate desired image quality.

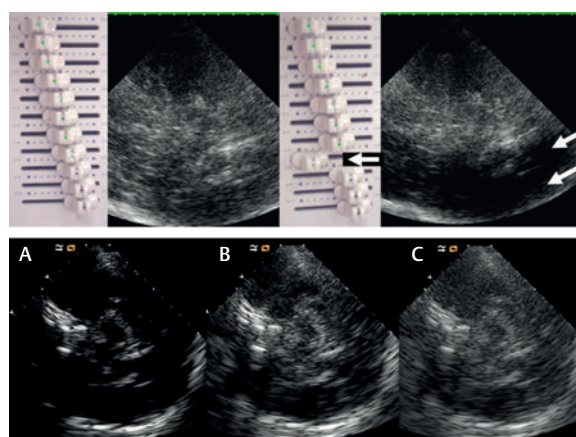


Fig. A1.39 TCCS, B-mode imaging, transtemporal axial midbrain plane. **Top:** Controls for compensation of depth-related signal weakening. **Bottom:** Image effect of different dynamic range settings. (A) 45 dB (high contrast, loss of image details). (B) 65 dB (optimal). (C) 95 dB (loss of contrast and of image details).

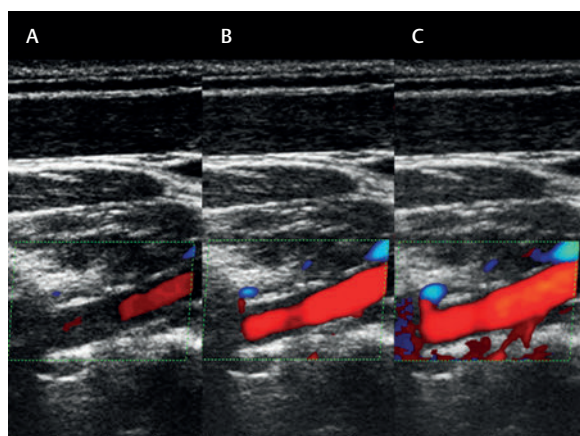


Fig. A1.40 Extracranial duplex: Vertebral artery in the V2 segment, longitudinal plane. Increasing color gain in images (A–C) leads to improved color signal.

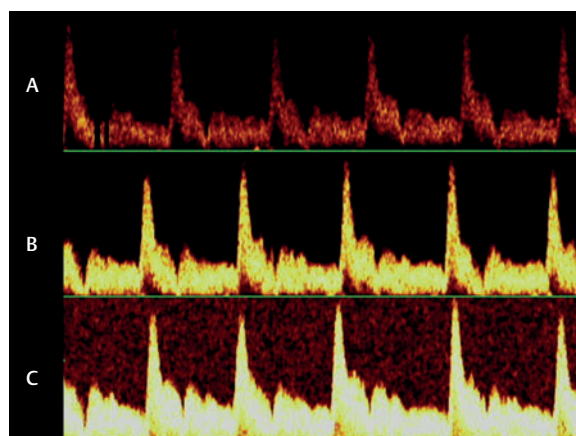


Fig. A1.41 Doppler spectrum image of the extracranial internal carotid artery: Effect of raising the gain function on image quality. Increasing gain from A to C leads to increasing image intensity. Note the high background noise in C and optimal adjustment in B.

increased. We do not recommend their use in routine practice as this might lead to the omission of low-flow vessels, such as veins. The filter does not affect the magnitude of the detectable flow velocity but might influence the calculation of mean and intensity-weighted mean velocities.

Artifacts

Even if all ultrasound settings are optimally adjusted, ultrasound images may be altered by artifacts specific to the ultrasound technique. The sonographer should be aware of this to avoid misinterpretation of findings. Several the most important artifacts are listed in this section; others are discussed in later chapters (Alexandrov 2013, Hindi et al 2013, Schmidt 2007).

Artifacts in Gray-scale Imaging

Shadowing

Shadowing is one of the most frequently observed artifacts, occurring behind insonated objects that completely absorb or reflect the ultrasound waves, leaving a black image without structural or flow details of the region in the “shadow zone”—that is, distal to the reflector. In neurosonology this phenomenon could be caused by bone (transverse processes) or calcified plaques. A partial shadowing effect may occur in tissue regions with greater ultrasound attenuation than the surrounding tissue or edge structures (such as the carotid vessel wall) while a structure with low ultrasound attenuation, such as a fluid-filled cyst, will result in distal “hyperechoic shadowing” (Fig. A1.43).

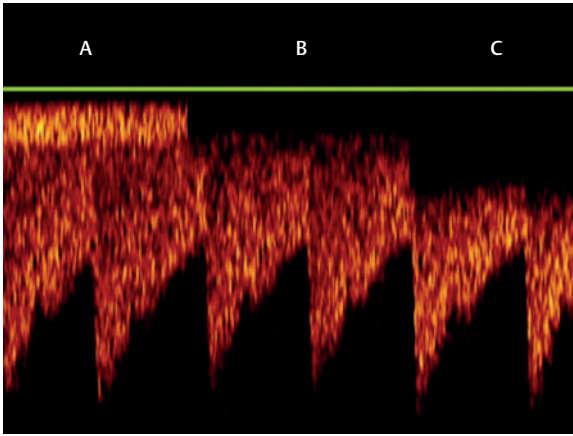


Fig. A1.42 TCCS, transtemporal approach: Doppler spectrum of the P2-PCA segment. (A) No filter; note the PCA signal and the low pulsatile flow signal of the basal vein of Rosenthal near the zero line. (B) Filter in use; the venous signal initially visualized has completely disappeared. (C) Maximal filter setting leading to distinct spectrum alteration. However, systolic and diastolic flow velocities can still be recognized in this example.

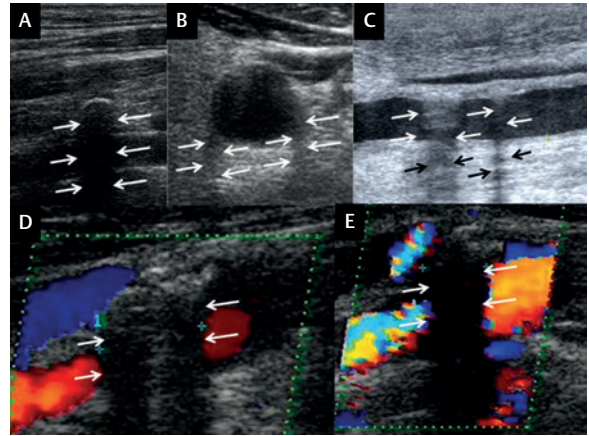


Fig. A1.43 Typical shadowing artifacts in B-mode and color-mode imaging (arrows): (A) Physiologic shadowing caused by the transverse processes of the C6 vertebra leading to a discontinuation of the vertebral artery B-mode signal. (B) Partial shadowing effect caused by the edge of the CCA. (C) B-Mode shadowing caused by vessel wall adherent plaques. (D,E) Color-mode shadowing by hyperechoic plaques in the carotid bifurcation.

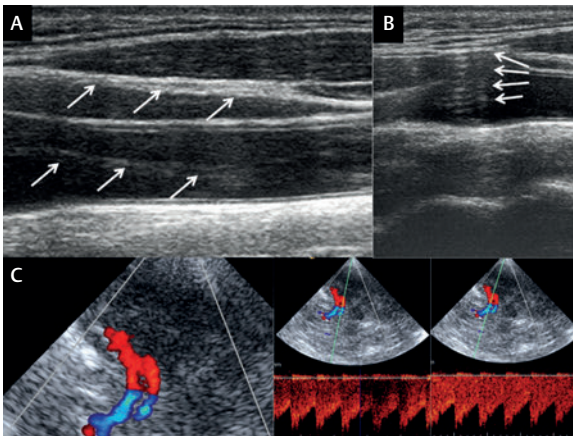


Fig. A1.44 (A) Reverberation artifact in extracranial B-mode imaging—the hyperechoic border between internal jugular vein and sternocleidomastoid muscle identical reappears within the lumen of the CCA (arrows). (B) Reverberation artifact with large number of repetitive echo signals extending deep into the underlying tissue. (C) Mirror artifact suggesting doubling of the MCA and anterior cerebral artery (ACA). Doppler spectrum analysis in both A1-ACA segments show identical Doppler signals confirming the classification as an artifact.

Reverberation

In case of multiple linear echo-reflecting structures within the ultrasound beam, the sound waves are not only reflected once by each layer but additionally travel between those layers before returning back to the ultrasound transducer, thereby generating signals with a falsely prolonged time span. This phenomenon results in equally spaced repetitive image structures. This is often seen on extracranial B-mode imaging of carotid arteries and jugular veins. If the reflecting

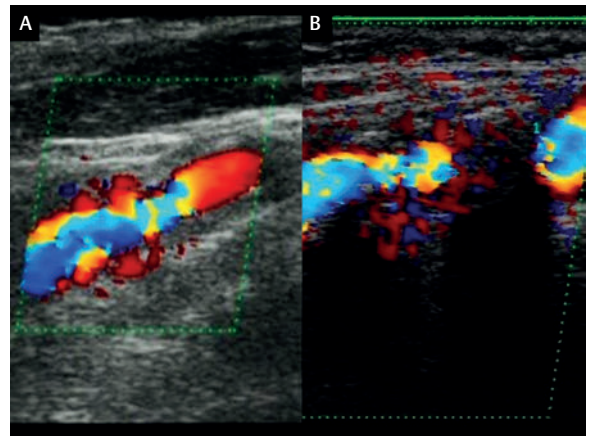


Fig. A1.45 Confetti effect—i.e., color signal outside the vessel. (A) Phenomenon occurring just distal to a high-grade internal carotid artery stenosis. (B) Confetti effect distal to a shadowing caused by hyperechoic plaque and concomitant stenosis.

layers are very close, the resulting reverberation artifact is described as a “comet-tail artifact” (Fig. A1.44A and Fig. A1.44B).

Refraction and Mirror Artifacts

Refraction leads to false duplication of insonated structures usually appearing identically side-by-side because of changes in ultrasound beam direction caused by tissue-dependent differences in the speed of sound

(Arning 1998). Transcranially, this can occasionally lead to a false double appearance of the basilar artery or middle cerebral artery (MCA) and might impair the differentiation between posterior cerebral artery (PCA) and superior cerebellar artery (SCA). To identify artifacts, the Doppler spectrum in both vessels in question should be compared. If they are identical, an artifact has to be assumed. *Mirroring* is a false duplication of insonated structures along an obliquely insonated reflector plane. Usually the mirroring structure, for example a calcified plaque, is clearly visible and the phenomenon may lead to a projection of flow signals into a structure without blood flow. Overall, it is necessary to recognize both phenomena although they are both infrequent neurosonological findings (**Fig. A1.44C**).

Artifacts in Color-mode Imaging

Shadowing

Shadowing, as in B-mode images, leads to a loss of signal, i.e., a loss of color.

Aliasing Phenomenon

See earlier section “Pulse Repetition Frequency, Insonation Depth, and the Aliasing Phenomenon.”

Color Signal Outside a Vessel with Blood Flow

This phenomenon can, depending on the specifics of the ultrasound system be caused if gain adjustments are too high, if the PRF is too low, or if the insonated tissue is moving (e.g., adjacent to an pulsatile artery) or close to a high-grade stenosis (confetti effect) (**Fig. A1.45**).

Artifacts in Doppler Spectrum Analysis

Aliasing Phenomenon

See earlier section “Pulse Repetition Frequency, Insonation Depth, and the Aliasing Phenomenon.”

Safety Considerations

By transmitting sound waves into the tissue ultrasound also transmits energy that could potentially cause tissue alterations. The observed effects are mainly heating and mechanical alteration of the insonated tissue either by energy absorption or by tissue movement and cavitation. The thermal effects increase with the insonation frequency, duration of insonation, and PRF. This means a simple B-mode image has the lowest risk of thermal effects, a triplex mode insonation with B-mode, color-mode, and pulsed Doppler analysis the highest. Classical transcranial Doppler (TCD) systems can be set to insonation energies that may cause local skin warming, but this is hardly noticeable in modern duplex ultrasound systems because of energy restrictions for manufacturers and heat diversion strategies, such as diverting heat away from the lens of the probe

and into the probe handle. According to the World Federation for Ultrasound in Medicine and Biology a temperature rise of up to 1.5 °C above physiologic levels can be applied without any restrictions. Several studies have analyzed whether transcranial insonation affects intracranial temperature but all have yielded negative results (Pfaffenberger et al 2013, Schlosser et al 2009, Vyskocil et al 2012). The measure of tissue heating is the thermal index (TI: the acoustic power output divided by the acoustic power to produce a 1 °C temperature rise). This is usually displayed on each ultrasound system during insonation. Depending on the tissues insonated, a soft tissue index (TIS), a bone index (TIB), and a bone near transducer index (TIC) have been defined.

Mechanical effects which can in general be achieved by the ultrasound technique range from tissue movements—the postulated mechanism of ultrasound in thrombolysis of ischemic stroke (for sonothrombolysis in acute stroke, see Case 10) to cavitation, which is a disruption of tissue integrity that has to be avoided in diagnostic ultrasound. For the mechanical effects, an increasing power output and insonation time increases the risk, while the insonation frequency shows an inverse relation. The on-screen measure for the nonthermal effects is the mechanical index (MI) (see also “Power, Gain, and Filter Settings” under “Imaging Modalities, Parameters, and Settings” earlier in this chapter).

For diagnostic ultrasound systems that comply with the current European or FDA regulations, in combination with the application of the ALARA (“As Low As Reasonably Achievable”) rule for diagnostic ultrasound, none of the adverse phenomena discussed above need be feared. Particular restrictions, however, are necessary when sensitive unprotected organs are insonated like the human eye or the brain in neurosurgical patients via the trepanation defect. For detailed information concerning accepted energy output see the current guidelines of the British Medical Ultrasound Society. Interestingly, for transcranial insonation, the current recommendation for the power output of duplex ultrasound systems do not apply in the same way and, in our opinion, may even be an obstacle to achieving good diagnostic results as only ~10% of the insonation energy penetrates the skull and is actually used for image generation. This results in the phenomenon that some “older” TCCS systems deliver better intracranial color-mode and Doppler spectra imaging than new high-end machines with the more recent power restrictions.

Several organizations and committees worldwide have published guidelines for ultrasound safety advice to manufacturers as well as sonographers. These can be reviewed on the relevant websites:

1. *Europe*: European Committee for medical ultrasound safety (EFSUMB, <http://www.efsumb-portal.org>), the British Medical Ultrasound Society (BMUS, www.bmus.org).
2. *United States*: Food and Drug Administration (FDA, <http://www.fda.gov>, section on radiation-emitting products, subsection on medical imaging).
3. *Worldwide*: World Federation for Ultrasound in Medicine & Biology (WFUMB, <http://www.wfumb.org>).

2

Vascular Anatomy and Structure of Ultrasound Examination

General Arterial Anatomy	18	General Venous Anatomy	61
Extracranial Arterial Anatomy	18	Intracranial Venous Anatomy	62
Intracranial Arterial Anatomy	21	Extracranial Venous Anatomy	62
General Structure of Arterial Ultrasound Examination	24	General Structure of Venous Ultrasound Examination	64
Special Arterial Anatomy and Ultrasound Anatomy	25	Special Venous Anatomy and Ultrasound Anatomy	64
Extracranial Arteries	25	Intracranial Veins and Sinuses	64
Intracranial Arteries	34	Extracranial Veins	71

General Arterial Anatomy

The analysis of the arterial vascular system of the brain and its pathologies has been the main focus of extracranial and transcranial ultrasound examinations for many years. The increasing quality of the available ultrasound systems, especially for intracranial examination, has led to more detailed visualization even of peripheral vessel segments. This consequently requires constant adaptation of examination techniques, including thorough knowledge and particularly a spatial sense of extracranial and intracranial anatomy. In all applied diagnostic techniques, including ultrasound, anatomic descriptions should be as precise as possible: e.g., for spatial orientation the approved notation should be used (**Fig. A2.1**). All vessels can be described and classified by their origin, course, caliber, and length, and are subdivided into different segments within the angiographic nomenclature. Comprehensive knowledge of cerebrovascular anatomy should also include awareness of anatomic variations. The terminology used here is a synopsis of several reference textbooks whose data are derived from postmortem anatomic examinations and angiographic studies (Huber 1982, Lang 2001, Osborn 1999, Yasargil 1984). Information from special reports is cited separately in the text. In particular, we attempt to elaborate specific anatomic definitions which are useful for ultrasound purposes, giving extra consideration to variations in anatomic nomenclature.

Extracranial Arterial Anatomy

Anterior Circulation

The common carotid arteries (CCAs) and vertebral arteries (VAs) are the four vessels securing the blood supply of the brain in a healthy individual. In ~70% of subjects the brachiocephalic trunk (BCT), left CCA, and left subclavian artery (SA) arise separately from the aortic arch. The right CCA originates from the BCT (**Fig. A2.2**). However, in up to 8% of cases the left CCA also originates from the BCT.

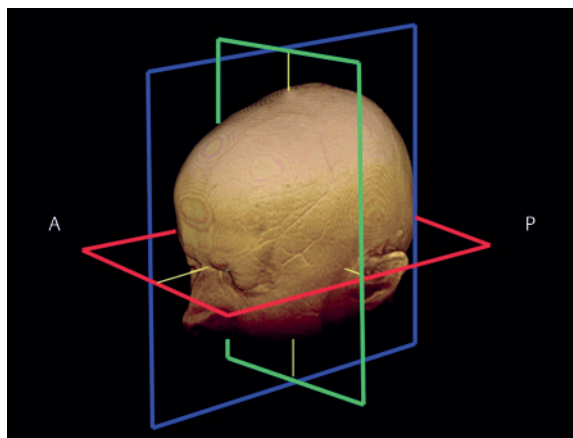


Fig. A2.1 Anatomic nomenclature used for spatial orientation. Red: axial plane; blue: sagittal plane, green: coronal plane. (A) Anterior, (B) posterior.

Other variations have also to be considered (Fig. A2.3). The CCA then usually continues without branching up to the level of the thyroid cartilage, i.e., the cervical 4/5 level, where it separates into the internal carotid artery (ICA), which supplies the brain, and external carotid artery

(ECA), which supplies the face and neck. However, the level of bifurcation may vary greatly and may be found more proximal in elderly subjects (Fig. A2.4).

At the carotid bifurcation the CCA widens and the dilatation continues into the proximal segment of the

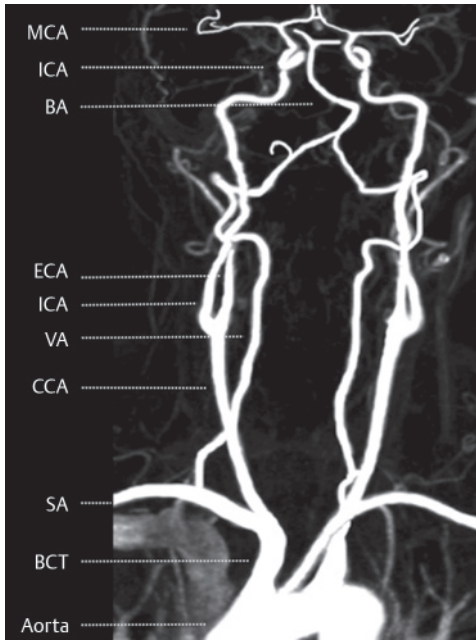


Fig. A2.2 Postprocessed contrast-enhanced 3D MRA, arterial phase, coronal MIP. Aortic arch and normal variant of brachiocephalic trunk (BCT). MCA = middle cerebral artery; ICA = internal carotid artery; BA = basilar artery; VA = vertebral artery; ECA = external carotid artery; CCA = common carotid artery; SA = subclavian artery.

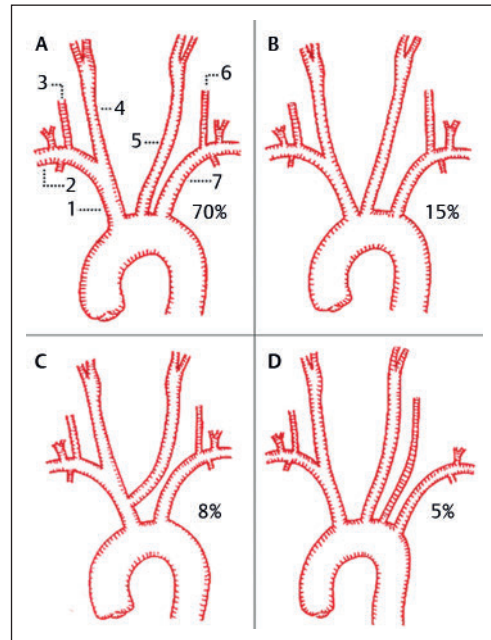


Fig. A2.3 Schematic drawing of normal anatomy and main variants of the aortic arch. (A) 70% of cases—normal type with direct origin of BCT, left CCA, and left SA from the aortic arch. (B) 15% of cases—left CCA originates from the right side of the aortic arch. (C) 8% of cases—left CCA originates from the BCT. (D) 5% of cases—left VA originates directly from the aortic arch. 1 = brachiocephalic trunk; 2 = right subclavian artery; 3 = right vertebral artery; 4 = right common carotid artery; 5 = left common carotid artery; 6 = left vertebral artery; 7 = left subclavian artery (adapted from Huber 1982, data from Toole 1974.)

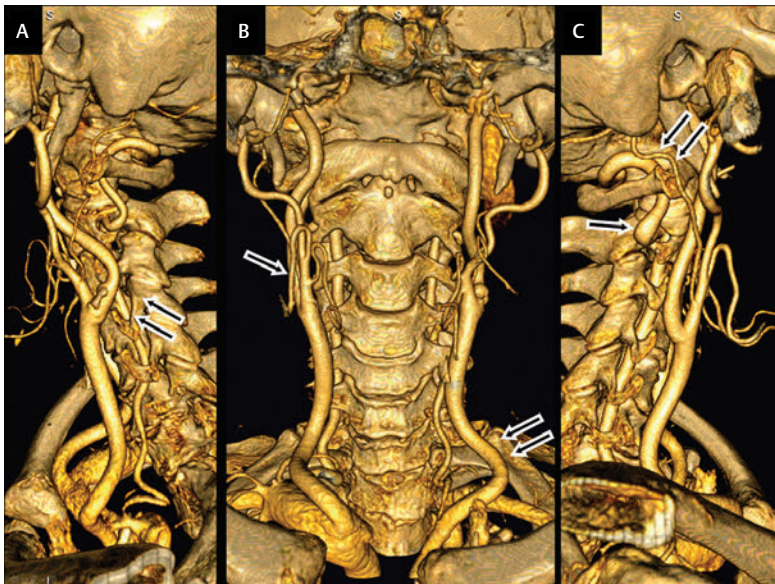


Fig. A2.4 CTA, 3D reconstruction (mandible removed) of the arteries of the neck. (A) Left lateral view. Note the dilatation and small atherosclerotic changes of the ICA at the carotid bifurcation (arrows). (B) Anterior view. Note the tortuous course of the superior thyroid artery (arrow) and of the proximal CCA (arrows). (C) Right lateral view. Note the clavicle obscuring the view of the proximal CCA segment. Note also the proximal (arrow) and the distal (arrows) V3-VA loop.

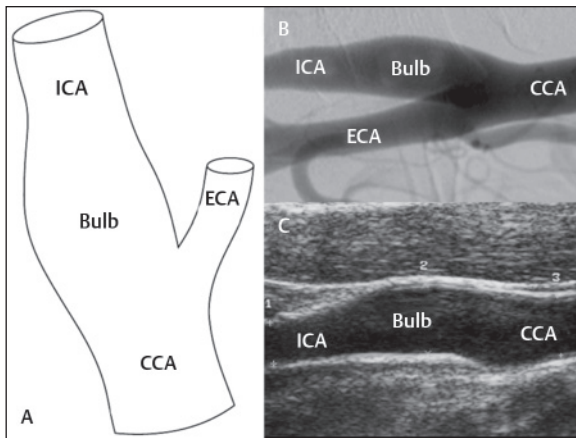


Fig. A2.5 Normal anatomy of carotid bifurcation. (A) schematic drawing. (B) DSA, selective CCA injection, lateral view, 90° counterclockwise rotated to correspond with the ultrasound image. (C) Duplex sonography, B-mode, longitudinal plane of the same subject demonstrating a wide bulb (6.8 mm) compared with the ICA (4.0 mm) and CCA (5.8 mm).

ICA. This segment is called the carotid bulb or carotid sinus. The diameters of the CCA, ECA, and ICA and the relationships between them vary greatly. Analyzing 1.969 nonaffected carotid bifurcations on DSA, the following ratios were reported: ICA/CCA 0.63 ± 0.11 (0.44–0.86), ICA/ECA 1.20 ± 0.29 (0.75–1.83), and ECA/CCA 0.55 ± 0.12 (0.34–0.79) (Schulz and Rothwell 2003). Ethnic differences have also been reported. In a study of 153 angiograms, African Americans had a proportionally smaller ICA and larger ECA compared with whites and Caribbean Hispanics. The carotid bulb revealed more or less the same diameter as the CCA (Koch et al 2009a). Others found a mean carotid bulb–CCA ratio of 1.19 ± 0.09 (Williams and Nicolaidis 1987) (Fig. A2.5 and Fig. A2.6). Loops, coiling, and tortuosities of the ICA are also common findings, the latter particularly in elderly people. Hypoplasia or aplasia of the ICA is rare, occurring in less than 0.001% of the population (Given et al 2001). It can also occur bilaterally (Viglianesi et al 2010) and affect the CCA (Drazin et al 2010). The left and right ICAs develop symmetrically and usually lie in a dorsolateral position in relation to the ECA. However, variations of their courses are frequent so that the vessel location should not be the only criterion of identification (Fig. A2.7). The ICA rises to the base of the skull without branching but may show elongations during its course before entering the skull through the carotid canal. The ECA also originates symmetrically on both sides but quickly branches into the superior thyroid, lingual, facial, maxillary, superficial temporal, and occipital arteries (Fig. A2.8). The first branch, the superior thyroid artery, is frequently visible on ultrasound examination and can be used for differentiating between the ECA and ICA as it arises in more than 70% as the first branch of the ECA. In ~20% the vessel may start at the bifurcation and in up to 10% from the CCA (Gupta et al 2014; Fig. A2.9).

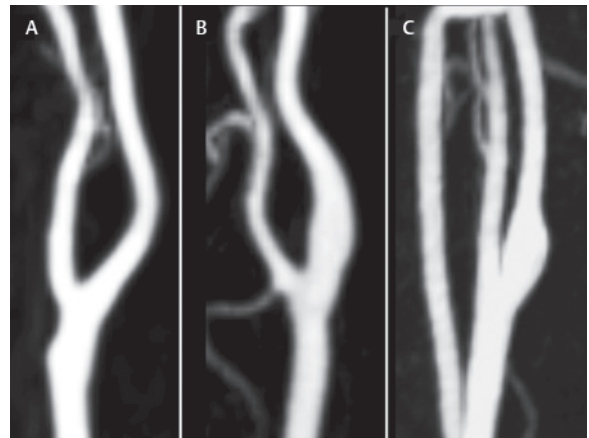


Fig. A2.6 (A–C) Variations of the carotid bulb. Contrast-enhanced MRA, lateral view. Note the variability of the carotid bulb and its relationship to the midpart and distal ICA (ICA in A–C on the right side).

Posterior Circulation

The VA originates from the SA as its first branch, which itself derives from the BCT on the right side and from the aortic arch on the left side. In ~5% of cases the left VA originates directly from the aortic arch. In contrast with the ICA, the VAs show considerable differences between the right and left sides, with the frequent finding of a dominant left-side artery. Using ultrasound and a lumen threshold diameter of 2.3 mm, VA hypoplasia has been reported in 7.8% on the right side and 3.8% on the left (Jeng and Yip 2004). In their extracranial course the VAs are divided into different segments. V0 is the point of origin, V1 is the extraforaminal segment of the VA before it enters the transverse foramen of the transverse process which occurs in ~93% at the sixth vertebra (Uchino et al 2013), V2 is the segment during its intraforaminal course up to the exit from the transverse foramen of the second cervical vertebra (axis, C2). Here V3 begins with its tortuous course and several loops allowing head mobility, also referred to as the atlas loop, before it enters the dura mater becoming the V4 segment. First V3 runs posteriorly and vertically between C2 and C1 for ~10 mm, forming a proximal loop. Then it enters the transverse foramen of C1 (atlas) and turns medially in a horizontal course within the VA sulcus of the atlas forming a distal loop, then it runs in an oblique course ventrally entering the foramen magnum. Here the intracranial V4 part starts after penetrating the atlanto-occipital membrane, the dura, and arachnoid mater (Fig. A2.10 and Fig. A2.11). It is important to know, that unlike the extracranial ICA, the VA has numerous segmental connections to muscular branches of the ECA, of which the occipital artery at the atlas loop is the most important one. These may be activated as collaterals in case of proximal occlusive VA processes.

Intracranial Arterial Anatomy

Anterior Circulation

The ICA enters the skull through the carotid foramen at the apex of the petrosal pyramid, where it follows an intrapetrosal course within the petrous carotid canal running in an

upward, forward, and medial direction (petrosal segment C6). It leaves the base of the skull via the foramen lacerum vertically along the side of the sphenoid bone (ganglionic segment C5). A persistent trigeminal artery, defined as a fetal-type connection between the C5-ICA segment and the upper third of the basilar artery (BA), may be found in

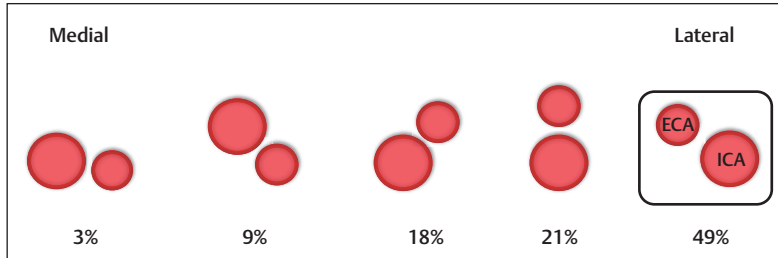


Fig. A2.7 Schematic demonstrating the spatial relationship of the ECA and ICA (Hennerici and Neuerburg-Heusler 2006).

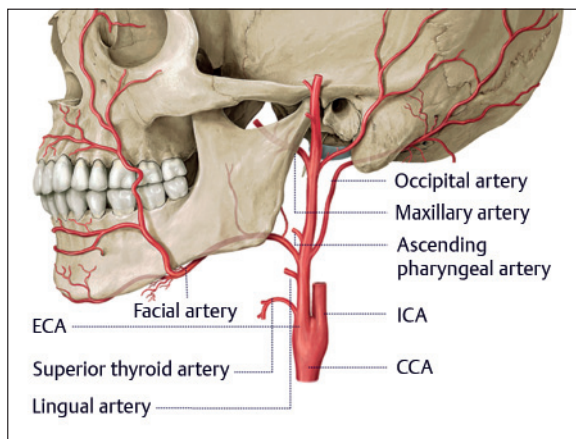


Fig. A2.8 Schematic of the ECA and its branches (Adapted from Schünke et al 2006; drawing: Karl Wesker.)

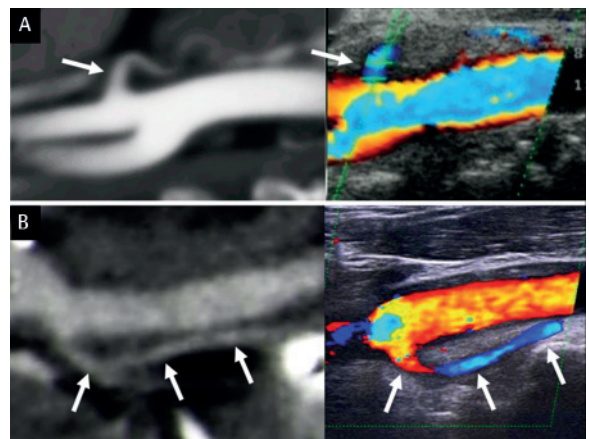


Fig. A2.9 Thyroid artery variants (arrows), ultrasound fusion imaging technique (Esaote MyLab Twice). **Left:** CTA. **Right:** Corresponding color-mode ultrasound image. **(A)** Most frequent variant with origin at the ECA (70%). **(B)** Rare variant with CCA offspring (10%).

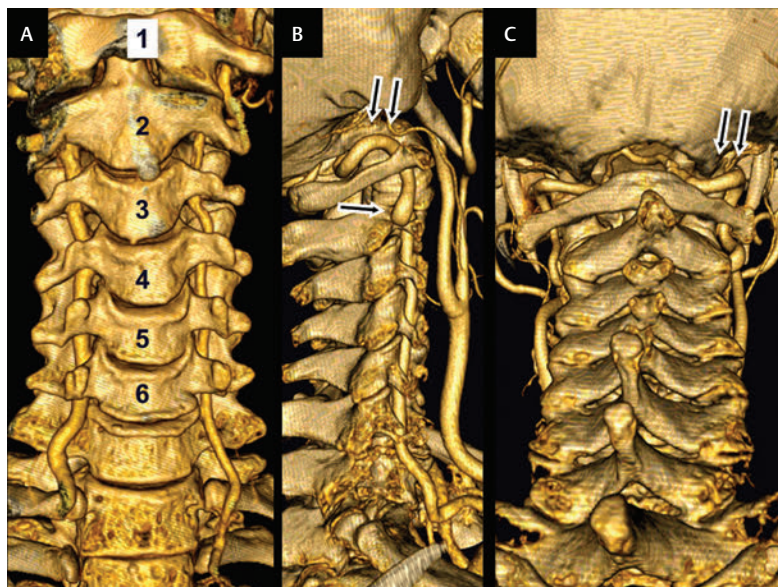


Fig. A2.10 CTA, 3D reconstruction (mandible removed) of the arteries of the neck to illustrate the posterior circulation. **(A)** Anterior view with numbered cervical vertebrae (1 atlas, 2 axis). Note the right dominant VA. The V2-VA segment starts bilaterally at C6. **(B)** Right lateral view. Note the intraforaminal V2-VA segments as well as the proximal loop between axis and atlas (arrow) and distal loop between atlas and occiput (arrows) at the V3-VA level. **(C)** Posterior view. Note the distal loop of the V3-VA segment at the atlanto-occipital joint before entering the foramen magnum (arrows).

up to 0.6% of all cases (Uchino et al 2000, 2003). From C5 the ICA turns upward and forms the carotid siphon (segments C2–C4) within the cavernous sinus (C3/C4). Here small hypophyseal and tentorial branches spring off. It enters the subarachnoid space (segment C2) and rises to its terminal part (segment C1) where it bifurcates into the middle cerebral artery (MCA) and the anterior cerebral artery (ACA). This termination is often referred to as the “carotid-T” because of its shape (or the “terminal” or “top” of the carotid). Before this, it gives off several branches: anterior at the C2/C3 level the ophthalmic artery (OA) and posterior at the C1/C2 segment the posteri-

or communicating artery (PCoA) followed by the anterior choroidal artery (AChA) (Fig. A2.12). In up to 10% of cases the AChA rises from the MCA or from the PCoA. The A1–ACA segment turns medially and slightly upward. It becomes the A2 segment at the point where the anterior communicating artery (ACoA), connecting both ACAs, originates. It then turns sharply upward to supply the ACA territory of the brain. The initial and horizontal M1 segment of the MCA may be symmetric but variations are not uncommon. It commonly bifurcates after 1–2 cm into two or more insular M2 branches, which supply the MCA territory (Fig. A2.13).

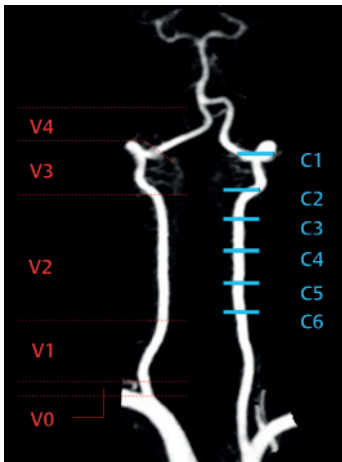


Fig. A2.11 Postprocessed contrast-enhanced 3D MRA, arterial phase, coronal MIP of the vertebrobasilar circulation. Red: Definition of VA segments from V0 to V4. Blue: Definition of cervical transverse processes from C1 to C6.

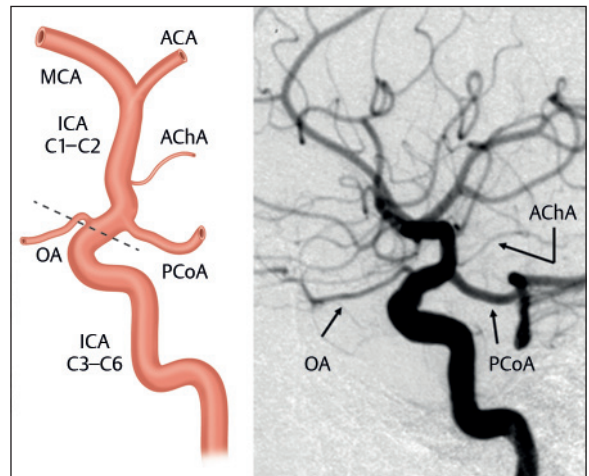


Fig. A2.12 Left: Schematic drawing of intracranial branches of the ICA (adapted from Lasjaunias et al 2001). The dotted line indicates the border between extra- and intradural compartment. Intradural OA origin occurs in 92.5%, extradural origin in 7.5% of cases. **Right:** DSA, ICA injection, lateral view showing the corresponding anatomic situs. ACA = anterior cerebral artery; AChA = anterior choroidal artery; ICA = internal carotid artery, MCA = middle cerebral artery, OA = ophthalmic artery, PCoA = posterior communicating artery.



Fig. A2.13 3D TOF-MRA, 3D volume-rendered reconstruction of the cerebral arterial circle (circle of Willis). (A) Anterior view. (B) Left lateral view. ACA = anterior cerebral artery; BA = basilar artery; ICA = internal carotid artery, MCA = middle cerebral artery, PCA = posterior cerebral artery; VA = vertebral artery.

Posterior Circulation

The VAs demonstrate considerable variation in length, course, and caliber. However, the intracranial caliber in general resembles the extracranial caliber. Both VAs enter the skull through the foramen magnum by piercing the atlanto-occipital membrane, the dura, and the arachnoid mater (V4 segment). Before merging to form the BA each VA gives off a posterior inferior cerebellar artery (PICA) which divides the VA into a proximal and a distal V4 segment. In people with VA hypoplasia, the VA can terminate partially or completely as the PICA, which then might not connect or contribute to the BA blood flow at all. The VA segment distal of the PICA up to the vertebrobasilar confluence can be separated from the pre-PICA segment and defined as the post-PICA V4 segment; sometimes it is

also called the V5 segment. The BA is in almost all cases a well-developed vessel which may become rather elongated with increasing age (Fig. A2.14). In bilateral FT-posterior cerebral artery (PCA), however, the BA appears hypoplastic. Apart from numerous small arteries providing the brain stem with blood it also gives off the paired anterior inferior cerebellar arteries (AICAs) and, near the basilar head, a pair of superior cerebellar arteries (SCAs). Finally it bifurcates into the two P1 segments of the PCA. The P1-PCA segment is short. It becomes the P2 segment at the point of origin of the PCoAs.

Cerebral Arterial Circle (Circle of Willis) and Its Variations

The anterior and posterior circulation connect via the paired PCoAs and the unpaired ACoA to form a circle known as the cerebral arterial circle or circle of Willis (CW), from which all further main arteries (ACA, MCA, and PCA) emerge (Fig. A2.15). Owing to the lack of a valvular system, blood flow through this circle can follow the direction of need. However, “perfect” anatomy with a completely developed CW is found in less than 30% of the population (Fig. A2.16).

Variations of the CW are the rule and a good knowledge of these is required for exact interpretation of findings during ultrasound examination. Functional assessment of communicating artery patency, which is probably more significant than the anatomic data alone, can be performed using transcranial ultrasound during extracranial carotid compression. Hoksbergen and coworkers (2000b) analyzed ACoA and PCoA function during an ipsilateral CCA compression maneuver. A functionally patent ACoA was assumed if CCA compression led to a reversed flow in the ipsilateral A1-ACA segment. A functionally patent PCoA was assumed if the flow velocity in the ipsilateral P1-PCA segment increased more than 20% over baseline levels (Hoksbergen et al 2000b). Using this approach they

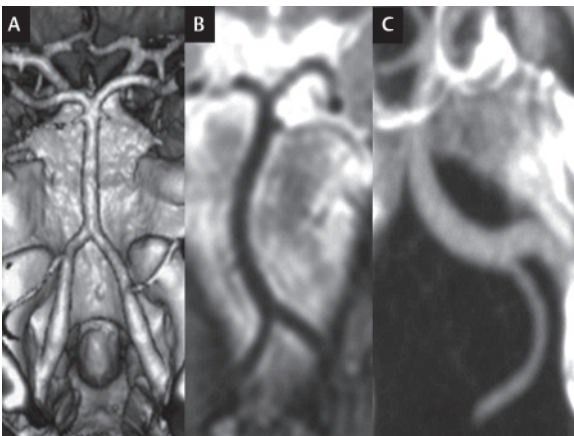


Fig. A2.14 Variations of the vertebrobasilar arteries. (A) CTA, 3D reconstruction: “Ideal” anatomic variant with two similar-sized VAs merging in a V shape into the BA. (B) MRI, T2-weighted image, coronal plane: Note the moderate elongation of the BA. (C) CTA, coronal MIP reconstruction: Note a left dominant VA and a hypoplastic right VA merging into a distinctly elongated BA.

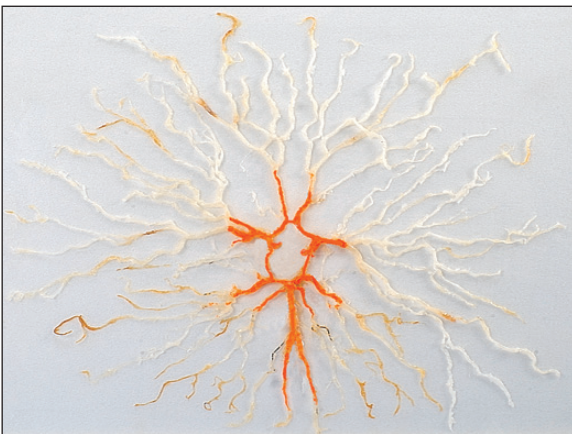


Fig. A2.15 Cerebral arterial circle (circle of Willis) and peripheral arteries: Anatomic preparation. Proximal vessel segments and circle of Willis shown in red. Note the fine distribution of the leptomeningeal peripheral vessels which show diameters comparable to the proximal vessel segments. (With kind permission from Prof. Bogusch, Center for Anatomy, Charité—Universitätsmedizin Berlin, Germany.)

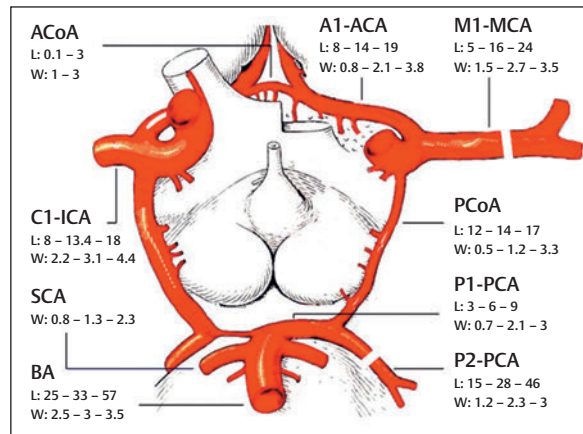


Fig. A2.16 Cerebral arterial circle (circle of Willis): Nomenclature and anatomic data of the basal cerebral arteries. All values (except for the ACoA) are given as: minimum—mean—maximum. L = length (mm), W = width (mm). (Adapted from Duus et al 2005; data: Lang 2001, Schulte-Altdorneburg et al 2000, Yasargil 1984.) Additional data not shown: ophthalmic artery diameter 0.8–1.2 mm; anterior choroidal artery diameter 0.5–1.5 mm.

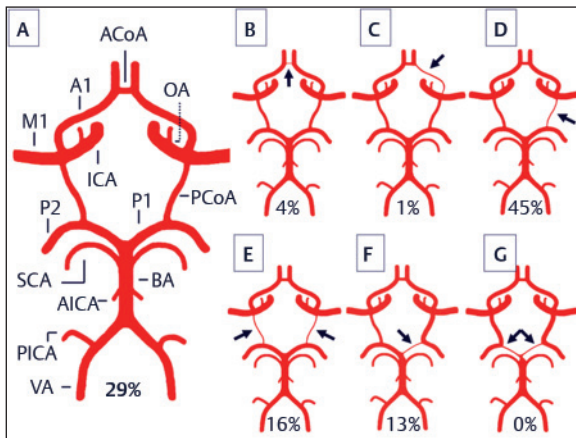


Fig. A2.17 Cerebral arterial circle (circle of Willis): Anatomic variations (arrows) as assessed by functional TCCS (according to Hoksbergen et al 2000b). (A) Normal type with complete circle of Willis (29%). (B) Impaired ACoA function (4%). (C) Unilateral impaired A1-ACA function (1%). (D) Unilateral impaired PCoA function (45%). (E) Bilateral impaired PCoA function (16%). (F) Unilateral impaired P1-PCA function corresponding to fetal-type variant of PCA (13%). (G) Bilateral impaired P1-PCA function (none). All data refer to subjects, not hemispheres. Combined variants are rare. A1 = A1 segment of the anterior cerebral artery; ACoA = anterior communicating artery; AICA = anterior inferior cerebellar artery; BA = basilar artery; ICA = internal carotid artery; M1 = M1 segment of the middle cerebral artery; OA = ophthalmic artery; P1 and P2 = P1 and P2 segment of the posterior cerebral artery; PCoA = posterior communicating artery; PICA = posterior inferior cerebellar artery; SCA = superior cerebellar artery; VA = vertebral artery.

found the absence of increased flow in the P1-PCA segment, i.e., impaired PCoA function, to be the most common variant in 61% of cases (45% unilateral, 16% bilateral). A unilateral fetal-type PCA, in which the PCA derives its blood directly from the ICA, resulting in a flow reduction or cessation in the vessel considered to be the PCoA during CCA compression, was seen in 13% of subjects. Impaired function of the ACoA was found in 4% of cases, while the A1-ACA segment was absent in 1% of cases (Fig. A2.17). A combination of the above variants can occur but represents a less frequent finding. A limitation of this study is that the compression tests could only be performed for a few seconds, so no conclusions can be drawn regarding the potential adaptation of collaterals over time (for further details see Chapter 5, "Collateral Pathways"). A bilateral fetal-type PCA may also be observed.

General Structure of Arterial Ultrasound Examination

Each radiologic imaging modality, such as DSA, CTA, and MRA, provides different aspects of anatomic information, reflecting its individual methodical basis which may be more closely related either to the real vessel anatomy or to vessel hemodynamics. Ultrasound with its unique methodical principles provides a specific view of vessel anatomy and cerebral hemodynamics, sometimes limiting its diagnostic yield but often providing additional or new

insights into brain perfusion. A comparison of DSA, CTA, and MRA makes it possible to appreciate especially the knowledge of intracranial vessel anatomy that can be gained by ultrasound techniques.

All the blood vessels that supply the brain are best studied with the patient in a comfortable supine position with the examiner investigating from behind the patient's head. According to the normal arterial flow direction, extracranial examination should be done prior to the intracranial insonation. To facilitate topographic orientation it is advisable to always start insonation in B-mode before color-mode imaging is used. Especially for transcranial insonation this approach finally leads to more rapid detection and identification of intracranial vessels. The sonographer should also be comfortably positioned. Ideally, the investigating arm should rest on the examination couch while one or two fingers of the hand holding the transducer are in contact with the patient's skin near the ear or the auditory canal. Just enough ultrasound gel should be applied to the lens of the transducer for the insonation; excessive amounts should be avoided. This approach will lead to optimal and stable guidance of the transducer even if the insonation should take longer than expected. It will also facilitate faster repositioning of the probe, e.g., after unplanned study interruptions.

For extracranial ultrasound, the head of the patient is preferably only slightly elevated, or not at all, to ensure maximum insonation space at the neck. Blood vessels are routinely insonated using 5–10-MHz transducers in the longitudinal and axial insonation planes and information is obtained regarding vessel wall alterations (B-mode), a potential lumen reduction (B-mode and color mode), and flow direction, as well as flow velocity (Doppler mode). Extracranially we recommend always obtaining and documenting angle-corrected flow velocities if a straight vessel course can be followed.

For transcranial insonation slight elevation of the head may be more comfortable for the patient, and 1–3-MHz transducers are used to enable the ultrasound beam to penetrate through the bone. However, compared with extracranial ultrasound, these low insonation frequencies reduce the spatial resolution of the ultrasound image, impeding the evaluation of vessel wall structures. Transcranial color-mode insonation is used to assess the vessel course, but is not sensitive enough for reliable evaluation of vessel lumen. Doppler analysis allows determination of flow direction and flow velocity. Angle correction of flow velocities is problematic because of the mostly tortuous course of intracranial arteries, especially in elderly people. In addition, often only a small segment of each vessel can be insonated. There is ongoing debate about whether or not to use angle correction. To improve reproducibility we recommend to measure the maximal achievable flow velocity without angle correction. In cases with a stenosis the corresponding insonation depth should be documented. If needed, angle-corrected velocities can be noted as additional data, provided the sample volume can be positioned in a satisfactory long vessel segment aligned with the direction of the vessel in the color-mode image (Nedelmann et al 2009b). For a detailed discussion see Chapter 1, "Doppler Shift and Flow Velocity" under "Ultrasound Principles".

The aim of the color-coded ultrasound investigation is to visualize the anterior and posterior circulations from the vessel origin at the aortic arch up to the main intracranial arteries. Even under optimal insonation conditions, however, this goal cannot be achieved for the origin of the CCA, which lies deep behind the clavicle, and for the vertical segments of the C6-ICA, which run within the petrosal bone of the skull base. Except for these locations, all other major brain-supplying arteries are accessible to ultrasound.

Video examples for the insonation of all relevant extra- and intracranial arteries are available online in the Thieme MediaCenter. ▶

Special Arterial Anatomy and Ultrasound Anatomy

The following section is ordered according to the blood flow from the heart into the brain, i.e., from the proximal cervical to the distal intracranial vessels. Instructions for insonation focus on color-coded duplex ultrasound only. Reference data of reported normal values for flow velocities are summarized in **Table A2.2** and **Table A2.3**.

Extracranial Arteries

A linear transducer with transmission frequencies between 5 and 10 MHz is sufficient for extracranial vessel analysis in most cases. Small and superficial arteries are easier to insonate with frequencies higher than 10 MHz. A sector transducer may facilitate the insonation of the SA and the origin of the VA. The pulse repetition frequency (PRF) should always be adapted to the

target vessel. Deep located and small arteries require a low PRF setting.

Common Carotid Artery (CCA)

Anatomic details: Apart from their variation in origin (see “General Arterial Anatomy” above), the CCAs are extremely stable and bilaterally symmetric blood vessels with hardly any anatomic variation. Elongated vessel courses can be seen with increasing age. The CCA has a mean caliber of ~6–7 mm (Yazici et al 2005).

Position and vessel identification: The CCA can frequently be visualized over a length of more than 5 cm proximal to the carotid bifurcation. The best insonation results are obtained if the head of the patient is turned away from the insonated side by 10–20°. Insonation should be performed in a cross-sectional as well as a longitudinal insonation plane over the whole visible length of the artery (**Fig. A2.18**). Differentiation from the internal jugular vein (IJV) is easy as the latter can be completely obstructed by applying slight pressure on to the neck (e.g., with the transducer). The origin of the CCA usually cannot be insonated as it lies behind and below the clavicle. Insonation is started in the B-mode. Longitudinal and axial planes are evaluated to analyze vessel wall configuration, thickness of intima media, or plaque formation (**Fig. A2.18**). Color-mode insonation and Doppler spectrum analysis are then performed (**Fig. A2.19**) (see also **Videos ▶ A2.1** and **A2.2**).

Normal values: Blood flow is usually laminar and not turbulent. For flow velocities, see **Table A2.2**.

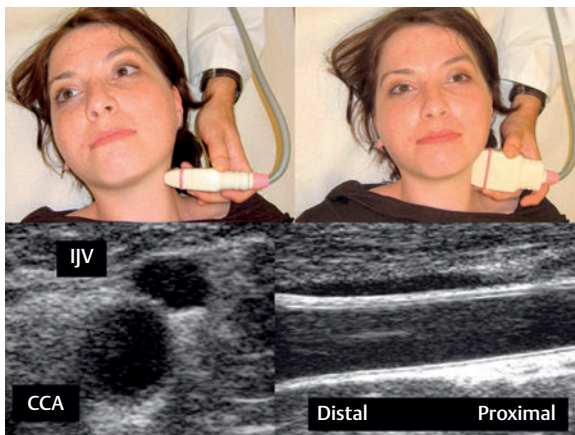


Fig. A2.18 **Top left:** Transducer position for axial CCA, ICA, and ECA insonation. **Top right:** Transducer position for longitudinal CCA, ICA, and ECA insonation. **Bottom:** Extracranial duplex, B-mode images of the CCA. **Left:** Axial plane. **Right:** Longitudinal plane. Note the close anatomic relationship of the CCA and the internal jugular vein (IJV). Note the spatial orientation used in all extracranial images: Left—distal vessel segment, Right—proximal vessel segment.

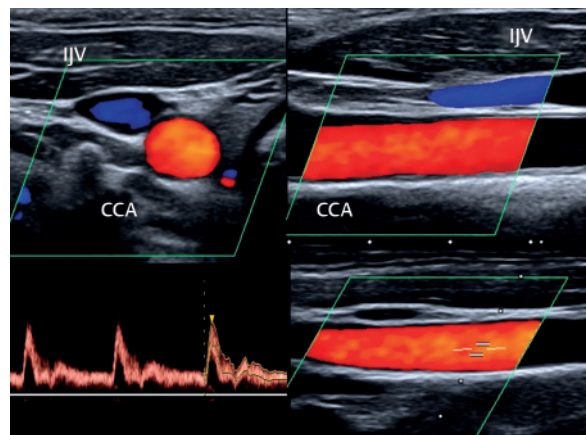


Fig. A2.19 Extracranial duplex, color-mode images of the CCA. **Top left:** Axial plane. **Top right:** Longitudinal plane. **Bottom:** Doppler spectrum analysis and color-mode image of the CCA (flow velocity 77/31 cm/s).

Internal Carotid Artery (ICA)

Anatomic details: At the carotid bifurcation the CCA divides into the ICA, which supplies the brain, and the ECA, which supplies the face and neck. The appearance of the carotid bulb and the spatial relation between the two vessels varies. The two main anatomic variants are illustrated in **Fig. A2.20**. In most cases, the ICA runs laterally. With increasing age the course of the ICA becomes more elongated. The diameter of the ICA ranges between 4 mm and 5 mm (Yazici et al 2005). Agenesis of the ICA is rare and several types of collateral pathways have been described (see also Case 42). In the most common type the cervical segment of the ICA is absent and the supraclinoid part and the MCA are fed by the PCoA (Uchino et al 2015).

Position and vessel identification: For ICA identification, the transducer is held in a position similar to the CCA insonation (**Fig. A2.18**). We recommend starting with a longitudinal or transverse approach by visualizing the CCA, following its course cranially, and examining the carotid bulb and the ICA–ECA bifurcation, rather than trying to identify an isolated distal vessel segment. If the longitudinal plane is used it is possible to visualize both ICA and ECA at the same time only in about one-third of cases. Otherwise the vessels are insonated individually, beginning at the transition from the CCA to the ICA. At that point, the ECA can usually be found if the distal part of the transducer is moved medially while the proximal part of the transducer rests above the CCA (**Fig. A2.21**). Once the proximal ICA is identified, the vessel is followed in the longitudinal plane as far distal as possible so as

not to overlook vessel coiling or kinking. In presumed ICA dissection axial examination may allow further distal insonation of the ICA. Routine documentation in the longitudinal plane with Doppler spectra should include the ICA at its origin and the most distal part as well as any relevant pathology, if present. **Table A2.1** lists the criteria for differentiating between the ICA and ECA.

The sequence of examination (B-mode followed by color-mode and Doppler spectrum analysis) is the same as for the CCA (**Fig. A2.22**). At the origin of the ICA, where the vessel widens to form the carotid bulb, the following peculiarity is frequently observed in the color mode and the Doppler spectrum analysis: As the blood flow in this region is less laminar and often disturbed, there may be an apparent flow reversal near the vessel wall with reversed color-code and blood flow direction. However, this is normal and present in almost all

Table A2.1 Ultrasound identification criteria for the extracranial ICA and ECA

ICA	ECA
Deep location (probe pointing toward the spine)	Superficial location (probe pointing toward the contralateral ICA)
No extracranial branches	Many extracranial branches
Lower pulsatility	Higher pulsatility
No or small reaction to digital tapping of the superficial temporal artery	Pronounced reaction to digital tapping of the superficial temporal artery

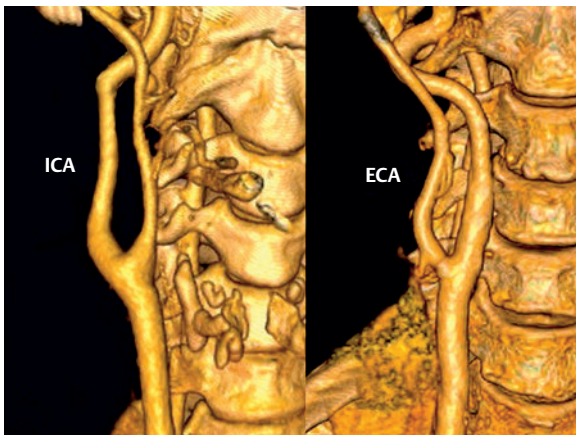


Fig. A2.20 CT angiography, 3D reconstruction, frontal view. Examples of the two most common anatomic ICA–ECA variants. **Left:** ~70% of cases—ICA lateral and/or posterior in relation to the ECA. **Right:** Remaining cases—ICA medial in relation to the ECA.

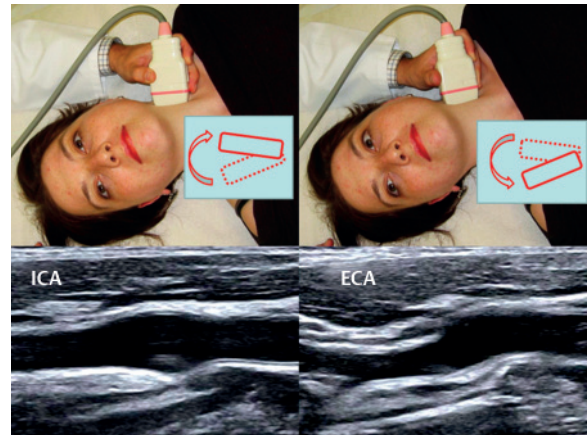


Fig. A2.21 **Top left:** Transducer position for longitudinal CCA and ICA insonation. **Top right:** Transducer position for longitudinal CCA and ECA insonation. **Bottom left:** Extracranial duplex, longitudinal plane, B-mode image of the CCA and ICA. **Bottom right:** Extracranial duplex, longitudinal plane, B-mode image of the CCA and ECA. Schematics indicate probe movements for insonation of the ICA and ECA together with the CCA.

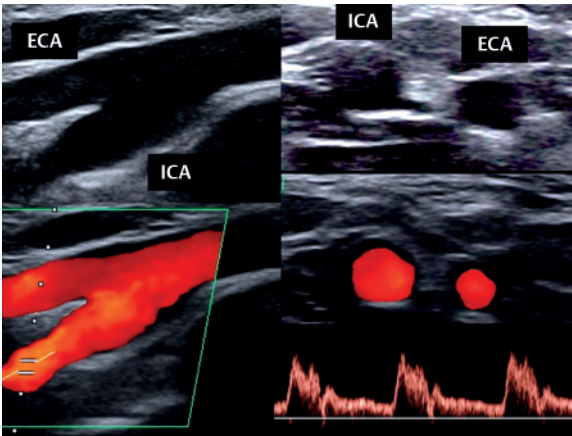


Fig. A2.22 Extracranial duplex. **Left:** B-mode (**top**) and color mode (**bottom**) images of the ICA and ECA just above the carotid bifurcation. **Right:** axial plane, B-mode (**top**) and color-mode (**middle**) imaging of the ICA and ECA; (**bottom**) Doppler spectrum analysis of the ICA (flow velocity 75/31 cm/s).

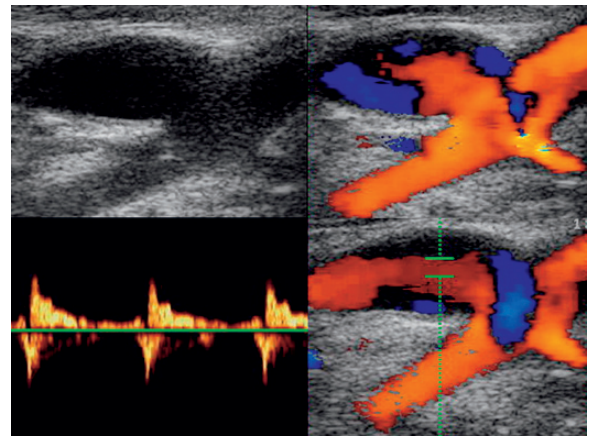


Fig. A2.23 Extracranial duplex, longitudinal plane. **Top left:** B-mode image of a wide carotid bulb. **Top right:** Color-mode image of the carotid bulb. Note the apparent flow reversal (blue-coded) caused by nonlinear flow within the bulb. **Bottom:** Doppler spectrum analysis and color-mode image of the carotid bulb. Note the retrograde flow component in the Doppler spectrum.

subjects (Middleton et al 1988). It should therefore not be interpreted as a pathologic finding as it is caused by the physiologic, highly variable, widening of the carotid bulb (**Fig. A2.23**) (see also **Videos** ▶ **A2.1** and **A2.2**).

Normal values: Within the carotid bulb the blood flow may be disturbed and may show low flow velocities. The flow pattern becomes laminar in the more distal ICA. The Doppler spectrum is less pulsatile than the spectrum in the ECA. For flow velocities, see **Table A2.2**.

External Carotid Artery (ECA)

Anatomic details: Unlike the ICA, which ascends without branching to the base of the skull, the ECA main stem quickly divides into branches that supply the face and neck. Its caliber is usually smaller than that of the ICA. The first ECA branch is the superior thyroid artery which can frequently be seen turning caudally toward the thyroid gland (see **Fig. A2.4**, **Fig. A2.9**, **Fig. A2.24**). Branches that can also be visualized by duplex ultrasound and that are routinely assessed within a clinical context are the occipital artery and the superficial temporal artery. Other branches that may be more difficult to detect by ultrasound are the ascending pharyngeal artery, the lingual artery, the facial artery, the posterior auricular artery, and the maxillary artery.

External Carotid Artery: Main Stem

Position and vessel identification: See ICA (**Videos** ▶ **A2.1** and **A2.2**). Main stem duplex imaging is demonstrated in **Fig. A2.24**. A useful differentiation criterion is the analysis of the Doppler spectrum of ECA and ICA during digital tapping of the preauricular superficial temporal artery, which reveals a stronger response in the ECA. The frequently detectable first branch—the superior thyroid artery—can also be used to identify the ECA. Its Doppler spectrum reacts positively to gentle digital tapping over the thyroid gland (**Fig. A2.24**). Also, the second branch of the ECA, the lingual artery, may be detected with a highly pulsatile flow which decreases upon pressing the tongue against the hard palate. Release of pressure leads to transient reactive hyperemia and subsequently to a pronounced increase in flow velocity (**Video** ▶ **A2.3**).

Normal values: Doppler spectrum analysis frequently shows a highly pulsatile flow compared with the ICA (**Fig. A2.24**). For flow velocities, see **Table A2.2**.

Superficial Temporal Artery (STeA)

Anatomic details: The main stem of the vessel ascends in the preauricular region and quickly divides mainly into a frontal and parietal branch, with variable vessel courses further ascending toward the temple and forehead (**Fig. A2.25**).

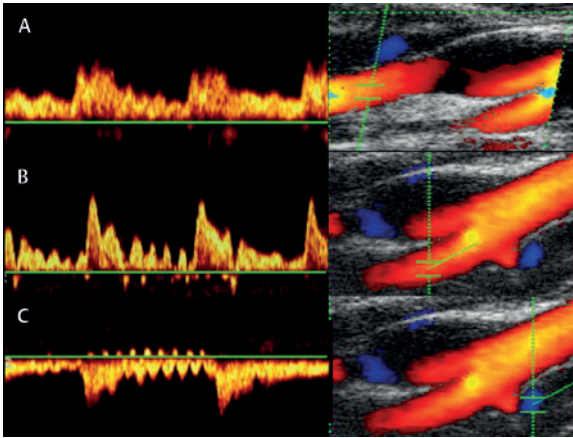


Fig. A2.24 Extracranial duplex, longitudinal plane. (A) ICA Doppler spectrum during preauricular superficial temporal artery tapping demonstrates a weak oscillation phenomenon. (B) Distinctly positive oscillation phenomenon in the ECA Doppler spectrum (flow velocity 68/12 cm/s). (C) Doppler spectrum of the superior thyroid artery. Note the positive oscillation phenomenon during slight digital tapping over the thyroid gland.

Position and vessel identification: Insonation is performed in the color mode with an insonation depth as low as possible (ideally 1.5 cm). The main stem is best identified in the preauricular region with a typical pulsatile external flow signal. According to the vessel's course the probe position needs to be adapted to display the maximum amount of the artery. In normal findings the color signal completely fills the vessel lumen. A hypoechoic vessel wall thickening is indicative of vessel wall vasculitis (**Fig. A2.25**). In patients with suspected vasculitis the branches of the STeA should be insonated as far as possible using the color mode to improve the detection rate of a regional hypoechoic vessel wall (so-called “dark halo” phenomenon). For better spatial resolution of the STeA vessel wall a linear transducer with transmission frequencies of 12–15 MHz is recommended (**Video ▶ A2.4**).

Normal values: For flow velocities, see **Table A2.2**.

Occipital Artery (OccA)

Anatomic details: The vessel has a variable course, ascending behind the ear (**Fig. A2.26**).

Position and vessel identification: For identification of the OccA, the transducer can be positioned in an axial plane cranially to the vertebral V3-VA segment and over the mastoid bone (see also “V3 segment” under “Extracranial Vertebral Artery” below). Insonation starts in the color mode with an insonation depth of ~2 cm. Doppler spectrum analysis of the OccA reveals a highly pulsatile arterial signal and may have variable flow directions. The transducer has then to be turned according to the vessel's course to display as much as possible of the artery and to analyze the flow pattern (**Fig. A2.26**; **Video ▶ A2.4**). Detection rates of 100% have been reported (Tee et al 2013).

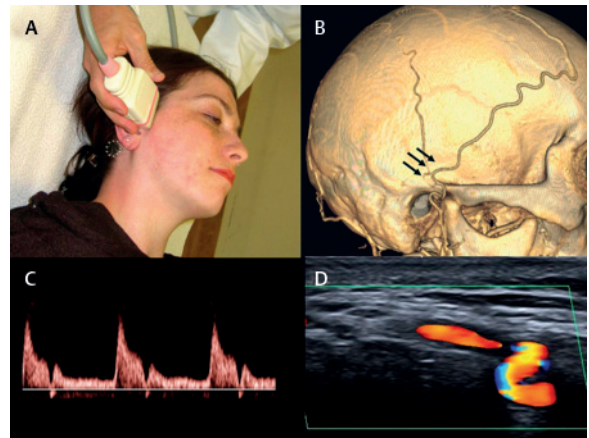


Fig. A2.25 (A) Transducer position for STeA insonation. (B) CTA, 3D reconstruction, lateral view. STeA: Main-stem course, ascending preauricular branches (arrows), and distal segments proceeding over the temporal and frontal bone. (C,D) Doppler spectrum analysis and color-mode imaging of the STeA (flow velocity 40/13 cm/s).

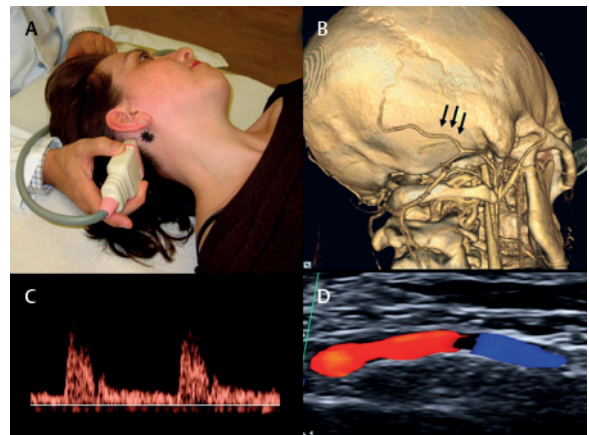


Fig. A2.26 (A) Transducer position for OccA insonation. (B) CTA, 3D reconstruction, right posterior oblique view: OccA main-stem course and branches ascending over the mastoid bone (arrows). (C,D) Doppler spectrum analysis and color-mode imaging of the OccA (flow velocity 10/2 cm/s).

Normal values: For flow velocities, see **Table A2.2**.

Subclavian Artery (SA)

Anatomic details: The anatomic variants of the aortic arch and its branches, including the SA, are described in “General Arterial Anatomy” above. Important SA branches to assess in a clinical context are the axillary and brachial arteries in addition to the VA.

Subclavian Artery: Main Stem

Position and vessel identification: Insonation of the SA is usually impaired as the vessel lies behind the clavicle and conventional longitudinal or cross-sectional images are

frequently difficult to obtain. We routinely approach the SA using a linear transducer while following the VA longitudinally or in mixed planes via the V1 segment to its origin from the SA (Fig. A2.27 and Fig. A2.28). Holding the probe laterally, the distal SA becomes visible usually with a flow away from the probe but it may show in its most proximal part a flow toward the probe. Pointing the probe in a medial direction reveals the proximal SA with a flow toward the probe. In impaired insonation conditions (e.g., a short neck or a greater than usual neck circumference) the use of a sector array might be helpful (e.g., see Fig. A2.39). Vessel identification is achieved by color-mode visualization and Doppler spectrum analysis. In many cases only a short vessel segment of the SA proximal and distal to the VA origin can be insonated.

Normal values: The Doppler spectrum profile normally shows a triphasic pulsatile flow signal with high velocities. Compression of the BrA leads to a marked reduction

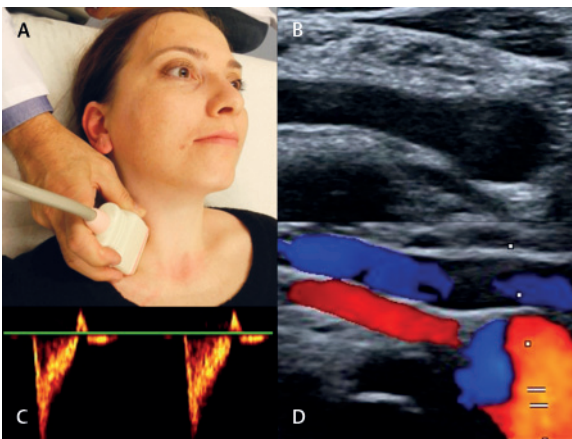


Fig. A2.27 (A) Transducer position for SA and proximal longitudinal V0/V1-VA insonation. (B) Extracranial duplex: B-mode imaging of the V0/V1-VA and SA. (D) Color-mode image of the same segment. (C) Doppler spectrum analysis of the SA with its typical triphasic pattern (153/–26 cm/s).

of systolic flow velocity (Fig. A2.27). No systematic values have been reported.

Axillary Artery (AxA)

Position and vessel identification: The AxA can easily be insonated in the axillary fossa in a longitudinal or an axial insonation plane (insonation depth 0.5–1.5 cm). As with the brachial artery the axial approach permits the fastest vessel identification and is also sufficient to evaluate the flow profile. For angle-corrected flow assessments the transducer has to be turned into the longitudinal insonation plane (Fig. A2.29; Video ▶ A2.5).

Normal values: The Doppler spectrum profile shows a triphasic pulsatile flow signal. For flow velocities, see Table A2.2.

Brachial Artery (BrA)

Position and vessel identification: The BrA can easily be insonated in the antecubital fossa in a longitudinal or an axial insonation plane (insonation depth 2–3 cm). The latter approach permits the fastest vessel identification and is also sufficient to evaluate the flow profile. For angle-corrected flow assessments the transducer has to be turned into the longitudinal insonation plane (Fig. A2.30; Video ▶ A2.5).

Normal values: The Doppler spectrum profile shows a triphasic pulsatile flow signal. For flow velocities, see Table A2.2.

Extracranial Vertebral Artery

Anatomic details: Unlike the carotid arteries, both VAs demonstrate considerable variations in length, caliber, and vessel course. Differences between the left and right side are common. There is no clear definition of VA hypoplasia: In general it is assumed if the diameter of a VA is less than 2–2.5 mm or the diameter equals less than 50% of the

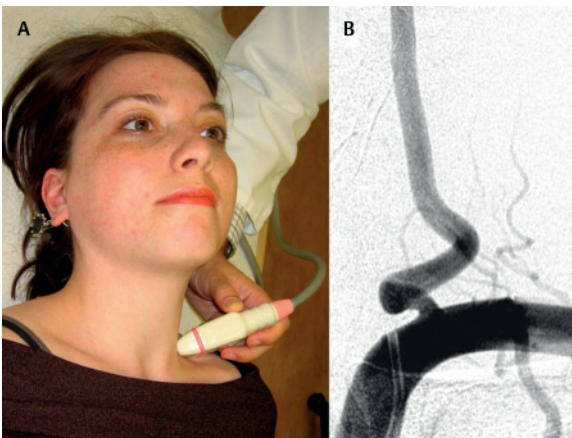


Fig. A2.28 (A) Transducer position for SA and V0/V1-VA insonation. (B) DSA, left SA injection, anteroposterior projection. Note the tortuous VA origin which may lead to misinterpretation of the VA origin as SA.

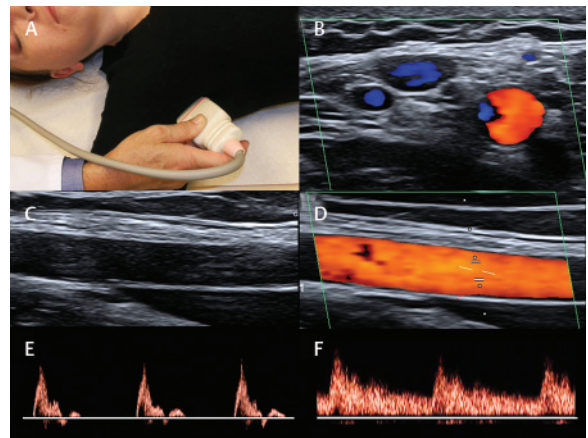


Fig. A2.29 (A) Transducer position for proximal longitudinal AxA insonation. (B) Color mode, axial insonation. Note the flat corresponding vein (blue) (C,D) Longitudinal insonation. (E,F) Doppler spectrum. Note the typical triphasic flow spectrum at rest (left) and the marked blood flow velocity increase during repeated hand grips (right).

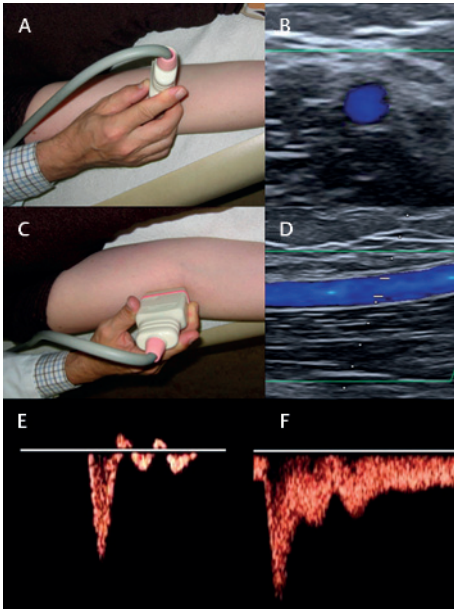


Fig. A2.30 (A) Transducer position for axial BrA insonation. (B) Corresponding color-mode image. (C) Transducer position for longitudinal BrA insonation. (D) Corresponding color-mode image. (E) Doppler spectrum analysis of the BrA at rest. Note the triphasic Doppler spectrum similar to that of the SA. (F) Doppler spectrum of the BrA shortly after repeated hand grips. Note the hyperemic response with marked flow velocity increase and decreased pulsatility.

contralateral VA. Alternatively, comparative volume flow measurements can be used to determine the differences between the two sides, and a cut-off of less than 40 mL/min may be used to define hypoplasia (Seidel et al 1999). Hypoplasia may be present in up to 10% of cases and is more frequently seen on the right side. Extracranially, the V0–V3 segments can be evaluated. VA examination should begin with the V2 segment as it is most easily identified.

V2 Segment

Anatomic details: The V2-VA segment starts at the point where the VA enters the transverse foramen. In 90% of cases this occurs at the level of the sixth vertebra (Fig. A2.31). The V2-VA segment ends when the vessel leaves its intraforaminal course at the second vertebra.

Position and vessel identification: The V2-VA segment can be insonated in nearly 100% of cases. This is best done with the patient's head in a straight position, chin slightly elevated. The transducer is held lateral to the larynx, aiming in a posterior and slightly medial direction toward the transverse foramen (Fig. A2.31). If starting from the CCA insonation, the probe is moved into an upright position until the transverse processes become visible (Video ▶ A2.6). Standard B-mode, color-mode, and Doppler spectrum analyses are usually done in the longitudinal insonation plane because of the small vessel size and the deeper location compared with the ICA. Routine examination should start with conventional B-mode to identify the transverse processes of the cer-



Fig. A2.31 Left: Transducer position for longitudinal V2-VA insonation. Right: CTA, 3D reconstruction, right anterior oblique view. Distal V1 and V2 segments of the VA. The sixth transverse process separates the V1 from the V2 segment (arrows).

vical vertebrae. A characteristic image pattern is found with a small visible vessel segment framed by the acoustical shadow of two transverse processes (Fig. A2.32 and Fig. A2.33). Then color-mode and Doppler spectrum analysis are performed (Video ▶ A2.6). Diameter, flow direction, and flow velocity within the V2 segment are routinely documented. We recommend measuring the diameter using B-mode but care must be taken not to include the outlining of the vertebral vein into the calculation. In case of doubt, measuring can be done in color mode avoiding color aliasing. In deeply located V2-VA segments it is helpful to reduce the PRF and switch off the beam steering of the color window. Furthermore, tilting the probe by slightly pressing the caudal end of the transducer into the skin of the neck optimizes color filling and facilitates angle correction in Doppler spectra assessment. In cases of impaired VA visualization we recommend first trying to examine the contralateral side where vessel identification might be easier. This will in particular be the case in VA hypoplasia, where the contralateral side is frequently hyperplastic. Once one VA is identified, contralateral insonation is easier as both VAs are located at a similar depth and the same transducer position can be applied on both sides. In case of a pathologic V2-VA finding, or if the clinical question suggests involvement of the posterior circulation, the routine measurement of the V2-VA in one intervertebral segment is extended to all VA intervertebral segments and the V0/V1 as well as the V3 segments. In individuals with a slender neck the V2-VA segment can also be seen in a transverse insonation plane (Fig. A2.34; Video ▶ A2.7).

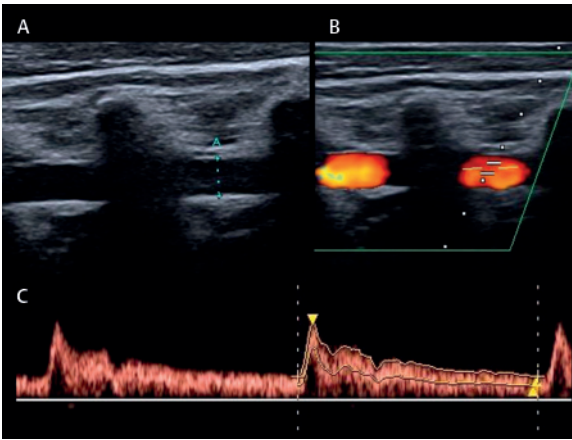


Fig. A2.32 Extracranial duplex, V2-VA insonation in the longitudinal insonation plane. (A) B-mode image, dominant VA, diameter 4 mm. (B) Color-mode image. Note the VA color-mode signal interruption by the transverse processes. (C) Doppler spectrum of the dominant VA (flow velocity 58/17 cm/s, PI = 1.5).

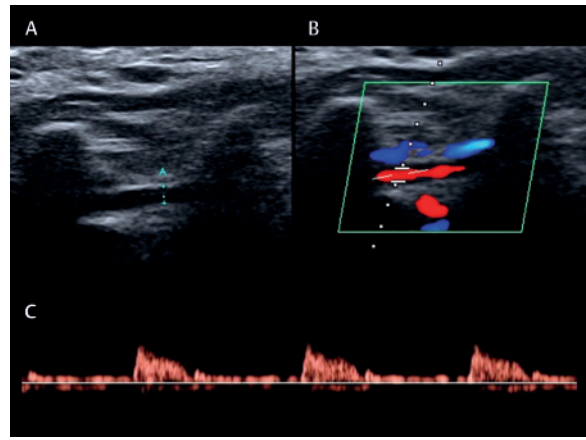


Fig. A2.33 Extracranial duplex, V2-VA insonation in the longitudinal insonation plane. (A) B-mode image, hypoplastic VA, diameter 1.9 mm. (B) Color-mode image. (C) Doppler spectrum of the hypoplastic VA (flow velocity 23/3 cm/s, PI = 2.6). Note the higher PI compared with a normal-sized VA (**Fig. A2.32**) typically seen in VA hypoplasia. The detectable diastolic flow indicates brain perfusion and argues against a distal flow obstruction.

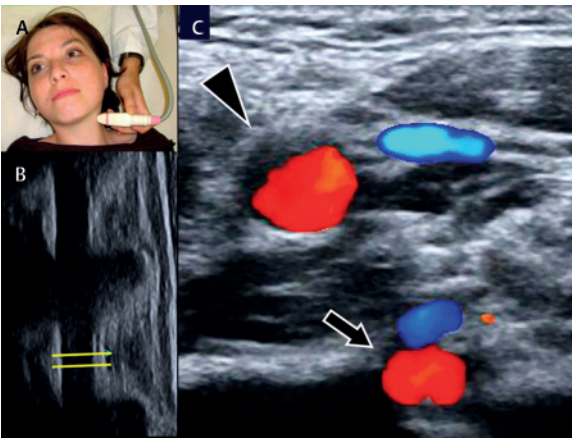


Fig. A2.34 (A) Transducer position for transversal V2-VA insonation. (B) Extracranial duplex, B-mode image, V2-VA insonation in the longitudinal insonation plane, 90° counterclockwise rotated. The yellow lines indicate the V2-VA segment between the fifth and sixth cervical transverse processes leading to image C. (C) Extracranial duplex, color-mode image, transversal plane as indicated in B. Note the prominent VA (arrow) with the corresponding vein and the CCA (arrowhead) with the IJV.

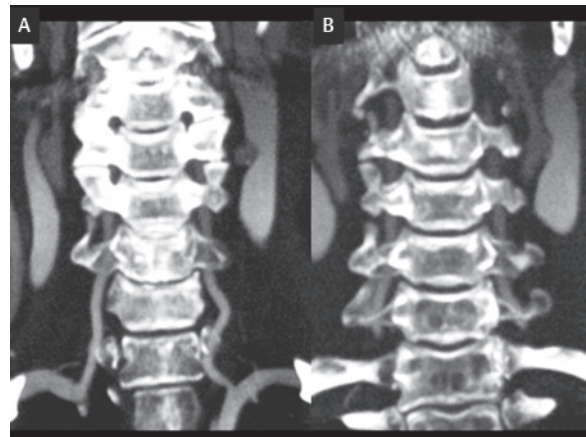


Fig. A2.35 CTA, 2D coronal MIP. (A) Anatomic situs of VA origin from both SAs in typical deep location. (B) In reality the VA origin is hidden by the clavicle.

Normal values: Pulsatility of the Doppler spectrum might vary from high pulsatility caused by low diastolic flow in a distinctly hypoplastic artery (**Fig. A2.33**) to low pulsatility with high velocities comparable with the ICA flow in a large vessel (**Fig. A2.32**). Even in a hypoplastic vessel a preserved diastolic flow component as indicator of remaining brain perfusion should be present. In this case the VA often ends as PICA. For flow velocities, see **Table A2.2**.

V0/V1 Segment

Anatomic details: Anatomic variations of the VA origin have already been described in “General Arterial Anatomy” above. As it lies behind the clavicle, inson-

ation may be difficult (**Fig. A2.35**). Larger ultrasound studies have demonstrated insufficient V0–VA visualization in 6–14% on the right side and in 14–40% on the left side (Trattnig et al 1993). The difference is mainly explained by the deeper origin of the left VA and the 5% of variants in which the left VA directly originates from the aortic arch. Apart from impaired insonation conditions caused by the deep vessel localization, other factors may also contribute to insufficient visualization. The VA originates at the SA apex in only ~50% of cases (**Fig. A2.36A**). In the remaining cases the vessel originates deeper in the aortic arch or at the apex but from the posterior wall, and in a minority even from the inferior SA wall which cannot be insonated by conventional ultrasound (Trattnig et al 1993). A tortuous

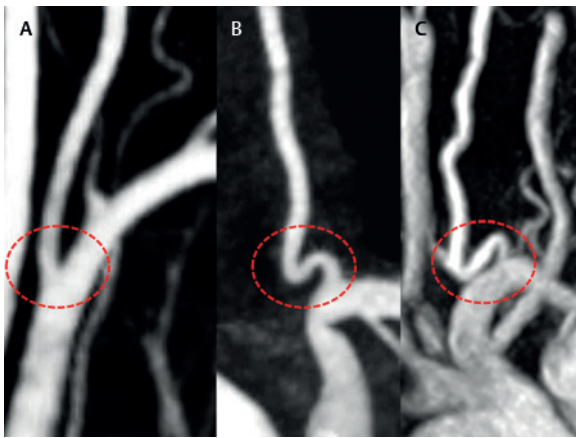


Fig. A2.36 Variations of the VA origin (encircled). (A) Straight but very deep (i.e., proximal) VA origin. (B) Marked elongation of the VA origin. (C) Kinking of the VA origin.

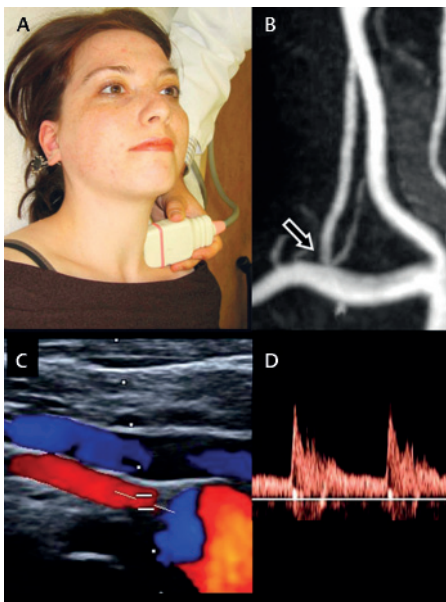


Fig. A2.37 (A) Transducer position for V0/V1-VA and SA insonation in the longitudinal plane. (B) Contrast-enhanced MRA, coronal view. Note the straight VA origin (arrow). Here the proximal VA and SA can concomitantly be visualized in a longitudinal examination plane. In elderly patients and elongated vessels (see **Fig. A2.35**) an axial insonation plane may facilitate the V0-VA segment evaluation. (C,D) Extracranial duplex, longitudinal insonation plane. Color-mode image and Doppler spectrum analysis of the VA origin (flow velocity 53/17 cm/s).

VA origin may be a further restricting factor. In elderly stroke patients, a tortuous proximal VA can be expected in up to 50% of cases (**Fig. A2.36B, C**).

Position and vessel identification: Insonation of the V0/V1-VA segment is started at the V2 segment, with the linear transducer used for the examination of the carotid arteries applying the color mode. From there the vessel is followed along its proximal extraforaminal

V1 path. Use of beam steering, for example by changing the linear beam into a partial sector field, if available, and beam steering of the color-mode field facilitates the identification of the proximal VA down to its origin at the supraclavicular fossa with the transducer pointed caudally and slightly ventrally (**Fig. A2.37**). In the case of tortuosities the course of the proximal VA may be visualized in the transverse plane. If identification of the VA is required because the vessel could not be followed continuously to its origin, confirmation can be achieved by digital tapping of the ipsilateral VA at the atlas loop. Tapping is easily done with one finger over the palpable groove behind the mastoid (**Video ▶ A2.8**). A typical modulation of the signal—similar to the tapping maneuver for the STeA—identifies the VA (**Fig. A2.38**). Compared with the V2 segment, the distal V1 segment runs rather superficially with a more inclined course, and it may therefore be examined even if the visualization of the V2 segment is insufficient. This may also help to clarify if a missing diastolic flow component in the V2 segment is “real” or just be caused by an unfavorable insonation angle. In difficult insonation conditions, the patient may be asked to reach toward their knee with the hand on the side of insonation (Alexandrov 2013). Also, a sector probe may facilitate the detection of the VA origin. As with the use of the linear probe, we recommend starting with the identification of the V2-VA segment and following the vessel in a longitudinal plane down to the SA (**Fig. A2.39**). Unlike the V0-VA segment, the V1-VA can be insonated in more than 90% of subjects (Kuhl et al 2000).

Normal values: Directly at the origin of the VA Doppler spectra might appear mildly turbulent and the pulsatility higher compared with the distal VA segments, without pathologic significance. This phenomenon is caused by the perpendicular branching off of the vessel from the SA. For flow velocities, see **Table A2.2**.

V3 Segment

Anatomic details: The V3 segment is a tortuous vessel segment with a complex three-dimensional anatomy (Ulm et al 2010). It encircles the atlas and the atlanto-occipital joint first in a posterior-vertical direction and then in a medio-horizontal direction, aiming for the foramen magnum. Two loops with a comma-shaped appearance can be distinguished. After leaving the transverse foramen of the second vertebra, the proximal loop runs in a vertical orientation between C2 and C1. The distal loop winds round the atlanto-occipital joint (**Fig. A2.40** and **Fig. A2.41**).

Position and vessel identification: Ultrasound insonation of the V3 segment traditionally focuses on the distal segment with its loop, also called the “atlas loop.” Insonation rates of 76% on the right side and 86% on the left have been reported (Trattnig et al 1990). In VA hypoplasia, confident identification may be difficult. For insonation the patient is asked to turn their head and the transducer is positioned in a transverse position just below the mastoid bone with a slight anterior and rostral orientation (**Fig. A2.42**).

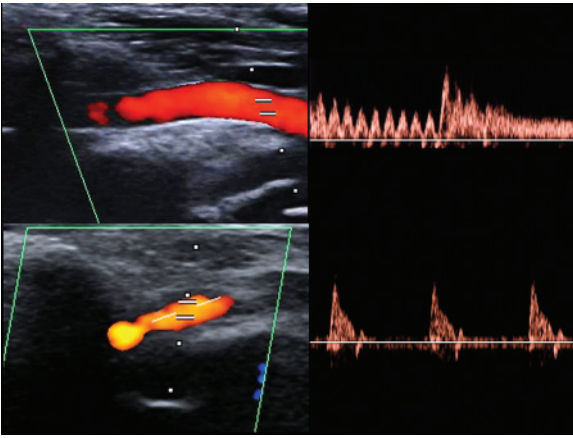


Fig. A2.38 Extracranial duplex, longitudinal insonation plane. Color-mode image and Doppler spectrum. **Top:** In case of doubt about VA identification—typical transients during VA tapping at the atlas arch confirms VA identity. **Bottom:** A distal V1-VA segment with a normal diameter (3 mm) and a flow pattern without diastolic flow is indicative of distal VA occlusion proximal of the PICA origin. Note that the signal here is quite similar to a normal SA flow signal. A distal VA occlusion should not be too readily assumed from V2-VA derived flow profiles, as a missing diastolic flow there might be attributable to an unfavorable angle of insonation, e.g., facilitated by vessel hypoplasia.

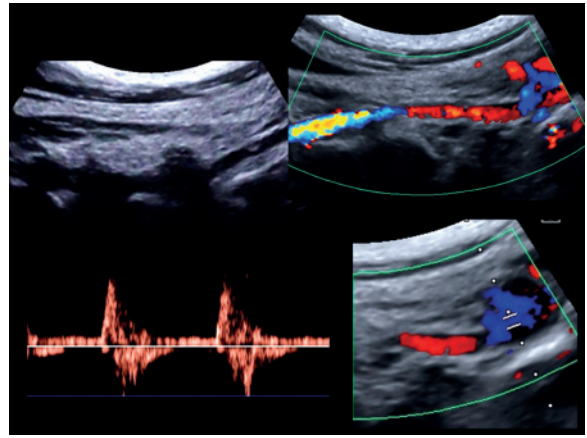


Fig. A2.39 Extracranial duplex, longitudinal insonation plane, sector probe. **Top:** B-mode (left) and color-mode image (right). The sector transducer may facilitate the examination of the VA origin in patients who are obese, have a short neck, or with a deep location of the VA origin. **Left:** Proximal V2 in B-mode imaging. **Right:** V0-1 and SA in color mode. **Bottom left:** SA Doppler spectrum with its typical triphasic flow pattern (flow velocity 85/-42 cm/s). **Bottom right:** Color-mode image of the VA origin and SA.

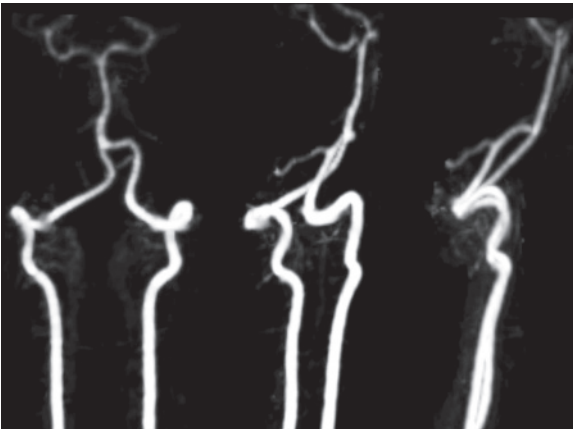


Fig. A2.40 Postprocessed contrast-enhanced 3D MIP MRA, arterial phase. Vertebrobasilar anatomy. **Left:** Posteroanterior view. **Middle:** 45° rotation to the left. **Right:** 90° rotation to the left. Note the tortuosity of the V3-VA.

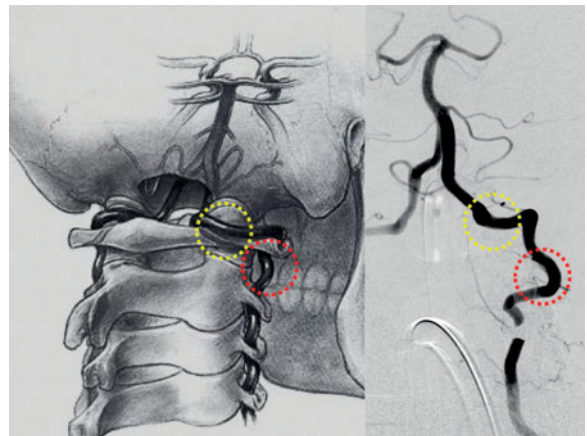


Fig. A2.41 **Left:** Drawing of the vertebrobasilar anatomy (adapted from von Reutern and von Büdingen 1993). **Right:** DSA, left VA injection, posteroanterior projection. Note the tortuous V3 course in both images and the two prominent loops: The proximal V3 loop (red circles) at the exit of the transverse foramen (C2) and the distal V3 loop (yellow circles) with its horizontal course behind the atlanto-occipital joint before entering the foramen magnum.

Pure B-mode imaging may fail to detect the artery. However, in color mode the segment appears with a flow away from the probe or, if slightly tilted downward, comma-shaped with a bidirectional color image, which makes confusion with the ICA unlikely (**Fig. A2.43**). Insonation depth varies according to the circumference of the neck but the vessel segment is usually detected in 1.5–4 cm of depth. The proximal V3 loop is best insonated with the linear probe following the V2 in the longitudinal plane (**Fig. A2.44**). The distal V3 segment can also be examined using the transcranial probe via the transforaminal approach

(**Video** ▶ **A2.9**; see also “V4 and Distal V3 Segment” under “Vertebral Artery” later in this chapter).

Normal values: Assessment of flow velocity has to allow for the fact that exact angle correction is impeded by the vessel course. We therefore recommend documenting the highest flow velocities without angle correction. As no systematic values have been reported, the available data from the V2 segment should be used as a guide for flow velocity evaluation (**Table A2.2**).



Fig. A2.42 Top left: Transducer position for distal V3-VA loop (atlas loop) insonation in a slightly oblique axial plane. **Bottom left:** Proximal V3-VA loop insonation in longitudinal plane. **Right:** CTA, 3D reconstruction, right posterior oblique view of the distal V2- and both parts of the V3-VA segment: the atlas loop (arrows) and the proximal V3 loop (white arrow). Note the OccA (dotted arrow), which should not be mistaken for the V3-VA (see **Fig. A2.26**).

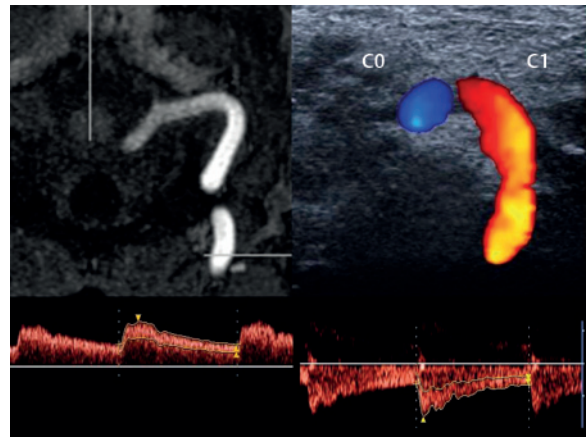


Fig. A2.43 Top left: Postprocessed contrast-enhanced 3D MIP MRA, arterial phase, axial MIP: V3 distal atlas loop. **Top right:** Extracranial duplex, axial insonation plane. Corresponding color-mode image. Note the straight horizontal vessel course behind the atlanto-occipital joint with a flow away from the probe (red) before entering the foramen magnum. **Bottom:** Extracranial duplex, Doppler spectrum analysis of the distal V3-VA (flow velocity 39/19 cm/s and 33/13 cm/s).

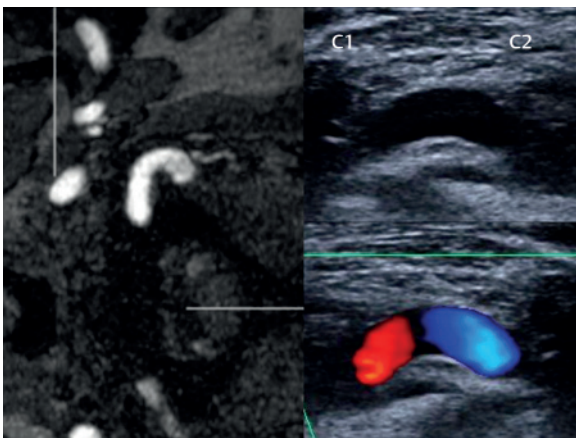


Fig. A2.44 Left: Postprocessed contrast-enhanced 3D MIP MRA, arterial phase, axial MIP, image rotated 45° counterclockwise to correspond with ultrasound plane: Proximal V3 loop. **Right:** Extracranial duplex, longitudinal insonation plane, B-mode image (**top**) and color-mode image (**bottom**). Note: the loop located between C2 and C1 appears similar to the atlas loop between C1 and skull base.

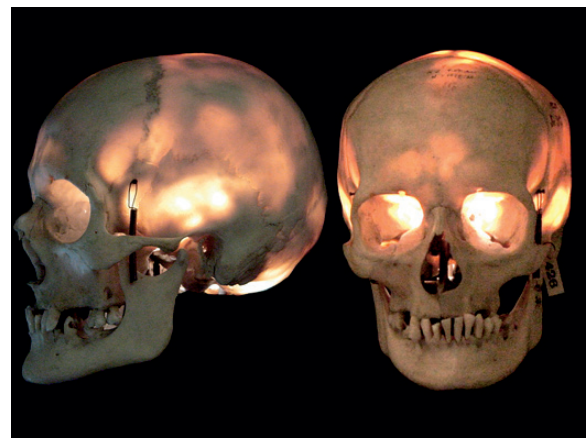


Fig. A2.45 Skull of a woman (aged 59), illuminated by flashlight from within. Note the transtemporal, transforaminal, transorbital, and transfrontal bone windows. (With kind permission from Prof. Schnalke, Berlin Museum of Medical History, Charité—Universitätsmedizin Berlin, Germany.)

Intracranial Arteries

A sector transducer with transmission frequencies of 1–3 MHz is required for intracranial vessel analysis using TCCS. The majority of ultrasound systems use 2- or 2.5-MHz transducers. Despite the use of low frequencies, insonation in adults can only be performed in regions where the skull is naturally thin: i.e., where a bone window is present (**Fig. A2.45**).

The dimension of each bone window is individual and depends on several factors. Kollár and coworkers (2004) correlated the thickness of the temporal bone and quality of the transtemporal bone window.

The reported thickness ranged from 0.7 mm in excellent transtemporal ultrasound conditions to 6 mm in poor conditions. The best insonation results come from the transtemporal bone window, which yields the majority of information about the intracranial blood circulation, and are achieved if the transducer is positioned in front of the external acoustic meatus just above the zygomatic arch. Transtemporal ultrasound penetration and subsequently insonation quality worsen with increasing age. In addition, gender differences at older ages are observed with worse insonation conditions in women. Finally, brain atrophy, whatever its cause, is also associated with worsening transtemporal insonation conditions.

Hoksbergen et al studied 112 European vascular patients aged over 60 years. Using the transtemporal window they found no signal in 1% of men and 23% of women while all signals (defined as M1-MCA, A1-ACA, and P1- and P2-PCA) were present in 83% of men and 40% of women. During transforaminal insonation 6% of men and 5% of women revealed no flow signal, whereas assessment of both V4-VA and BA was possible in 91% and 79%, respectively (Hoksbergen et al 1999). Of 198 ethnic South Asian stroke patients (mean age 64 years, 70% males) an inadequate acoustic bone window was seen in 16.2% of cases (De Silva et al 2007). A prevalence as high as 23% has been reported for Thai stroke patients (Ratanakorn et al 2012). For clinical practice, the patency of the acoustic bone window can be divided into five categories:

1. Excellent—all main segments of the basal intracranial arteries are visible throughout their entire length.
2. Good—the intracranial arteries can be reliable judged.
3. Fair—a complete assessment is not possible.
4. Bad—only parts of certain vessels are visible.
5. Missing—no vessel signal is available.

In most ultrasound systems the quality of the B-mode image correlates well with the visibility of the CW, i.e., the quality of the color-mode image. However, sometimes these findings may also differ, with missing color-mode signals despite a reasonable B-mode visualization of parenchymal structures such as the midbrain. Transcranial color-mode quality can be optimized by reducing the depth of insonation, the size of the color window, and the PRF. The latter may lead to “dirty” images with a profound color aliasing phenomenon. Although this might seem to impair the detection of circumscribed stenoses and the analysis of flow direction, we recommend use of this strategy to obtain good spatial information on the insonated vessel segment as a “road map” and to prove the vessel’s integrity. Doppler spectrum analysis of vessel segments should be performed as a second step, which then allows exact assessment of flow velocity and flow direction. The latter is facilitated by using the ultrasound system’s “triplex examination mode,” which allows real-time examination with B-mode, color mode, and Doppler mode simultaneously active. The triplex mode especially facilitates the examination of elongated vessels through different insonation planes—a constellation which is true for most of the intracranial arteries and veins. Unfortunately, many ultrasound systems suffer a substantial reduction of image quality as soon as the triplex mode is activated, which is probably due to limited calculation power. Even so, the triplex mode helps to quickly identify the required vessel segment and the system may then be switched into the duplex mode as required, e.g., to analyze a turbulent flow or raised flow velocity in more detail.

In spite of ongoing technical and system improvements, the patency of the bone window will probably remain crucial. The development and use of ultrasound contrast agents—consisting of stabilized microbubbles that can be injected intravenously to improve

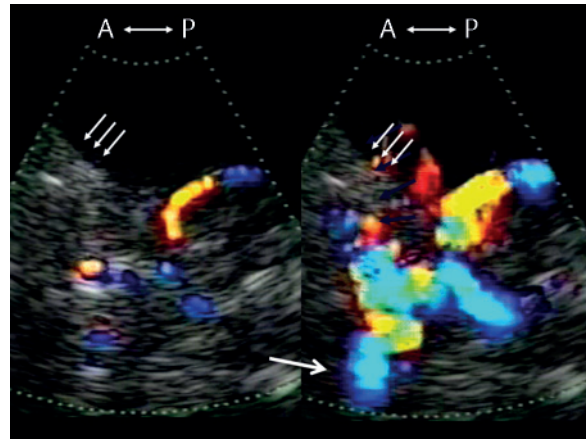


Fig. A2.46 TCCS, transtemporal approach, axial plane. **Left:** Color-mode imaging in a stroke patient with impaired transtemporal bone window; color signals of the A1-ACA and M1-MCA (arrows) are not visible, apart from the P1- and P2-PCA segments. **Right:** Color-mode image after intravenous administration of 1 mL SonoVue. Excellent images of all basal cerebral arteries are seen except for the ipsilateral M1-MCA (arrows), although the contralateral M1-MCA becomes visible (arrow), confirming M1-MCA occlusion. Note the blooming effect and aliasing phenomenon artificially enlarging the insonated vessels. (A = anterior, P = posterior)

signal-to-noise ratio—help to overcome this problem. Currently available in a large number of countries is the sulfur hexafluoride-based agent SonoVue (Bracco Imaging), sold as Lumason in the United States. Using echo-contrast agents, intracranial vessel visualization is improved and detection rates reach ~90%, even in the elderly population (Gerriets et al 2002). In another study at least the main stem of the MCA was visible after the administration of echo-contrast agents, which was not possible before in 12% of subjects (Postert et al 1998). An example of color signal improvement after contrast application is shown in **Fig. A2.46** and **Video A2.10**. (For further details concerning ultrasound contrast, see also Chapter 1, “Harmonic Imaging and Ultrasound Contrast Agents” under “Imaging Modalities, Parameters, and Settings.”)

Like MRI and CT, TCCS uses well-defined examination planes to achieve reliable and reproducible images of parenchyma and vessels. As with MRI and CT, axial planes are the standard examination planes. Coronal planes are helpful for visualizing vessel segments with a vertically orientated course and sagittal planes may be used for vessels with a rostrocaudal course (Stolz et al 1999b). Fusion imaging with MRI facilitates the recognition of planes and vessel assignment (for methodological aspects see Chapter 1, “Ultrasound Fusion Imaging” under “Imaging Modalities, Parameters, and Settings”).

Applying TCCS through the transtemporal bone window, five main axial insonation planes (**Fig. A2.47**; see also **Videos A2.11–A2.13** for transtemporal insonation with and without fusion imaging) and two coronal insonation planes (see **Fig. A2.54** and **Video A2.14**) can be distinguished. Within these planes different structures such as bone, parenchyma, or cerebrospinal fluid (CSF)

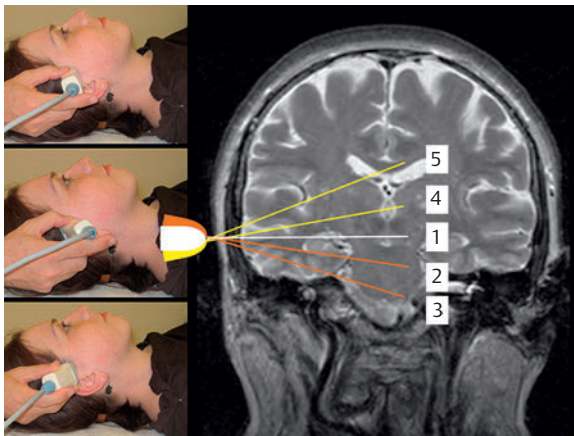


Fig. A2.47 Transducer position and schematic drawing of the five axial insonation planes in a coronal T2-weighted MR image. **1** = midbrain plane; **2** = upper pontine plane; **3** = lower pontine plane; **4** = thalamic plane; **5** = cella media plane.

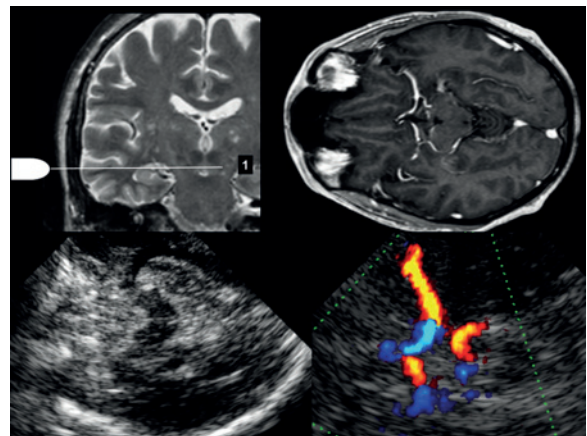


Fig. A2.48 Midbrain plane. **Top left:** Probe position. **Top right:** Corresponding MR ce-MP-RAGE images rotated by 90° to correspond with ultrasound images, axial plane. **Bottom left:** Corresponding TCCS B-mode image. **Bottom right:** Color-mode images demonstrating M1-MCA, M2-MCA, A1-ACA, P1-PCA, P2-PCA, and BA tip.

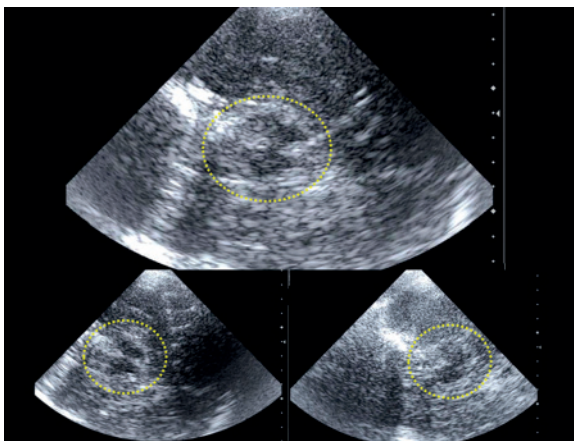


Fig. A2.49 TCCS, axial B-mode image of the midbrain plane. **Top:** Optimal midbrain positioning in the center of the ultrasound image, facilitating anatomic orientation and optimizing vessel visualization. **Bottom:** Nonrecommended midbrain positioning.

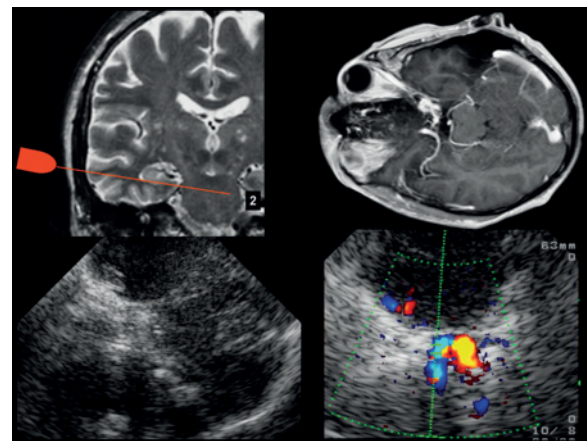


Fig. A2.50 Upper pontine plane. **Top left:** Probe position. **Top right:** Corresponding MR ce-MP-RAGE images rotated by 90° to correspond with ultrasound images, axial plane. **Bottom left:** Corresponding TCCS B-mode image. **Bottom right:** Color-mode images demonstrating ICA siphon.

within the cisterns and fissures can be assessed on conventional B-mode imaging and used as landmarks for intracranial orientation and insonation of main vessels. We recommend beginning in the midbrain plane as most vessel segments of the CW can be identified there and the probe can be placed perpendicular. The best temporal acoustic window (i.e., the thinnest temporal bone) is usually found preauricular above the zygomatic arch. From here the probe is moved in small circles to pick up the best B-mode image. The brighter the whole image, the closer the probe is to the optimal window. The hypoechoic midbrain should easily be distinguished from its surrounding hyperechoic basal cisterns (**Fig. A2.48**). From here, only minimal probe movements are needed for further image optimization, controlled by one or two fingers of the transducer-holding hand that are kept in contact with the patient's skin during insonation.

For a standardized insonation approach, the midbrain should be centered within the ultrasound monitor (**Fig. A2.49**). By lowering the insonation angle by ~10° the upper pontine plane is displayed, and another 10–20° decrease displays the lower pontine plane at the border to the medulla oblongata (**Fig. A2.50** and **Fig. A2.51**). Ultrasound landmarks are anteriorly the sphenoid and posteriorly the petrosal bone forming the middle temporal fossa and—especially for the upper pontine plane—the hypoechoic pons and cerebellum as well as the hyperechoic fourth ventricle. Pointing the transducer 10° upward from the midbrain plane, the thalamic plane is displayed with both hypoechoic thalami embracing the third ventricle and the hyperechoic pineal gland behind the third ventricle (**Fig. A2.52**). Further increasing the insonation angle by 10–20° reveals the cella media plane with angular cut of the hypoechoic lateral ventricles (**Fig. A2.53**).

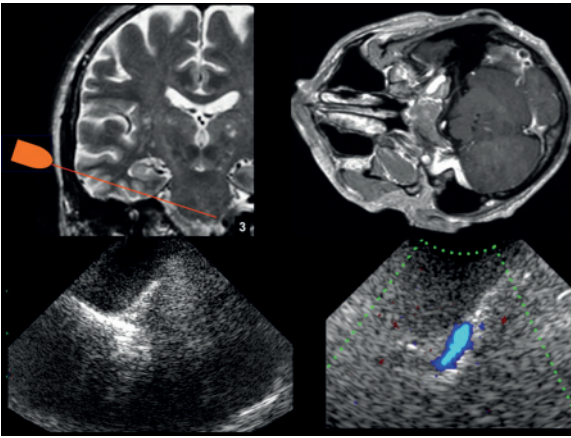


Fig. A2.51 Lower pontine plane. **Top left:** Probe position. **Top right:** Corresponding MR contrast-enhanced MP-RAGE images rotated by 90° to correspond with ultrasound images, axial plane. **Bottom left:** Corresponding TCCS B-mode image. **Bottom right:** Color-mode images demonstrating C6-ICA.

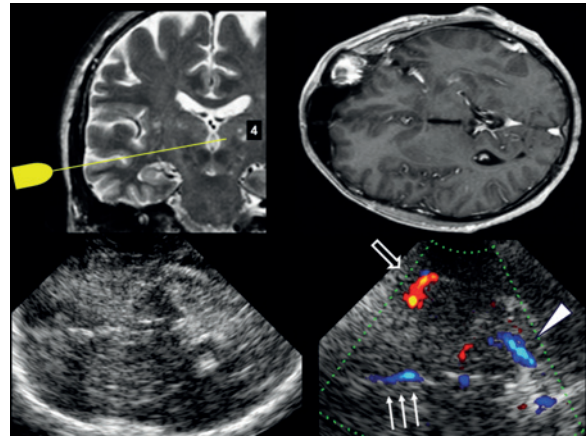


Fig. A2.52 Thalamic plane. **Top left:** Probe position. **Top right:** Corresponding MR contrast-enhanced MP-RAGE images rotated by 90° to correspond with ultrasound images, axial plane. **Bottom left:** Corresponding TCCS B-mode image. **Bottom right:** Color-mode images demonstrating M2/M3-MCA transition (arrow), A2-ACA (arrows), and P2/P3-PCA transition (arrowhead).

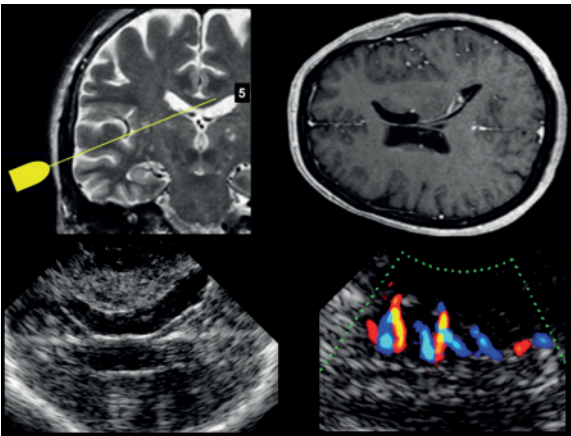


Fig. A2.53 Cella media plane. **Top left:** Probe position. **Top right:** Corresponding MR contrast-enhanced MP-RAGE images rotated by 90° to correspond with ultrasound images, axial plane. **Bottom left:** Corresponding TCCS B-mode image. **Bottom right:** Color-mode images demonstrating insular M3-MCA branches.

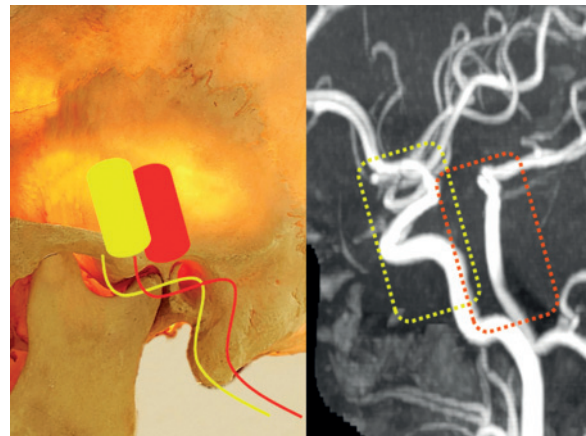


Fig. A2.54 **Left:** Illuminated skull demonstrating location and best transducer position over the transtemporal bone window for the anterior coronal plane (yellow) and posterior coronal plane (orange). **Right:** 3D TOF-MRA, lateral MIP. Insolation field of the anterior coronal plane (yellow) and the posterior coronal plane (orange).

Insonation through a bone window is comparable to peering through a keyhole. Depending on the region of interest, the position of the transducer might need to be adjusted, e.g., moved cranially but aiming downward to visualize basal structures (as if looking through a keyhole and trying to see the floor behind the door). Alternately, the probe might need to be moved caudally but aiming upward to see thalamus or lateral ventricles (like trying to see the ceiling in our keyhole example).

Transtemporal coronal planes may be the first choice to analyze craniocaudally orientated vessels and may help to render stenotic lesions more precisely. The anterior coronal plane in particular facilitates the complete analysis of the intracranial ICA and makes it possible to differentiate more precisely between the terminal ICA, the beginning of the MCA, and the ACA. The posterior coronal

plane can be used to analyze at least the distal BA and to distinguish the proximal PCA from the SCA but may also visualize the entire course of the BA and even parts of the ipsi- or contralateral V4-VA. Also, the C6-ICA segment can be visualized in the posterior coronal plane (**Fig. A2.54** and **Fig. A2.55**). As B-mode reference points, the hypochoic vessel sheath of the proximal ICA segments may be used in the anterior coronal plane and the hyperechoic prepontine cistern and clivus in the posterior coronal plane.

The proximal intracranial posterior circulation is examined through the transtemporal window, i.e., through the foramen magnum. Further access paths are via the transorbital or the transfrontal bone window (although the latter is rarely used). In the transtemporal approach up to 90% insonation energy is absorbed by the bony structures, but the transorbital approach requires reduction of

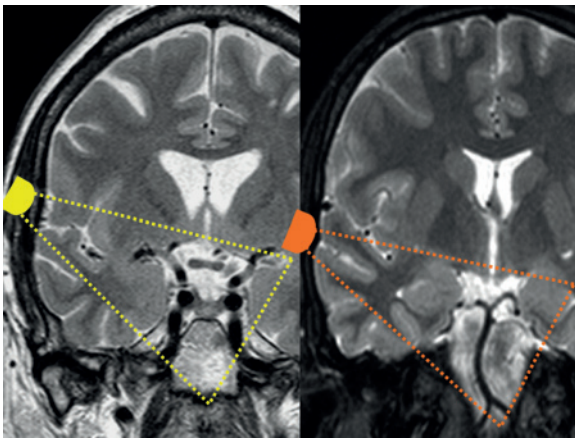


Fig. A2.55 MR T2-weighted image, coronal plane. **Left:** Anterior coronal plane comprising at least the distal ICA, and proximal MCA and ACA segments. **Right:** Posterior coronal plane comprising BA, proximal PCA segments, and superior cerebellar artery.

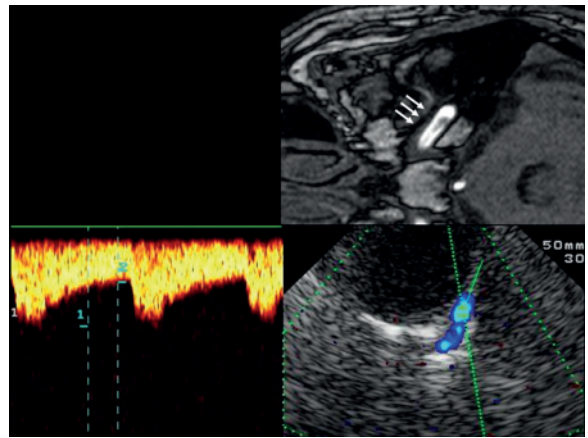


Fig. A2.57 Top: 3D TOF-MRA, axial source image, lower pontine plane, image rotated by 90° to correspond with the ultrasound image. Horizontal part of the C6 segment (arrows). **Bottom:** TCCS, transtemporal approach, axial lower pontine plane. **Right:** Color-mode image demonstrates the horizontal part of the C6 segment. **Left:** Doppler spectrum analysis (angle-corrected flow velocity 66/37 cm/s).

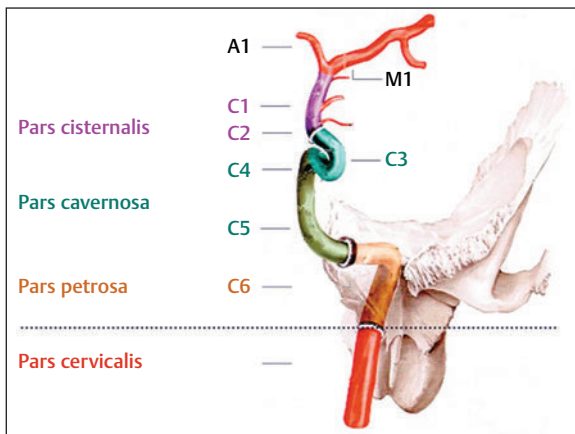


Fig. A2.56 Schematic of the intracranial part of the ICA. Extracranial part: pars cervicalis. Intracranial parts: pars petrosa, C6 segment; pars cavernosa, C5–C3 segments; pars cisternalis, C2 and C1 segments. (Adapted from Schünke et al 2006; drawing: Karl Wesker.)

the insonation energy to prevent side effects to the human eye. Therefore the former approaches allow a mechanical index (MI) of up to 1.5, the latter—in accordance with the US Food and Drug Administration (FDA) recommendations for insonation of the orbit and eye—should not be higher than 0.26.

Internal Carotid Artery

Anatomic details: According to its anatomic course, the intracranial ICA is by neurosonologic definition divided into three parts and six segments (**Fig. A2.56**). Radiologists, however, commonly divide the ICA into seven segments according to its flow direction, with the C1 at its extracranial origin and C7 at its intracranial ending. Provided that a sufficient bone window is present, all intracranial segments can be insonated by TCCS in combined

axial and coronal planes. If the axial plane is used, the transducer has to be focused between the midbrain and lower pontine planes (see **Fig. A2.50** and **Fig. A2.51**). For coronal insonation the probe is turned 90° upward without changing its position over the preauricular transtemporal bone window (**Fig. A2.54**). Mixed planes sometimes allow insonation of longer segments, especially of the ICA (see also **Videos** ▶ **A2.15** and **A2.16**).

C6 Segment

Anatomic details: The most proximal segment is C6 with its ascending and horizontal part within the petrosal bone, leaving the skull at the foramen lacerum (**Fig. A2.57**). Anatomic length including the vertical and horizontal parts is 25–35 mm, the major part corresponding to its horizontal course. The horizontal C6-ICA is partly covered by a thin osseous and/or cartilaginous layer and the inferior sphenoparietal ligament. The lateral rim of the petrosal bone serves as a readily identifiable anatomic landmark.

Position and vessel identification: Only the horizontal part of this segment can be visualized at the deepest point of the skull base (**Fig. A2.57**) with a flow direction away from the transducer. The axial lower pontine plane is recommended but the posterior coronal plane also allows a good visualization of the first intracranial segment of the ICA. In subjects with a good transtemporal bone window it is visible in up to 97% over a length of 15 ± 4 mm (Eggers et al 2009). Angle-correction is often possible because its straight course. Failure to detect the C6 segment in spite of excellent temporal acoustic bone window and detection of all other basal arteries may be due to the thickness of the fibro-osseous layer on the horizontal part of this vessel.

Normal values: For flow velocities, see **Table A2.3**.

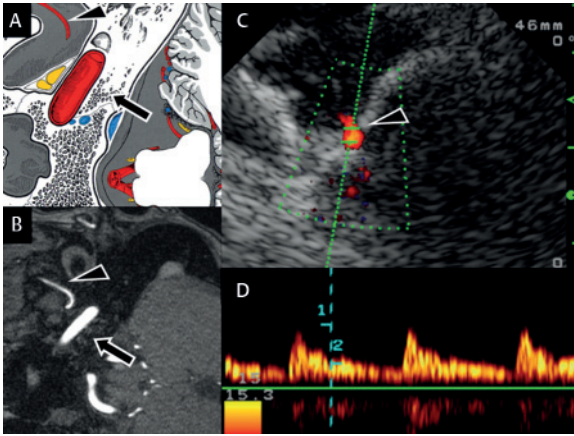


Fig. A2.58 (A) Schematic of the relationship between the C6-ICA, the petrosal bone (arrow), and the MMA in the temporal fossa (arrowhead). (Adapted from Kretschmann and Weinrich 2003.) (B) Corresponding 3D TOF-MRA, axial source image, rotated 90° counterclockwise, indicating C6-ICA (arrow) and MMA (arrowhead). (C,D) TCCS, color-mode image and Doppler spectrum analysis, lower pontine plane, revealing the MMA spectrum analysis (flow velocity 20/8 cm/s, PI = 1.5).

Excursion: Middle Meningeal Artery (MMA)

Anatomic details: The MMA is one important branch of the maxillary artery which itself is the last branch of the ECA. After originating from the maxillary artery in the infratemporal fossa, it runs through the foramen spinosum to supply the dura mater and the calvaria. The MMA is the largest artery that supplies the meninges. In 1.2% of cases the MMA alone ensures the blood flow of the OA (see Case 42) (Hayreh and Dass 1962). Recently a major focus has been given to the MMA in patients with migraine studied by MRA (Nagata et al 2009, Schoonman et al 2008) and also by duplex ultrasound (Alijagic-Schultze et al 2010). The MMA may also serve as an important feeder or collateral in dural arteriovenous fistula (see Case 34), meningioma, and moyamoya disease (see Case 9) (Deng et al 2014, Hori et al 2015, Shah et al 2015).

Position and vessel identification: The MMA is identified by its anatomic relationship to the C6-ICA. In a series of 27 subjects with excellent temporal acoustic bone window and a detectable C6-ICA and MCA, the MMA was visualized in 63% of cases (Alijagic-Schultze et al 2009). When the C6-ICA is visualized the probe has to be tilted slightly downward. The MMA can be insonated medially of the mid or distal third of the C6-ICA and usually just below it with a red-colored signal and low flow velocities as well as high pulsatility. The PRF, color window size, and color gain therefore have to be adapted (Fig. A2.58; Video ▶ A2.17).

Normal values: For flow velocities, see Table A2.3.

C5 Segment

Anatomic details: This segment is the ascending part up to the beginning of the carotid siphon (Fig. A2.59).

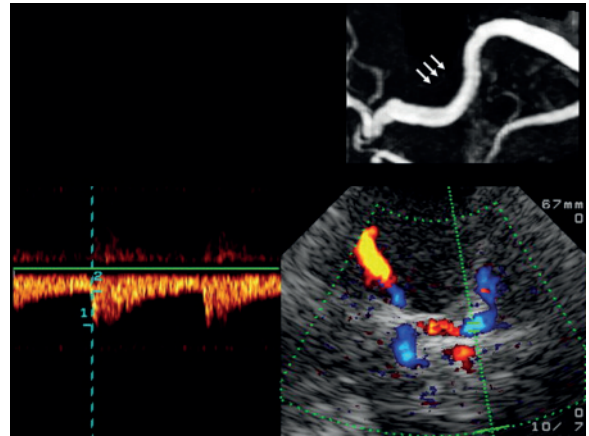


Fig. A2.59 Top: MR contrast-enhanced T1-weighted image, coronal plane, image rotated 90° counterclockwise to correspond with the ultrasound image. Arrows: C5 segment. Bottom: TCCS, transtemporal approach, coronal plane. Right: Color-mode image demonstrates the C5 segment. Left: Doppler spectrum analysis (flow velocity 31/13 cm/s).

Position and vessel identification: The C5 segment can best be visualized in one of the coronal planes (Jurgita et al 2002) (Fig. A2.54 and Fig. A2.55). Because of an unfavorable insonation angle, blood flow velocity measurements are usually not recommended (Fig. A2.59).

Normal values: For flow velocities, see Table A2.3.

C3/C4 Segment

Anatomic details: The C3/C4 segment and the C2 segment form the carotid siphon, which can have a variable appearance. Its shape can vary from an almost straight course in young subjects to a C-shaped or a tortuous S-shaped vessel course, the latter more often seen in the elderly population (Fig. A2.60). Anatomic length including C5 is 30–50 mm.

Position and vessel identification: The C3/C4 segment can best be visualized in the axial upper pontine plane (Fig. A2.50; Video ▶ A2.18). It is visible in subjects with good insonation quality without exception (Eggers et al 2009). Exact measurements of flow velocities are difficult as angle correction is impaired by the vessel course (Fig. A2.61). A straight course with a flow away from the probe is observed in young subjects. Elderly subjects present variable elongations and often a bidirectional flow (Fig. A2.62). The highest measured velocity should be recorded. In cases of a missing transtemporal bone window, visualization of the carotid siphon via the transorbital approach can be attempted. Because of the restrictions on insonation power, a low detection rate can be expected. The OA, the PCoA, and the AChA arise from C2 and C3. Due to their diameter the OA and PCoA may be insonated (see below).

Normal values: For flow velocities see Table A2.3.

	0–20 years	21–50 years	51–74 years
Normal 	100%	74%	41%
Omega 	0%	24%	51%
Tortuous 	0%	2%	8%

Fig. A2.60 Anatomic variants of the carotid siphon in relation to age. (Adapted from Huber 1982.)

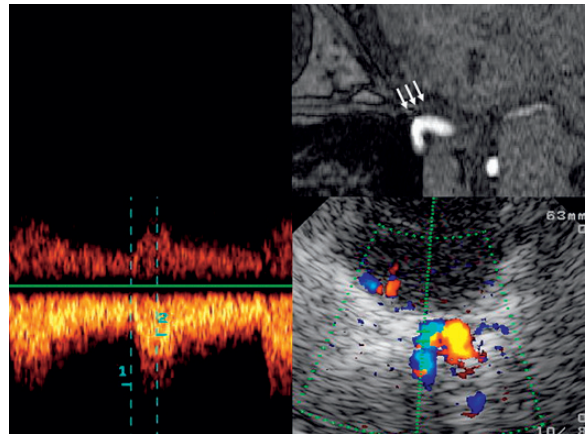


Fig. A2.61 **Top:** MRI, 3D TOF-MRA, axial source image, upper pontine plane, image rotated 90° counterclockwise to correspond with the ultrasound image revealing the C3/C4 segment (arrows). **Bottom:** TCCS, transtemporal approach, axial upper pontine plane: **Right:** Color-mode image demonstrates the C-shaped part of the carotid siphon. **Left:** Doppler spectrum analysis (flow velocity 50/25 cm/s).

C1/C2 Segment

Anatomic details: Both segments form the rising cisternal, most distal part of the vessel—also called the terminal ICA (TICA)—before it bifurcates to form the carotid-T, which also refers to its anatomic shape. The anatomic length is 13–18 mm.

Position and vessel identification: The C1/C2 segment usually follows a mediolateral course, which allows good color imaging in the coronal plane. Color-mode visualization might be impaired if the vessel runs perpendicular to the ultrasound beam (Fig. A2.54, Fig. A2.55, Fig. A2.63). It is visible over a length of 11 ± 2 mm in 100% of cases with a patent bone window (Eggers et al 2009). Often the C1/C2 segment follows a long, straight course and in these cases angle-corrected flow velocity measurement may be obtained (Fig. A2.64). If the vessel anatomy is unclear the distal ICA can also be studied in successive transverse slices by using the conventional transtemporal axial approach starting at the midbrain plane and tilting the probe caudally toward the carotid siphon in the upper pontine plane. Such an approach impedes correct flow velocity measurements but allows the assessment of vessel integrity and evaluation of high-grade stenosis.

Normal values: For flow velocities see Table A2.3.

By using an intermediate plane between the axial and the coronal plane (called the oblique coronal plane) the intracranial ICA may become almost completely visible. Together with the proximal M1-MCA it then forms a U-shaped color signal (Fig. A2.65; Video A2.16).

Ophthalmic Artery (OA)

Anatomic details: After arising from the C2 or C3 segment of the ICA, the OA runs through the optic canal into the

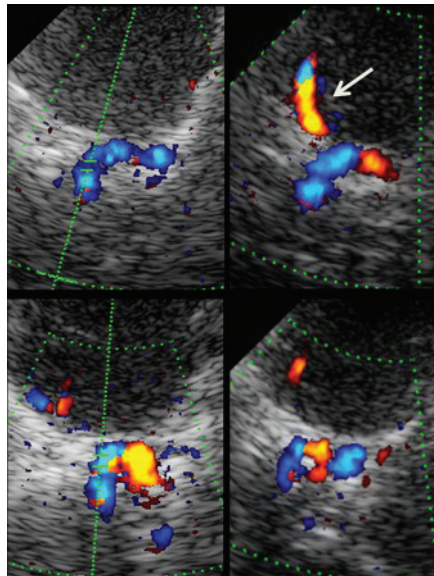


Fig. A2.62 TCCS, transtemporal approach, upper pontine plane, color-mode images. **Top:** Carotid siphon anatomy in younger people with a straight or only mild elongated course. **Bottom:** Elderly or hypertensive subjects—the carotid siphon may reveal severe elongations, coils, and loops. Note that a prominent temporal M2 branch of the MCA may be observed in the upper pontine plane (arrow).

orbital socket, where it branches into the orbital arteries (lacrimal artery, supraorbital artery, anterior and posterior ethmoidal artery, medial palpebral artery, dorsal nasal artery, supratrochlear artery) and the ocular arteries (central retinal artery [see below], ciliary arteries, muscular branches). The main stem has a mean diameter of 0.8–1.2 mm. A dual origin with a dominant contribution via the MMA has been observed in 2.4% of cases. In 1.2% of cases the OA arose solely from the MMA (Hayreh and Dass 1962). Its origin is usually intradural; an extradural

origin has been observed in 7.5% of cases (Yasargil 1984). The OA can be partially insonated during its intracranial course via the transtemporal bone window and during its course through the orbital socket via the transorbital insonation approach.

Intracranial Ophthalmic Artery

Position and vessel identification: For intracranial insonation the transtemporal upper pontine imaging plane is chosen and the carotid siphon is visualized (Fig. A2.50). The color-mode signal of the OA can then be identified at least as a small color dot in ~90% of cases with a patent transtemporal bone window ~5–10 mm anterior of the

carotid siphon and ~5 mm medially of the lesser wing of the sphenoid bone (Schreiber et al 2006). To maximize color gain the PRF has to be reduced, i.e., optimized for detection of low flow velocities. The color box should be small. The insonation depth may vary between 55 mm and 70 mm. The OA shows a Doppler spectrum with flow direction toward the transducer. Vessel identification can be confirmed by slight tapping of the ocular bulb (two fingers applied flat on the closed eye). This results in a positive oscillation phenomenon within the OA Doppler profile (Fig. A2.66; Video A2.18).

Normal values: For flow velocities, see Table A2.3.

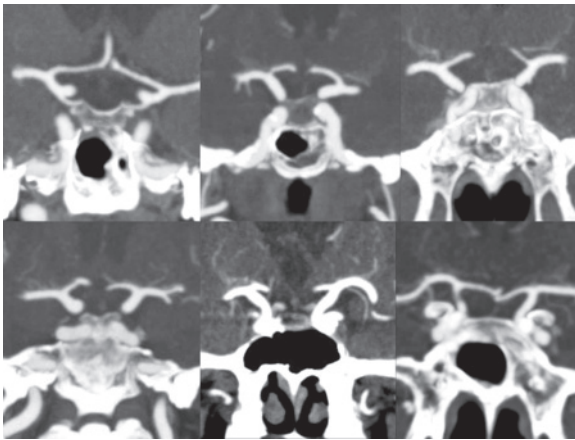


Fig. A2.63 CTA, coronal MIP. Examples of variations in carotid-T anatomy. **Top left:** A marked oblique course facilitating TCCS insonation in the anterior coronal plane. **Bottom right:** A more vertical course which may impede duplex color imaging.

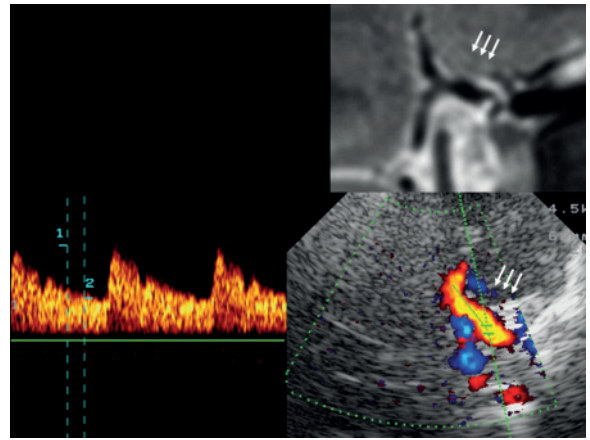


Fig. A2.64 **Top:** MRI, T2-weighted image, coronal plane, image rotated 90° to correspond with the ultrasound image. Note the flow void in the C1/2 segment (arrows). **Bottom:** TCCS, transtemporal approach, anterior coronal plane. **Right:** Color-mode image demonstrates a flow signal in C1/C2 toward the probe. **Left:** Doppler spectrum analysis (angle-corrected flow velocity 113/36 cm/s).

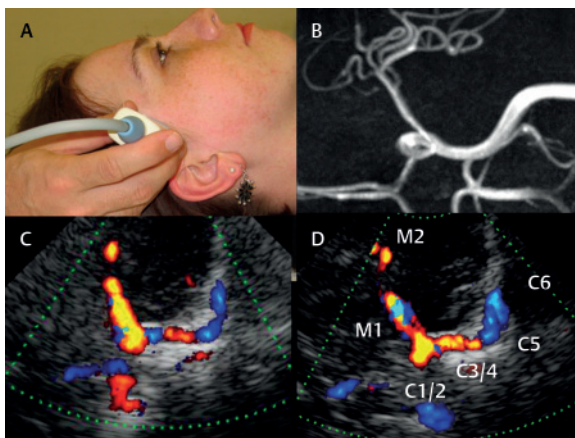


Fig. A2.65 (A) Probe position in an oblique coronal plane. (B) 3D TOF-MRA, coronal MIP, 90° counterclockwise rotated to correspond with ultrasound image. (C,D) TCCS, transtemporal approach, oblique plane showing two examples of a large part of the ICA and MCA in one insonation field.

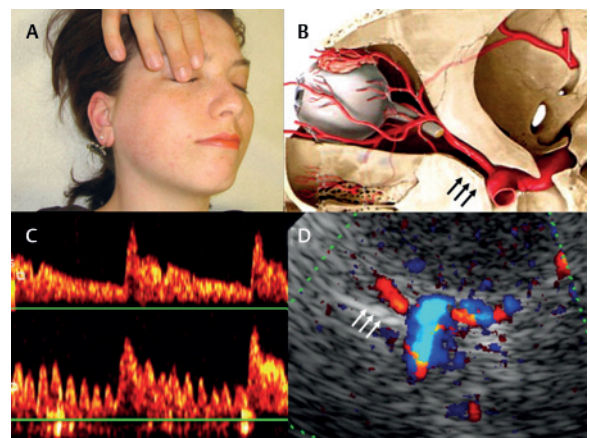


Fig. A2.66 (A) Tapping maneuver. (B) Schematic of the origin of the OA from the carotid siphon (arrows). (Adapted from Schünke et al 2006; drawing: Karl Wesker.) (C,D) TCCS, transtemporal approach, upper pontine plane. (C) Doppler spectrum demonstrates low flow velocities (top) and a positive oscillation phenomenon on digital tapping of the ipsilateral optic bulb (bottom). (D) Color-mode image demonstrates a red-coded OA signal toward the probe, anterior and slightly laterally to the carotid siphon (arrows).